DEPARTMENT OF PETROLEUM AND GEOSCIENCE

Master of Science Thesis

Author: **Raymond Mushabe**

NORWEGIAN UNIVERSITY OF SCIENCE AND TECHNOLOGY

TOPIC: EFFECT OF WATER QUALITY ON SPONTANEOUS IMBIBITION IN CARBONATE CORES

June 2021

EFFECT OF WATER QUALITY ON SPONTANEOUS IMBIBITION IN CARBONATE CORES

Raymond Mushabe
Supervised by: Associate Prof. Carl Fredrik Berg and Associate Prof. Antje van der Net

2021.06.11

Abstract

The research topic in this work was the effect of water quality on spontaneous imbibition (SI) in carbonate cores. The target was to alter the oil wetting state in outcrop cores to a more water wet state in order to have spontaneous imbibition of brine and improved crude oil recovery. The main aim was to understand how the ionic composition of imbibing brine dictates the wettability change. In order to carry out these experiments a rig designed to operate at 96°C for an uninterrupted SI was needed. Outcrop cores used were of two origins; outcrop cores from Ainsa in Spain and from Angola, and these outcrop cores were considered representative of an Equinor operated oil field off-shore Brazil. Based on petrophysical properties, the core material sourced from Angola was more heterogeneous than that from Ainsa. X-ray diffraction (XRD) and back-scatter electron imaging (SEM) results classified the rock materials as limestone without anhydrite. The research also compares two aging processes, and design for the most efficient process.

The effect of ionic composition on wettability alteration was studied by analysing oil recoveries due to SI of formation water (FW), synthetic seawater (SSW) or modified versions of synthetic seawater at 96°C . The ionic composition of SSW was altered by increasing the Mg^{2+} and SO_4^{2-} ion concentrations. Three different modified synthetic sea waters; one with two times sulfate concentration and four times magnesium concentration (SSW-2S4Mg), a second water with two times sulfate concentration and eight times magnesium concentration (SSW-2S8Mg), and finally a low salinity water where the NaCl concentration is reduced to 10% of the SSW concentration (0.1-NaCl-SSW). For reproducibility of results, two cores were used in each run of SI experiment. Contact angle measurements conducted at room temperature on polished rock chips aged both at 25°C (room temperature) and at 96°C were also done using the same set of brines to supplement results of spontaneous imbibition. Zeta potential measurements were conducted on Angola 8 μm rock particles suspended in each of the test brines to study the rock-brine interface at 25°C and 70°C .

An improved SI rig that allows an uninterrupted SI process was set up and worked smoothly without leakages, pressure build up and water boiling. From SI experiment, improved oil recoveries of 6-10% with SSW after FW, showed that SSW is an EOR fluid in limestone cores. Recoveries of 4-6% and 4-10% with SSW-2S4Mg and SSW-2S8Mg, respectively, showed that enriching SSW with Mg^{2+} and SO_4^{2-} ions improves the water wetting state in limestone cores and causes more spontaneous imbibition. The experiment with Ainsa cores gave a recovery of 5% with 0.1-NaCl-SSW after SSW showed the impact of selective dilution. Additional recovery of 13% with SSW-2S4Mg confirmed that reducing the NaCl content in SSW improves the activity of potential determining ions in the wettability alteration process in limestone cores. This was also confirmed with contact angles on water wet samples after aging in 0.1-NaCl-SSW for 3 days.

Different aging methods were studied by aging two Ainsa cores with either dynamic or static aging. For this comparison, a new experimental set up for dynamic aging was designed and built. This setup could handle high temperatures and pressures below 35 bars. Spontaneous imbibition results showed that dynamic aging is a better wettability alteration process than static aging. A recovery of 12% was recorded in the core aged dynamically and 4% for the statically aged when SSW was introduced in a tertiary mode.

Acknowledgement

Thanks be to God the Almighty for enabling me to compile this work. It is by His strength that I have been able to do it. I will always be grateful to my parents that have given me the gift of education. Thank you Mr.Rhobert Korutaro and Mrs.Josephine Bazira. Many thanks to the rest of my family for the moral, financial, spiritual and emotional support you have given me over years.

My sincere appreciations go to my beloved supervisors that have consistently and persistently guided, corrected and encouraged me to pursue more. Thank you Associate Prof. Carl Fredrik Berg and Associate Prof. Antje van der Net. In your presence I have learnt a lot and will always cherish my experience with you. My humble appreciations go to Equinor AS for your material support. Thanks to Rex M.s Wat and Thomas Ramstad for your guidance and help through out my project time.

My kind appreciations go to Roger Overå for laboratory guidance you gave me. I would like to thank people at the thin section laboratory and SINTEF workshop for the profound work you offered in core handling and laboratory equipment improvisation. Thank you Gunnar Vistnes and the rest of the team.

Thanks Gbadebo Adejuma. You were indeed an amazing laboratory partner. I had great experiences with you and thanks for always pushing me to do my best. Thanks Shirin Safar Zadeh, Lay Nimeshkumar Trivedi, and Haili Long-Sanouiller for the amazing time we had togther in the laboratory and thank to Alberto Luis Bila for laboratory help. My sincere appreciation go to Alex Baguma Muhairwe and Maria Assumpta Nakibuule for your editorial inputs into my work and constructive criticism.

Contents

Figures

Tables

Code Listings

Acronyms

[Ca^{2+}]/[$SO_4{}^{2-}$] relative concentration between Ca^{2+} and SO_4^{2-}. 21

[a] concentration of component a. 3

% wt percentage weight. 62

Φ_{eoi} surface electrical potential of surface i at infinite separation. 39

κ_B Boltzmann constant. 40

ψ_i surface potential at interface i. 40

ρ_g grain density. 57

ζ_i zeta potential at interface i. 40

$^-$OH hydroxide. 25

0.1-NaCl-SSW 10x-NaCl-diluted synthetic seawater. vii, xix, 46, 47, 61, 62, 65, 74, 78–81, 83, 84, 87, 89, 90, 103

0.1-SSW ten times diluted SSW. 24, 46, 47, 59, 62, 79–81, 90

AN acid number. xv, xvi, 8, 11–13, 15, 16, 19–21, 27, 45, 46

ANP National Agency of Petroleum, Natural Gas and Biofuels. 1

BN base number. 8, 46

C_i local ion concentration. 42

Ca^{2+} calcium. xi, xvi, xxiii, 3, 6–11, 16–31, 39, 74, 78, 79, 83–86, 90

$CaCl.2H_2O$ calcium chloride dihydrate. 47

$CaCO_3$ calcium carbonate. 6

$CaSO_4$(s) anhydrite precipitate. xv, xvi, 9–11, 19, 20, 24, 26, 27, 29, 30, 64

Cl^- chloride. 9, 31, 39, 74, 78, 84

D-60 Exxsol D60. 48, 49, 52, 53, 67, 68, 82, 106, 107

DLE double-layer expansion. 4, 35, 62, 81, 85, 86

DLVO Derjaguin, Landau, Verwey, and Oberbeek. 35

EDL electric double layer. xi, xvii, 5, 11, 30, 35, 41–44

EOR enhanced oil recovery. vii, xvi, 11, 22, 24, 85

Fe iron. 73, 74

FW formation water. vii, xi, xv, xvii, xix, 3, 5–10, 21, 22, 24, 27–31, 33, 46, 47, 49, 52, 56–58, 60–62, 65, 66, 74–76, 78–83, 85, 87, 89, 101, 102, 106

GC Gouy-Chapman. xvii, 41, 43

HCO_3^- hydrogen carbonate. 74

I_w amott-harvey water index. xv, 15

IFT interfacial tension. 3, 17, 31, 33, 36

K^+ potassium ion. 74

KCl potassium chloride. 47

LS-EOR low salinity enhanced oil recovery. 5, 31, 35

mD milidarcy. xix, 73, 75

Mg^{2+} magnesium,. vii, xi, xii, xvi, xviii, xxv, 3, 6, 9, 10, 16–19, 23–31, 46, 48, 49, 61, 64, 65, 74, 78–81, 83–86, 89, 90

$MgCl.6H_2O$ magnesium chloride hexahydrate. 25, 47

MIE multi-ion exchange. xi, xvi, 3–5, 11, 21, 28, 31, 32, 78, 81, 84, 86

ml mili litre. 47, 49, 52, 53, 57, 59, 60, 66–68, 82, 102

N_2 nitrogen gas. 68

Na^+ sodium. 31, 39, 74, 78, 84

NaCl sodium chloride. vii, xii, xviii, 3, 9, 10, 18, 23, 25, 28, 29, 47, 48, 61, 64, 65, 78, 80, 83–85, 89

$NaHCO_3$ sodium hydrogen carbonate. 47

$NaSO_4$ sodium sulphate. 47

OIIC oil initially in the core. xvii, xviii, 48, 71, 77, 84, 86

OIIP oil initially in place. 1

P-B Poisson-Boltzmann. 39

P_c capillary pressure. 17, 40

PDI potential determining ion. xv, xviii, 3, 5, 17–21, 23, 28, 31, 44, 61, 62, 84, 86

PDIs potential determining ions. vii, xvi, 19, 20, 23, 47, 64, 65, 78, 79, 81, 83–85, 89, 90

pH pH. xix, 10, 11, 18, 62

PPM parts per million. 30

PRV pressure relief valve. xvii, 60

PTFE polytetrafluoroethylene. xvii, 48, 60, 67, 82

PV pore volume. 72, 75

R-COO- organo-metallic bond, where x is either Mg or Ca. 10, 86

RCA Routine Core Analysis. xii, 45, 53, 71

RF recovery factor. 1

RPM rotations per minute. 53, 59, 63, 75

RT room temperature of 23°C. xvi, xviii, 25, 48, 49, 79, 80, 89

SCAL Special Core Analysis. xii, 45, 59, 71

SCN^- thiocyanate. 21, 22, 25, 26

SEM back-scatter electron imaging. vii, xii, xvii, 59, 64, 72–74

SI spontaneous imbibition. vii, xv–xix, 8–10, 12–17, 19, 20, 22, 24, 27, 28, 31, 45–51, 60, 64–68, 71, 72, 74–77, 82, 83, 86, 88–90, 105–107

SIP Specific interaction potential. xvi, 37, 39–41

SO_4^{2-} sulfate. vii, xi, xii, xv, xvi, xviii, xxiii, xxv, 3, 8–10, 16–29, 31, 32, 46, 48, 49, 61, 64, 65, 74, 78–80, 83–86, 89, 90

Sr^{2+} strontium ion. 74

$SrCl.6H_2O$ strontium chloride hexahydrate. 47

SSW synthetic seawater. vii, viii, xv, xvi, xviii, xix, xxiii, xxv, 3, 5, 16, 20, 22–25, 27, 30, 31, 33, 46–49, 59, 61, 62, 65, 74, 76–81, 83–87, 89, 90, 101–103, 107

SSW-2S4Mg 10 times NaCl-diluted SSW with $[Mg^{2+}]$ and $[SO_4^{2-}]$ respectively 4 and and 2 times above that in SSW. vii, xix, 46, 47, 49, 52, 53, 60–62, 65, 74, 78–81, 84, 85, 87, 89, 101, 102, 107

SSW-2S8Mg 10 times NaCl-diluted SSW with $[Mg^{2+}]$ and $[SO_4^{2-}]$ respectively 8 and and 2 times above that in SSW. vii, xix, 46, 47, 49, 52, 53, 60–62, 65, 74, 78–81, 85, 87, 89, 101, 102, 107

SW sea water. xii, xvi, xix, 3, 16–18, 20, 22, 24, 27, 29–31, 46, 49, 52, 60–62, 64–66, 83, 85, 89, 90, 103

Swi irreducible water saturation. xii, 59, 63, 74, 75, 83, 85

T temperature. 40

TDS total dissolved salt. 47, 74

XRD X-ray diffraction. vii

ZP zeta potential. xv, xix, 17, 18, 23, 46, 62, 79–81, 89, 90, 102

Chapter 1

Introduction

Brazil has emerged to be among key players in global oil production. According to the Brazilian National Agency of Petroleum, Natural Gas and Biofuels (ANP), Brazil produced on average 3 million barrels/day of crude oil in 2020. Most of the Brazilian fields are marginal and mostly located on the eastern coastal waters. The oil field under study in off-shore Brazil is made of Aptian bivalve carbonate rocks and located within the same coastal marine basin, as shown in Figure 1.1(a). The field was discovered in 1974, and as of 2008 had produced about 600 million barrels of crude oil, which makes up about 10% of oil initially in place oil initially in place (OIIP) (Spadini et al., 2008), and had grown by only 5% in 2020. The field is structurally heterogeneous with multiple fractures at different scales as shown in Figure 1.1(b) in form of multiple reservoir units. A recovery of 15% in such a field is way below the average global recovery in carbonate reservoirs at approximately 30% figure which itself is quite low.

Primary production of oil from a reservoir by pressure depletion in an oil field is not an optimal way of maximising recovery during the life span of the field. Due to heterogeneity in petrophysical properties of carbonate reservoirs, mainly permeability, porosity and wettability, in comparison with those of sandstone reservoirs, the recovery factor (RF) is even lower. Therefore, pressure maintenance mostly by water flooding or gas injection is usually started at the beginning of the production phase to maximise recovery.

Traditional water flooding in carbonate oil reservoirs is difficult to implement, and in most cases unsuccessful (Yi et al., 2012). Treiber et al. (1972) showed and reported that carbonate reservoirs are mostly mixed wet, and lean more to being oil wet in comparison with sandstone reservoirs. Fluid flow in a porous medium is in part governed by wettability. In petroleum reservoirs, its usually either oil or water wet. This parameter partly dictates how much residual oil remains behind (Tiab and Donaldson, 2015; Thomas et al., 1993; Yi et al., 2012). This implies that recovery by either spontaneous imbibition or water flooding is higher in sandstones than in carbonates due to the natural wettability states of the two reservoir types. In the end more residual oil is expected in carbonate reservoirs than in sandstones.

The other challenge with water-flooding carbonate oil reservoirs is the difficulty in directing flow of injected brine to contact residual oil. Carbonate reservoirs are naturally fractured. These fractures have varying degrees of fracture width, and with permeabilities in orders of magnitude larger than permeabilities in matrix blocks. Therefore any form of water-flooding into such a system will result in wide fractures as thief zones and almost no water injection from fractures into matrix blocks as was observed by Yi et al. (2012).

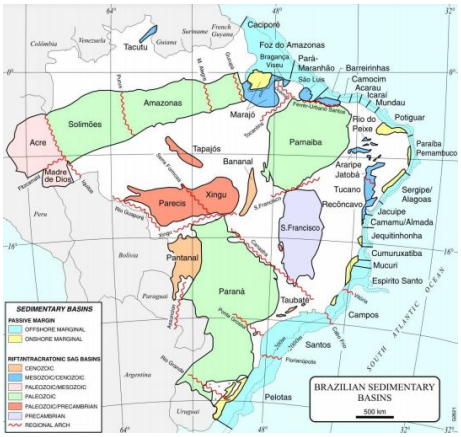

(a) A map showing sedimentary basins of the Brazil

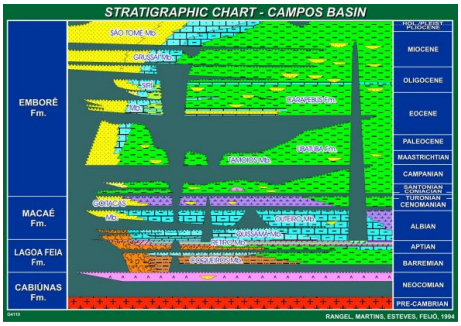

(b) The structuring in the off-shore field under study showing major multiple fractures in form of numerous reservoir units on a macro scale

Figure 1.1: The off-shore oil field in Brazil under study, Spadini et al., 2008

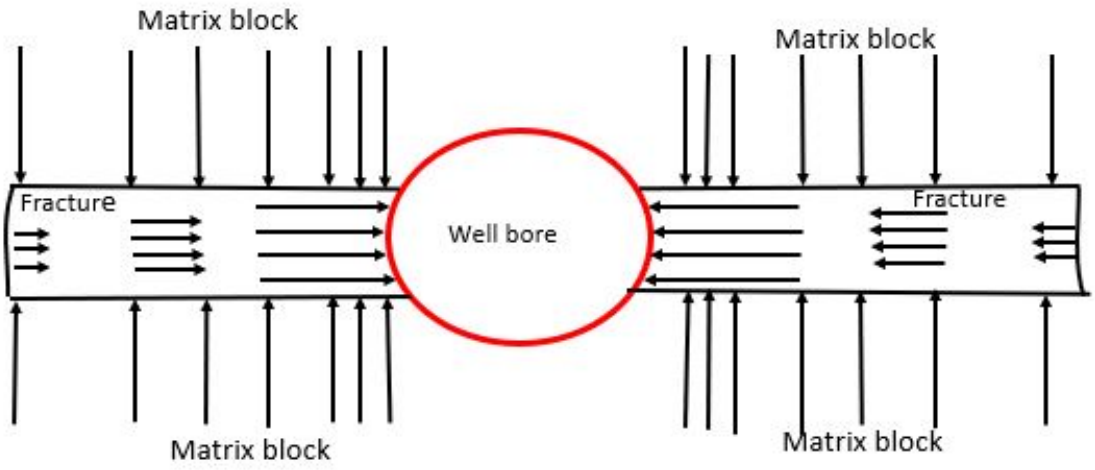

Figure 1.2: Fracture-Matrix communication in carbonate reservoirs. Flow from matrix blocks to fractures and finally to production in a well bore

However, considering that over 60% of the world oil reservoirs are carbonates (Chandrasekhar, 2013), there is a technical and technological need to improve oil recovery from them. The off-shore field in Brazil is no exception. One way to achieve higher recoveries is by altering the wettability state to a more water-wet. As a result, spontaneous imbibition from fractures into matrix blocks harboring oil takes place as illustrated in Figure 1.2. Spontaneous imbibition is a process where a wetting phase displaces a non-wetting phase in a porous medium by capillary action (Yu et al., 2008). For spontaneous imbibition of water (brine) to occur, the capillary pressure curve of the flow system needs to be positive (Hirasaki et al., 2004), and preferably with large magnitude values for higher imbibition rates. According to the Young-Laplace formulation of capillary pressure, one of the key parameters that can be altered to make capillary pressure positive is the contact angle, which directly defines wettability. A small change in wettability can result in a significant spontaneous imbibition and hence more recovery. Strand et al., 2008, noted that a wettability change of 19% at previously oil wet sites resulted an extra oil recovery of 45% on limestone cores from the Middle East reservoir. Yi et al. (2012) attributed the improved oil recovery to wettability alteration on cores that were flooded.

During production from the Ekofisk field in the North sea, it was discovered that there was more recovery when sea water (SW) was injected as a pressure maintenance fluid during secondary flooding than when water with composition like initial formation water was injected (Strand et al., 2008). It was attributed to SW being able to alter wettability of the chalk Ekofisk to be more water wet which instantly initiated spontaneous imbibition from fractures into matrix blocks. Recent studies by Yi et al. (2012), Tweheyo et al. (2006), Yousef et al. (2010) and Zhang et al. (2006a), support this idea of wettability alteration by SW. The imbibing brine displaces more oil in the matrix and results in an improved recovery. In the case of the Ekofisk field, when the composition of the produced water was measured, it was found out that effluent composition was different from that which was injected and formation water. The produced water had different concentration ofpotential determining ion (PDI)s, (Mg^{2+}, Ca^{2+}, SO_4^{2-}), than that in injected sea water. This was in line with chromatography wettability test by Strand et al. (2008), Zhang et al. (2006a) and Zhang et al. (2007), which indicated that these divalent ions were responsible for the wettability alteration. Yousef et al. (2010) also noted that diluted version of synthetic seawater (SSW) were able to alter wettability in carbonates and even do it more effectively than synthetic seawater. Yousef et al. (2012(b)) conducted a field experiment using both synthetic seawater (SSW) and diluted versions of SSW and made similar observations on $[SO_4^{2-}]$ and $[Ca^{2+}]$ and higher than conventional recoveries. From here on, '[a]', means ionic concentration of component a. Selective dilution of SSW with respect to sodium chloride (NaCl) which significantly changes the ionic strength of SSW was suggested by Yousef et al. (2012(b)) to also enhance the wettability alteration processes in carbonate reservoirs.

Several explanations and theories have been put forward to explain the effects of low salinity and composition of injection water on oil recovery. However, the majority of the research has been done on sandstone core samples and less on carbonate reservoirs. Yi et al. (2012) summaries the five generally accepted theories behind low salinity effects in both reservoir types and these include: multi-ion exchange (MIE), rock dissolution, fines migration, interfacial tension (IFT) reduction, and double layer expansion effects. Yi et al. (2012) also summaries that lack of clay minerals and strong bonding energy between the polar components in oil and the carbonate rock surface have over the years limited understanding the main mechanism(s) behind low salinity effects in carbonates. However, over the last 15 years, a lot of research has been done to try to explain water composition effects in carbonates both by salinity reduction and composition alteration of the injection/imbibing brines.

In this work, the aim is to understand how the ionic composition of imbibing brine dictates the wettability change when imbibing in secondary and tertiary modes by the spontaneous imbibition process in crude oil-containing limestone core plugs at a high temperature of 96°. The result is visualised by the improved oil recovery between change of brines. Contact angle measurements in different test brines are made to supplement observed oil recoveries. The key objectives of the study are;

1. To optimise the composition of synthetic seawater with regards to potential determining ions with the main focus on the magnesium, (Mg^{2+}) and sulfate (SO_4^{2-}) ions to improve oil recovery
2. To study the impact of selective dilution of synthetic seawater with respect to sodium chloride (NaCl) content on the wettability alteration process in limestone cores
3. To improve the laboratory experimental set up for spontaneous imbibition experiments designed for high temperatures and pressures less than 2 bars. The new set up is to be

used in objectives 1, 2 and 4

4. To study the best aging process for restoring a representative initial oil-wetting state suitable for wettability studies
5. To set up a new experimental rig for the suggested aging style, (dynamic aging)

In the rest of the document, the *Abstract* gives an overview of the work done and summarise key observations and conclusions. The *Background* section gives an account of summarised literature review. Detailed description of the carbonate reservoirs and mechanisms behind low salinity in both carbonates and sandstone reservoirs is provided. The chapter also summaries previous work that has been done in the area of wettability restoration in line with core aging. The *Theory* chapter gives a detailed description of thin water films and the role they play in the multi-ion exchange (MIE) and double-layer expansion (DLE) mechanisms. The two commonly suggested mechanisms responsible for wettability alteration. In the *Materials and Methods section* experimental set ups and procedures followed to achieve the objectives are reported. The chapter includes also a brief description of the core material and fluids. Experimental results and detailed discussion on those results is provided in the *Results and Discussion* section whereas the *Conclusion and Recommendations* section outlines the key findings that have been found in this study and suggestions for further research. Any other supporting information is found in Appendices A, B, C and D.

Chapter 2

Background

Over years, water has been the most and widely used fluid for pressure maintenance and volumetric sweep recoveries. Limited focus has been put to understand its effects on reservoir properties that control flow and ultimate oil recovery (Yi et al., 2012). Recent studies on injection brines, into oil-containing cores, especially synthetic seawater and its diluted versions, a process commonly called low salinity enhanced oil recovery (LS-EOR), have stimulated a series of studies in this area (Yousef et al., 2010). Research has been and still being done to understand mechanisms behind observed low salinity oil recoveries when brines are injected or imbibed in either secondary or tertiary mode (Yi et al., 2012; Yousef et al., 2010).

Wettability modification as a result of surface charge alteration at the carbonate rock-brine interface is the most supported and prominent mechanism behind the effect of low salinity flooding and imbibition (Yi et al., 2012; Tweheyo et al., 2006; Yousef et al., 2010; Zhang et al., 2006a; Zhang et al., 2007; Yousef et al., 2012(b); Yousef et al., 2012(a); Zhang et al., 2006b). A process commonly termed as multi-ion exchange (MIE) mechanism. Nazari et al. (2020) note that the MIE mechanism happens as a result of complex formation between cationic potential determining ion (PDI)s and the organic groups adsorbed to the rock surface as was envisioned by Zhang et al. (2006a) and Zhang et al. (2007). Electric double layer expansion at the water-wet sites is also a prominent mechanisms that can be used to explain improved oil recovery during LS-EOR (Nazari et al., 2020; Firoozabadi et al., 2015; Hirasaki et al., 1991). Rock dissolution and subsequent fines migration due to concentration gradient between formation water (FW) and injected/imbibing brine, and inter-facial tension reduction due to saponification at crude oil-brine interface electric double layer expansion have also been suggested as probable mechanisms Sheng (2010), Yi et al. (2012), Yousef et al. (2010) and Nasralla et al. (2014).

In this thesis, focus is mainly put on the multi-ion exchange (MIE) and the electric double layer (EDL) expansion mechanisms. Processes that are initiated at water wet sites in thin water films. However, to understand mechanisms of wettability alteration at play during LS-EOR in carbonates, it is vital to first understand carbonate reservoir types and their striking contrasts in morphology and environment of formation, definition of wettability, and the initial wetting state that we are trying to modify and factors that control it. Section 2.4 will look at the wettability restoration processes in outcrop cores and summarise work that has been done in regard to restoring the initial oil wet state.

2.1 Carbonate reservoir types

Carbonates reservoirs originate from calcareous skeletons of organisms that generally lived in shallow marine waters. When these organisms died, their skeletons and shells formed bioclastic sediments within the same basin (Darling, 2005). Over geologic time these fragments were cemented by calcium carbonate precipitating from pore water forming. In addition to other diagenetic processes, this process formed carbonate reservoirs we know today (Lucia, 2007).

Carbonate reservoirs are broadly classified into three categories. These are limestone, chalk, and dolomite. This broad classification is based on the skeletal material, environment of formation, mineralogical composition and intrinsic structures unique to each type. All the three rocks are of made of calcium carbonate, $CaCO_3$, as the main mineral. Limestone forms in shallow waters and consists of only two minerals, calcite and aragonite. Its a massive rock and of low porosity. Due to diagentic processes such as compaction, leaching and dolomitization, limestone can have porosity and permeability conducive for fluid storage and flow. Chalk is a friable, fine-textured limestone composed dominantly of coccolith calcite and forms in relatively deeper waters than other carbonates (Friedman, 1996). Dolomite is a limestone in which some of the calcium in the mineral lattice was substituted by magnesium,, a process known as dolomitization. The core material used in this study is representative of a limestone off-shore field in Brazil. The reservoir is a bivalve limestone but the whole core was drilled from an outcrop in Angola.

Majority of the studies in the field of low salinity flooding in carbonates have been done on either chalk reservoir cores or chalk outcrop cores. Less work has been done on limestone and far less on dolomite reservoirs. In this experimental study about limestone cores, a generic summary about carbonate reservoirs is first given at the start of most sections, and mostly contains work studies on chalk cores. This format has created a base upon which a discussion about limestone cores under study is anchored.

2.2 Wettability

In petroleum reservoirs, wettability is a rock-fluid property characteristic of the reservoir. In a porous medium containing two or more immiscible fluids, wettability is a measure of the preferential tendency of one of the fluids to spread and wet the rock surface (Tiab and Donaldson, 2015). It is a property that depends on rock-fluid specific surface energies (inter-facial tension). In a rock-brine-oil system, if the rock-brine interface has lower specific energy δ_{sw} than the rock-oil interface energy δ_{so}, then brine (FW) will wet the rock. If the reverse is true then oil wets the rock. It is not possible to practically measure rock-fluid specific energies in the reservoir. A relative measure by the inter-facial tension at the crude oil-brine interface δ_{ow} and the contact angle θ are fortunately possible, and the two parameters are correlated through Young's Equation (2.2). If the contact angle θ is greater than 115, the rock is oil wet, less than 75°it is considered water wet, and mixed wet between 75°and 115°(Anderson et al., 1986).

$$\tau = \delta_{so} - \delta_{sw} = \delta_{ow} cos\theta \tag{2.1}$$

- Where τ is the adhesion force (effective inter-facial tension), δ_{so} is specific surface energy at rock-oil interface, δ_{sw} specific surface energy at rock-brine interface, δ_{ow} inter-facial tension at crude oil-brine interface and θ contact angle measured through the denser fluid.

$$cos\theta_{ow} = \frac{\delta_{so} - \delta_{sw}}{\delta_{ow}} \tag{2.2}$$

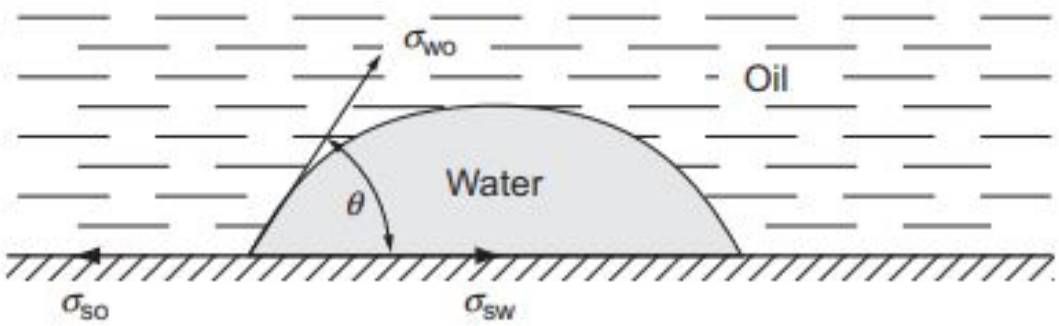

Figure 2.1: Surface energy at rock-fluid interfaces are responsible for wettability state in a rock, Tiab and Donaldson (2015)

If a rock surface is completely water wet, water will occupy all smaller pores and will also form a continuous film (thin water film) in larger pores. If the rock surface is fully oil wet, oil occupies smaller pores and the thin water film is absent in larger pores. However either cases are in-existent in actual reservoirs, whether sandstone or carbonate. Carbonate reservoirs are usually preferentially oil wet or mixed wet. Mixed wettability can also be defined as a wetting state where micro pores in the rock are occupied by water and are water wet, but larger pores are oil wet and a continuous film of oil exists throughout in the larger pores (Tiab and Donaldson, 2015). The wettability state in a reservoir has a dominant influence on fluid flow and electrical properties of the water-hydrocarbon-rock system. It controls the capillary pressure and relative permeability behavior and thus the rate of hydrocarbon displacement and ultimate recovery (Tiab and Donaldson, 2015).

2.3 Initial wetting State in carbonates

Generally clean carbonate cores or carbonate reservoirs before oil migration are 100% water wet (Tiab and Donaldson, 2015). However, when oil migrates into a porous carbonate the wetting state is altered. Carboxylic molecules in oil make the crude oil-brine interface negative due to their dissociation. At the rock-brine interface, the net surface charge is positive due to excess calcium ions (Ca^{2+}) present in formation water (Tweheyo et al., 2006; Zhang et al., 2006b; Zhang et al., 2006a). When there are no or few negative polar functional groups in oil, the repulsive forces between the rock and the crude oil-brine interface are strong and this results in positive disjoining pressure and thick water films (Firoozabadi et al., 2015; Hirasaki et al., 1991) and (Tweheyo et al., 2006). The film is then stable and the rock is more water wet.

Unfortunately, the net negative potential at the oil water interface due to dissociation of carboxylic groups in oil usually creates a strong force of attraction between crude oil-brine and rock-brine interfaces bounding the thin water film. In the end, the thickness of the thin water film shrinks until it raptures which allows the carboxylyic molecules to strongly and almost irreversibly adsorb on the pore walls. Thomas et al. (1993) showed that fatty acids in oil permanently adsorb on the carbonate surface after the rapture of thin water film. These two types of hydrocarbon molecules make the carbonate rock oil wet. Over a geologic time,

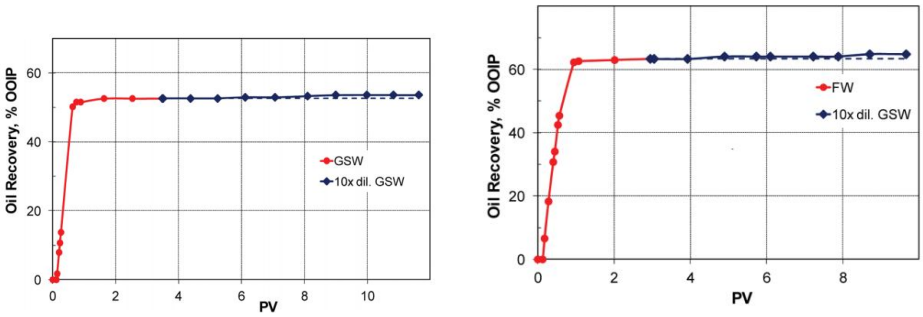

(a) SI using FW (red) when Low AN= 0.08 mgKOH/g, crude oil is used in aging

(b) SI using FW (red) when high AN= 0.34mgKOH/g, crude oil is used in aging

Figure 2.2: Impact of AN on the initial wetting properties. A recovery of 63% with high AN compared with 50% with low AN (Austad et al., 2012)

carbonate reservoirs end up being mixed wet and more strongly oil wet if rich in carboxylic groups. Thus the composition of the oil, in terms of the acid number (AN) and base number (BN), dictates and sets the pace for the initial wettability state in carbonates (Shariatpanahi et al., 2010; Austad et al., 2012). The acid number defines the amount of the carboxylic functional group in the oil phase while the base number defines the amount of the amide or amine functional group in the same phase. Austad et al. (2012) working on limestone reservoir cores, observed that the AN of crude used in core aging dictated the imbibition rate and ultimate oil recovery for low salinity experiments in carbonates. High AN made the substrate more oil wet. Observations made in such a case would be substantial when a low salinity brine is introduced as displayed in Figure 2.2. Other physical and chemical factors, as discussed below, dictate the extent of carboxylic adsorption.

2.3.1 Effect of temperature

Generally, high temperatures during core aging result in poor (low) initial water wetness whether the rock has anhydrite or not as shown in Figure 2.3 with formation brine enriched and depleted in sulfate . However, Thomas et al. (1993) showed that long and polymeric structures of the carboxylic and fatty acid molecules in crude oil are unstable at high temperatures. The two hydrocarbons are affected in the same way like polymers during polymer flooding. Thus high temperatures may minimise the carboxylic and fatty acid adsorption. The acid number of crude is also dependant on temperature (Zhang et al., 2005). High reservoir temperatures results in decarboxylation of crude over geologic time where the carboxylic end is replaced by hydrogen with carbon-dioxide as the second product. The reaction is catalysed by the substrate itself, calcium carbonate (Zhang et al., 2005). This reaction reduces the carboxylic and fatty acid groups that would otherwise have adsorbed on the pore walls.

Favourable high temperatures that are below the decarboxylation window catalyse hydrocarbon adsorption at the rock-fluid surface in carbonates and provide the necessary energy, that would otherwise be absent at subsurface conditions, to initiate wettability change (Tweheyo et al., 2006). Shariatpanahi et al. (2010) also observed high temperatures below 100°C favour anhydrite dissolution which avails sulfate ions, SO_4^{2-}, that can adsorb at and make pore surfaces more water wet. Unfortunately, due to high concentration of calcium ions, Ca^{2+}, in FW, this dissolution is hard to occur. Using a software, Austad et al. (2012) observed that temperatures above 110°C in limestone reservoirs are unfavourable for anhydrite dissolution in formation water. The test was conducted using FW of different salinities, Figure 2.4a. Such

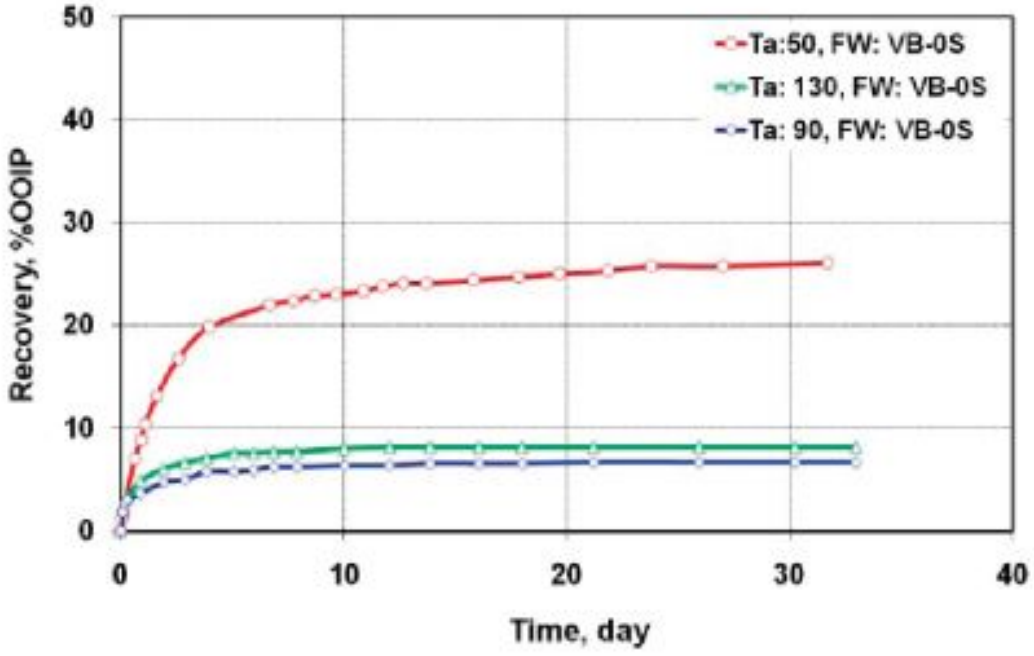

Figure 2.3: Effect of aging temperature on SI for cores with dissolvable anhydrite which loosely indicates that high temperatures cause low water wetness (Shariatpanahi et al., 2011)

temperatures therefore only favour hydrocarbon adsorption.

2.3.2 Effect of initial composition of formation water

Carbonates have formation water highly saturated with calcium ions, Ca^{2+}. This makes dissolution of other similar ions, such as CO_3^{2-} and SO_4^{2-} that are potential determining to the carbonate surface and can define initial wetting state, difficult (Shariatpanahi et al., 2010). However, the content of sodium chloride, (NaCl), in formation water in a carbonate reservoir that has anhydrite has an effect on the initial wetting state. Shariatpanahi et al. (2011) found out that cores with formation water rich in NaCl had a more water wetting state than those with lower NaCl content. This was explained by the substitution of adsorbed SO_4^{2-} in the stern layer of the double layer system by the chloride ions, Cl^-. The Cl^- increase the availability of aqueous SO_4^{2-} ions which are active in improving the wetting state. This therefore implies that presence of dissolvable anhdrite will also have a strong effect on the initial wetting state, for the anhydrite will act as an in-situ source of the SO_4^{2-} ions (Yi et al., 2012) and (Shariatpanahi et al., 2010). However, the SO_4^{2-} ions have to be in the aqueous state for them to have an effect on wettability (Shariatpanahi et al., 2011), and the reservoir temperature high enough for both anhydrite dissolution and SO_4^{2-} adsorption. Shariatpanahi et al. (2011) and reference to Figure 2.5 showed that favourable temperatures need to be less than 50°C. Above this temperature anhydrite dissolution in FW decreases.

Shariatpanahi et al. (2010) showed that anhdrite in carbonate reservoirs dissolves according to Equation (2.3) with equilibrium shifting to the right as temperatures increase. They also conclude that even though $CaSO_4(s)$ precipitation occurs at temperatures above 100°C, still adsorption of SO_4^{2-} together with Ca^{2+} and Mg^{2+}, if in-situ, can occur and in the end make

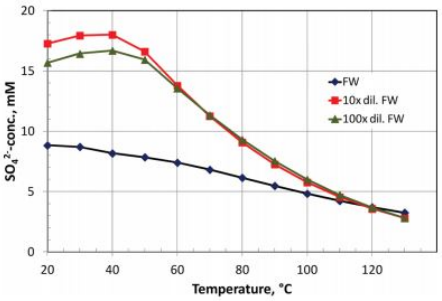

(a) Effect of temperature on anhdrite dissolution in limestone reservoirs (Austad et al., 2012)

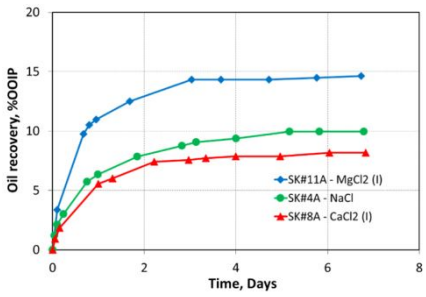

(b) The impact the initial $[Ca^{2+}]$ and $[Mg^{2+}]$ have on the initial wetting state in carbonate reservoirs (S. Shariatpanahi et al., 2016)

Figure 2.4: Left: Temperature and $CaSO_4(s)$ dissolution relationship. Right: The impact of divalent cations in FW on the initail wetting state in carbonate cores

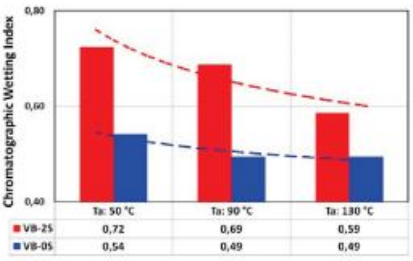

(a) Water wet fraction (Wetting Index) of the cores containing FW without sulfate, VB-0S, and with sulfate, VB-17S. The values are at different temperatures.

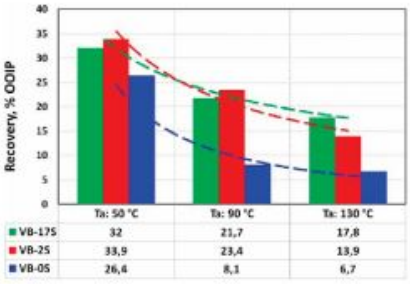

(b) Oil recovery by SI from the cores with VB-OS and VB-17S as FW. The core were imbibed with VB-OS in the secondary mode.

Figure 2.5: Wettability state and oil recovery by SI with core having different FW compositions and aged at different temperatures (50,90 and 130C, Shariatpanahi et al. (2011)

the initial wetting state more water wet.

$$CaSO_4(s) \leftrightarrow Ca^{2+} + SO_4^{2-} \Longleftrightarrow [CaSO_4(s)...(SO_4^{2-})] \tag{2.3}$$

The presence and amount of Mg^{2+} and Ca^{2+} ions in the initial FW also define the degree of the initial water-wetness in carbonate reservoirs. S. Shariatpanahi et al. (2016) conducted experiments at room temperature by isolating the Ca^{2+} and Mg^{2+} ions in the initial FW and then imbibing the test core with Valhall FW depleted in either of the two ions. With reference to Figure 2.4b, high $[Ca^{2+}]$ in FW makes a chalk pore surface less water wet while $[Mg^{2+}]$ makes it more water wet. The NaCl content is considered inert to a chalk surface and therefore was used as a base case. The R-COO-Ca bond is stronger than the R-COO-Mg bond by a factor of 10. S. Shariatpanahi et al. (2016) concluded that the organo-metallic bond could be the reason why Mg^{2+} makes a chalk surface more water wet than Ca^{2+}

2.3.3 Effect of pH

The pH of formation water determines the potential at the substrate (Firoozabadi et al., 2015). Gupta and Mohanty (2011) observed that as the pH increases, the calcite surface charge

changes from positive to negative after crossing the point of zero charge. For limestone, this point is around a value of 9.2. Strand et al. (2008) concluded that the optimal pH range for the carbonate rock to exhibit good equilibrium with the fluid system is 7-8. That implies around neutral pH. This pH range favours the dissociation of both basic and acidic components at the crude oil-brine interface (Tweheyo et al., 2006).The basic components are easily neutralised whereas the excess carboxylic group, ($R-COO^{-}$,) molecules are attracted to the Ca^{2+} at the rock surface (Tweheyo et al., 2006). This alters the wettability and makes the rock more oil wet. The same process would occur if the oil has some soaps in it. Therefore both the acidic and basic conditions make the carbonate rock surface more oil wet or mixed wet.

2.3.4 Pore wall surface area

The total surface area of the internal pore walls also have an effect on the degree of water wetness (Strand et al., 2008). Reservoirs with large pore surface areas, i.e highly porous and consisting of small grains, are usually more oil wet than those with with larger pores. This explains why biogenic chalks that are made of cocoolith organic matter, which are smaller in size than the fragmented calcite crystals in limestone are usually more oil wet than limestone or dolomite reservoirs. The experimental analysis on the effective pore surface area by Shariatpanahi et al. (2010) found outcrop chalk from Denmark having an area of $1.7 m^2/g$ whereas actual limestone reservoir core having an area of $0.29 m^2/g$. In their case, this would imply that the chalk surface area is ≈6 times larger than that of limestone. The large surface area provides a good platform for surface reactions. The adsorption of the carboxylic groups. In the proceeding discussion, Section 2.5, it will be found out that the area difference also explains why chalks are more reactive to low salinity EOR fluid.

In conclusion, the initial wettability state in carbonate reservoirs is mainly controlled by the oil composition (AN), temperature and presence of anhydrite precipitate. The rest of the factors are enhanced by the extremes of these three factors. Therefore, if we can play around on these parameters then we can be able to alter the wettability in carbonates and build further understanding about the MIE and EDL hypothesises.

2.4 Core Aging: Restoration of initial wettability

This section is about comparing the efficiency of two core aging processes that are commonly used in laboratory core studies. Static aging and dynamic aging. Either of the two methods is opted for in restoring the initial oil wetting state in either reservoir cores or outcrop cores that are reservoir analogues. The wettability state in core plugs determines microscopic fluid distribution in the pore space, and affects fluid flow, recovery rates and ultimate oil recovery (Fernø et al., 2010; Tiab and Donaldson, 2015; Graue et al., 1999). The discussion in this section is based on the work that was done by Fernø et al. (2010), Graue et al. (1999) and Standnes and T. Austad (2000).

2.4.1 Wettability in outcrop cores

In laboratory experiments on wettability, outcrop rock core plugs are commonly used instead of actual reservoir cores. The costly nature of the coring program either during drilling or logging, and the logistics involved thereafter limit the accessibility of reservoir cores. Therefore, outcrop cores are usually resorted to as the quickest and and cheapest option. In order to do a good petrophysical analysis, both during routine and special core analysis, outcrop cores used

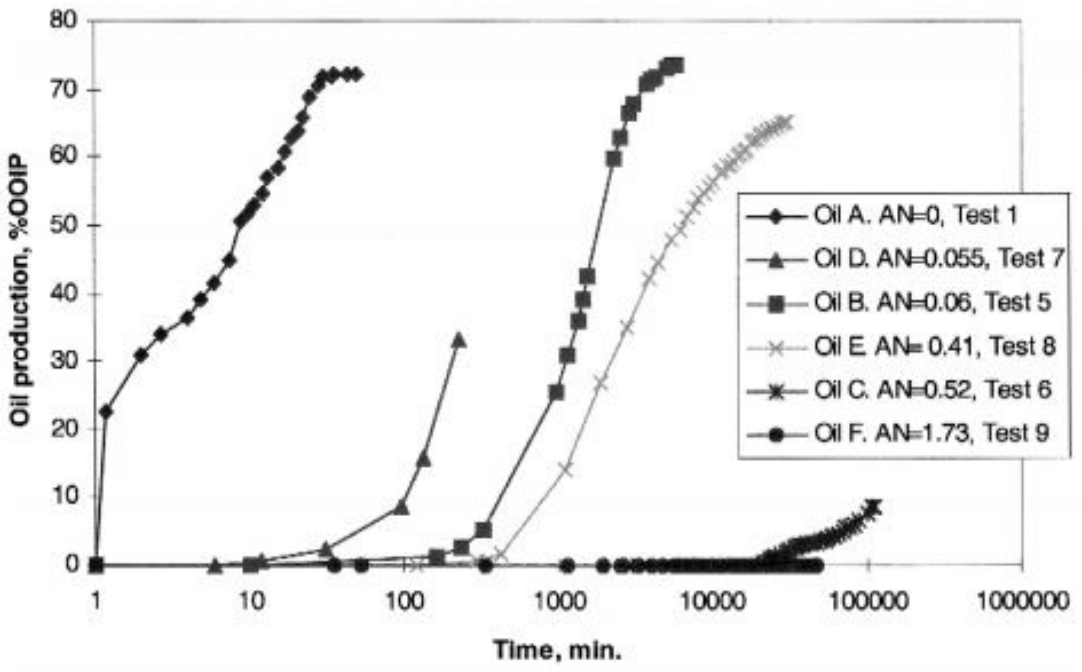

Figure 2.6: Any Crude oil has a carboxylic group content that can make a mineral surface oil-wet. SI results at 40°C by Standnes and T. Austad (2000). using oil of diffrent AN

in the process need to be good analogues to the reservoir rock under study.

The wettability of cores used in laboratory experiments need to be representative enough of existing wettability state in the oil reservoir under study. Even when actual reservoir rock plugs are used, the process of coring, core retrieval, transportation and storage, and cleaning and drying alter the wettability preexisting in them at reservoir conditions (Fernø et al., 2010). Carbonate reservoir rocks are mixed wet and lean more to oil wetness (Standnes and T. Austad, 2000), but by the time cores are cut into plugs for use, the pristine wettability state no longer exits. Standnes and T. Austad (2000) have shown, through spontaneous imbibition (SI) experiment, that any crude oil has the ability to make a mineral surface oil-wet. Outcrop crops, close representative of the actual reservoir rock, are commonly drilled from a rock outcropping at the surface. This implies that the rock is exposed to atmospheric condition and if porous , then its pores are occupied by water and air. Therefore, the original wetting state in the case of outcrop carbonate cores is completely water-wetting. To make these easily-available outcrop cores reservoir analogues to study fluid flow properties that include wettability, needs to be changed to mixed or oil-wet in carbonate core plugs. This process of wettability restoration is commonly done during core aging.

2.4.2 Core aging styles - Static vs Dynamic

Initial wettability state in core plugs controls initial fluid distribution in them. To restore a reservoir-representative wettability, core plugs are normally aged by contacting them with crude oil at elevated temperature for a long period normally in weeks or months. There are two kind of core aging and include static and dynamic. During static aging the core plugs are submerged in crude oil in an aging cells closed and placed in an oven set at a target aging temperature. Under dynamic aging, core plugs are placed in a high-temperature, high-pressure

hassler core holder, under confining pressure and flooded with fresh crude oil at a constant rate over a definite time. During aging, surface active components in crude oil react or get attached to the rock pore walls.

Carboxylic groups in Asphaltenes and resins, and long-chain carboxylic acids are the main active components involved during initial wettability restoration (Thomas et al., 1993) and (Standnes and T. Austad, 2000). Standnes and T. Austad (2000) confirmed through SI that mere asphaltene content does not necessarily define the activeness of crude oil in wettability modification. In Figure 2.6, crude oil D had the highest asphaltene content of 2.57 wt% and lowest AN of 0.055mgKOH/g among all the oils. Standnes and T. Austad (2000) reported that the degree of homogeneous distribution of these surface active components in crude oil in the core together with aging conditions of temperature and time, and the magnitude of initial water saturation determine the extent of their reactivity. Fernø et al. (2010) also reported that the thickness of the thin water film and amount of active polar components in crude oil are the controlling parameters for surface reactions. When the thin water film thickness is below its threshold, it easily ruptures and surface-active components in crude oil attach to the rock surface. In so doing the pore surface wettability becomes more oil wet. In addition, the overall bulk oil composition during the process plays a key role in restoring wettability. The bulk oil compositions dictates the solubility of asphaltenes and other polar components. If these surface active components are poorly dissolvable in crude, then that crude is good for wettability restoration (Fernø et al., 2010).

Traditionally, static aging is the most commonly used aging method. Fernø et al. (2010) high-

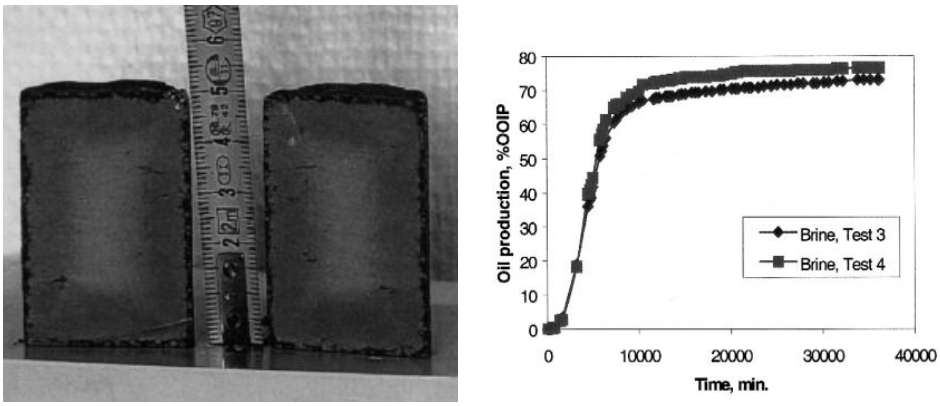

(a) Residual oil saturation in a cleaved core statically aged at 50°C. A thick black lining around the cleaves indicate that heavy crude oil molecules are more adsorbed to the outer surfaces than the inner sections of the core

(b) Low early oil production in the first ≈1000 minutes and a drastic rise thereafter from an unshaven statically aged core. An indicator of a slow initial SI process due to a strongly oil wet outer surfaces of the core

Figure 2.7: Inhomogeneity in wettability distribution in a core statically aged at 50°C (Standnes and T. Austad, 2000)

lighted challenges and inefficiencies associated with it. The keys ones being non-uniform wettability distribution, inefficiency during the aging process and poor or uncertain reproducibility of experimental results. Inhomogeneous wettability distribution effects had earlier been observed and confirmed by Standnes and T. Austad (2000) in a 100% crude oil-saturated cores by picture analysis of residual oil saturation distribution in a cleaved core that had been aged statically at 50°C shown in Figure 2.7(a). Low oil recovery by SI in the first 1000 minutes in Figure 2.7(b) supported the observation. Further analysis by shaving the same core to different

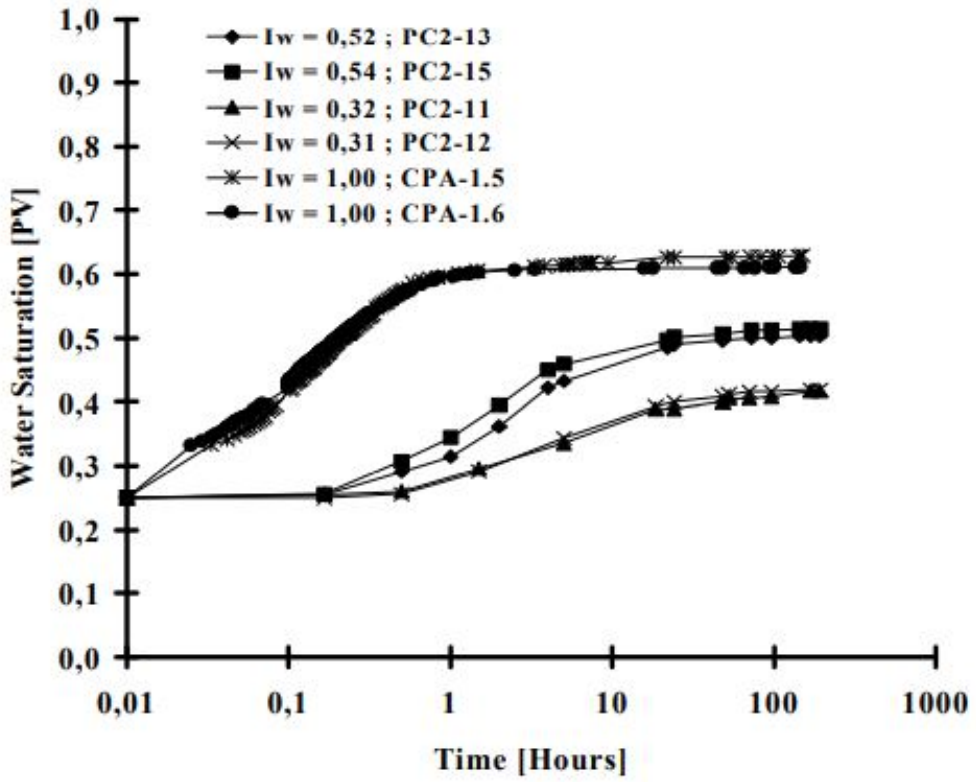

Figure 2.8: Effect of aging temperature during static aging . The lower pair of curves is for cores aged at 161°C, middle at 83°C and top is the reference fully water wet case. The proximity in pairs shows good reproducibility of results (Graue et al., 1999)

diameters showed that outer diameters were more oil wetting and had minimal SI whereas inner smaller diameters had strong SI with crude oil production from larger diameter oil-wet sections. Graue et al. (1999) was able to confirm poor wettability distribution in aged core plugs by conducting magnetic resonance imaging on them, to map the water saturation after spontaneous imbibition of water. Graue et al. (1999) observed a radial saturation with pores on and close to the surface having lower saturation than those at and close to the core axis.

During static aging, physical parameters especially temperature and duration of aging play a key part in wettability restoration. Basing on aging studies and experience, aging conducted at 60°C is less effective than one conducted at 90°C, no matter the nature of the rock. Long time aging results also turn out to be better than short time aging results. From the work that was conducted by Graue et al. (1999) on identical outcrop chalk cores from Denmark shown that core aged aged at 161°C had lower water saturations and Amott-Harvey water indices than those aged at 83°C as summarised on Figure 2.8. All aging was done for the same period of time, 90 days.

As already pointed out, during dynamic aging crude oil is forced through the core at the target aging temperature. Fernø et al. (2010) showed with cores aged at 90°C that to achieve better aging results with dynamic aging over static aging, aging needs to last more than 72 hours. Form the Amott-Harvey water indices, imbibition rates and ultimate oil recovery from spontaneous imbibition (SI), Fernø et al. (2010) was able to compare the two aging styles. Cores aged for less than 72 hours had smaller Amott-Harvey water index. While the indices were

lower in those aged dynamically than statically when aging was greater than 72 hours. By I_w index, cores aged statically failed to reach values lower than 0.25 within 24 days whereas that value and smaller were reached within 7 days with dynamic aging.

The difficulty to reach the lower I_w values indicates how challenging it is to restore the actual wetting stating through static aging. It also shows poor microscopic fluid distribution with in the core with more SI occurring along the core axis, for cylindrical cores, than from outer parts. In static aging, the composition of crude, in terms of acid number (AN), also plays a key role. Comparing cores that were aged in paraffinic-lamb oil with those in crude oil, recovery rates and longer induction time were observed in the crude oil category as shown in Figure 2.9a.

In conducting dynamic aging studies, Fernø et al. (2010) also observed that there exists an optimum injection rate that results in the best and lowest water-wetting state. At a constant aging time, Fernø et al. (2010) observed that the this rate is within in the interval from 1ml/hour to 5ml/hour. The optimum rate could be dependant on the nature of core material under study, in-terms of permeability and degree of heterogeneity. For Fernø et al. (2010)'s study, the optimal rate was 3ml/hour. The minimum in Figure 2.9b at this rate indicates the dependence of core dynamic aging efficiency on injection rate.

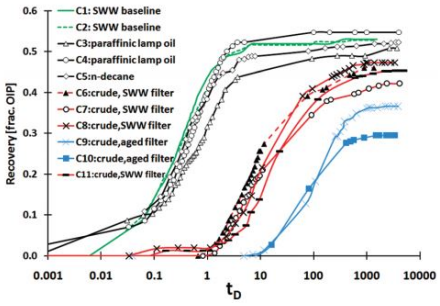

(a) Recovery factor vs dimensionless time. Comparing the effect of oil composition in terms of AN on static aging. A look at recovery rate, I_w and induction time. Aging was done at 90°C (Fernø et al., 2010)

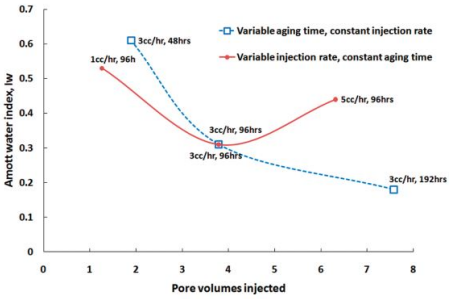

(b) Using the I_w to compare the effect of injection rate at constant aging time (96 days). The minimum exists at 3ml/hour. Aging was done at 90°C

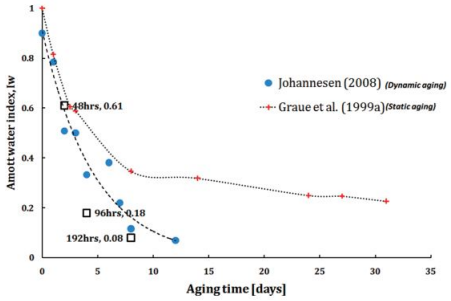

(c) Smaller I_w values for Dynamic aging in comparison with those for static aging show that it restores the initial wetting state better than static aging. Aging was done at 90°C.

Figure 2.9: Left: The I_w as a wettability quantitative measure. Right and bottom: Static vs dynamic aging Amott Harvey water indices, I_w for aging done at 90°C (Fernø et al., 2010)

Basing on this literature study therefore, the dynamic aging style was adopted and used in

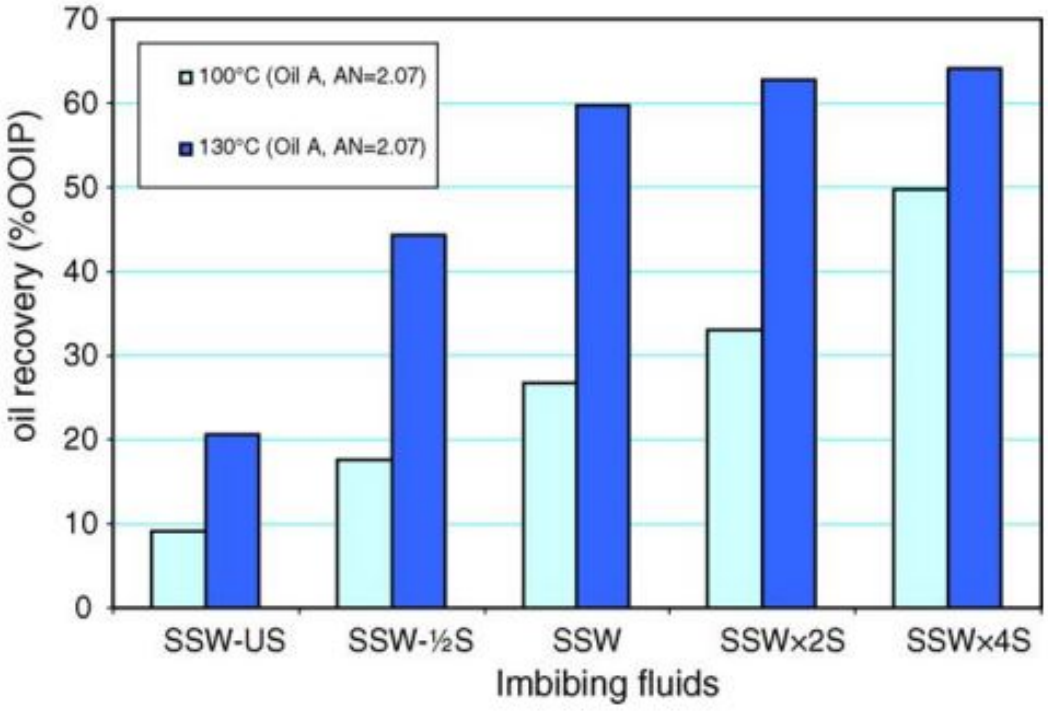

Figure 2.10: Recoveries using crude oil of AN=2.07mgKOH/g at 130°C and 100°C by SI in chalk cores. Depleting or enriching SSW with SO_4^{2-} ions has an effect on the ultimate oil recovery in carbonate cores. The sulfate effect is supplemented by temperature. Dark blue peaks at for light blue peaks (Zhang et al., 2006b)

the aging process of all Angola and Ainsa cores except core B8. The two aging styles have also been studied using two cores from Ainsa. Core B1 was aged dynamically while core B8 aged statically.

2.5 Wettability alteration

Generally the initial reservoir conditions stimulate the wetness of the carbonate reservoir to be mixed to oil wet. In addition to already discussed physical factors, Section 2.3, the wetting phase is controlled by surface reactions at the crude oil-water interface and the rock-water interface (Tweheyo et al., 2006). Carboxylic groups in crude oil, commonly quantified by the AN, dictate the degree of oil wetness as they adsorb on the rock surface. In order to have more production from such an oil wet state, commonly fractured, there is need to alter wettability to a more water wet. Crude oil recovery by spontaneous imbibition of brine then displaces more residual crude oil to production wells. Recent studies (Strand et al., 2008; Tweheyo et al., 2006; Zhang et al., 2006a; Zhang et al., 2007; Austad et al., 2015; Zhang et al., 2006b; Yousef et al., 2010) have shown that it is possible to alter the wettability state in and make carbonate outcrop and reservoirs cores more water wet through injection or spontaneous imbibition of synthetic seawater or its modified versions. In the paper series by Zhang et al. (2006a), Zhang et al. (2007) and Zhang et al. (2006b), they showed that sulfate ions (SO_4^{2-}), calcium ions (Ca^{2+}) and magnesium, ions (Mg^{2+}) at right physical and chemical conditions and appropriate relative compositions can symbiotically alter wettability in chalk cores. All the three divalent ions are prevalent in SW in substantial amounts that are coincidentally ideal for wettability

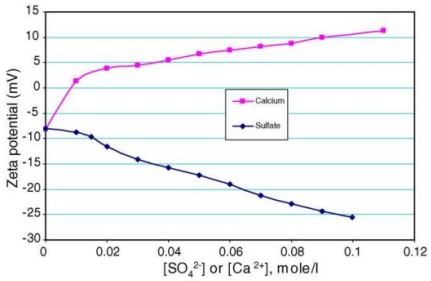

(a) Both SO_4^{2-} and Ca^{2+} are potential determining ions to a carbonate surface.

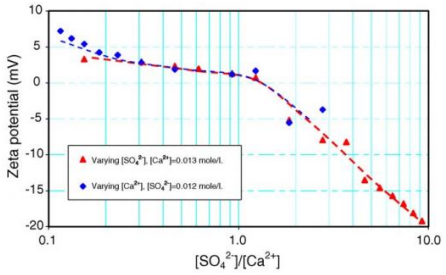

(b) Relative impact of $[SO_4^{2-}]$ and $[Ca^{2+}]$ to the carbonate-brine interface on the surface potential

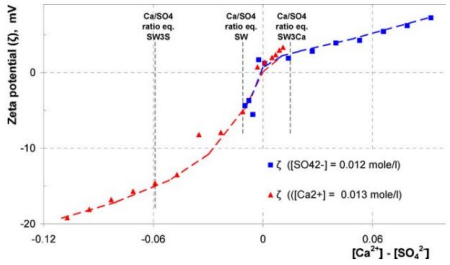

(c) The two-part zeta potential measurement by Strand et al. (2006)

Figure 2.11: Zeta potential measurements were made at room temperature. The increase in relative concentration of each ion makes its charge dominant at the carbonate surface which is directly correlated with zeta potential (Zhang et al., 2006b; Strand et al., 2006)

alteration. In north-sea sea water, $[SO_4^{2-}] = 2[Ca^{2+}] = 2[Mg^{2+}]$. Other multivalent ions, such as Ba^{2+}, also exit in sea water in trace amounts but will not be discussed in this work. Strand et al. (2008) also showed that SO_4^{2-}, Mg^{2+}, and Ca^{2+} ions can alter wettability in limestone cores from the Middle East in almost the similar manner as in chalks by relatively increasing their concentrations.

In majority of the experiments (Yi et al., 2012; Tweheyo et al., 2006; Yousef et al., 2010), the observed improved oil recovery was correlated with surface reactions that altered the wetting state and boosted spontaneous imbibition, and far less to interfacial tension reduction at the water-oil interface. This confirmed that SO_4^{2-}, Ca^{2+} and Mg^{2+} are potential determining ion (PDI) to a carbonate surface, and the boosted spontaneous imbibition was due to capillary pressure being more positive. Zhang et al. (2006b) showed that normal sea water composition can still be altered to provide a more optimal composition for wettability alteration to a stronger water wet state that ultimately improves spontaneous imbibition (SI) as shown in Figure 2.10 with the SO_4^{2-} ion composition altered both above and below the concentration in SW. With more water imbibing the matrix blocks, more oil is contacted and recovered by gravity as the capillary pressure values in the porous regions contacted by sea water become more positive. Zhang et al. (2007), at the end of their paper series about wettability alteration in carbonates suggested a surface chemical mechanisms responsible for wettability alteration, as will be discussed in Section 2.5.4. It is however important to first understand the role played by each ion in the process and the conditions that optimally enhance its reactivity.

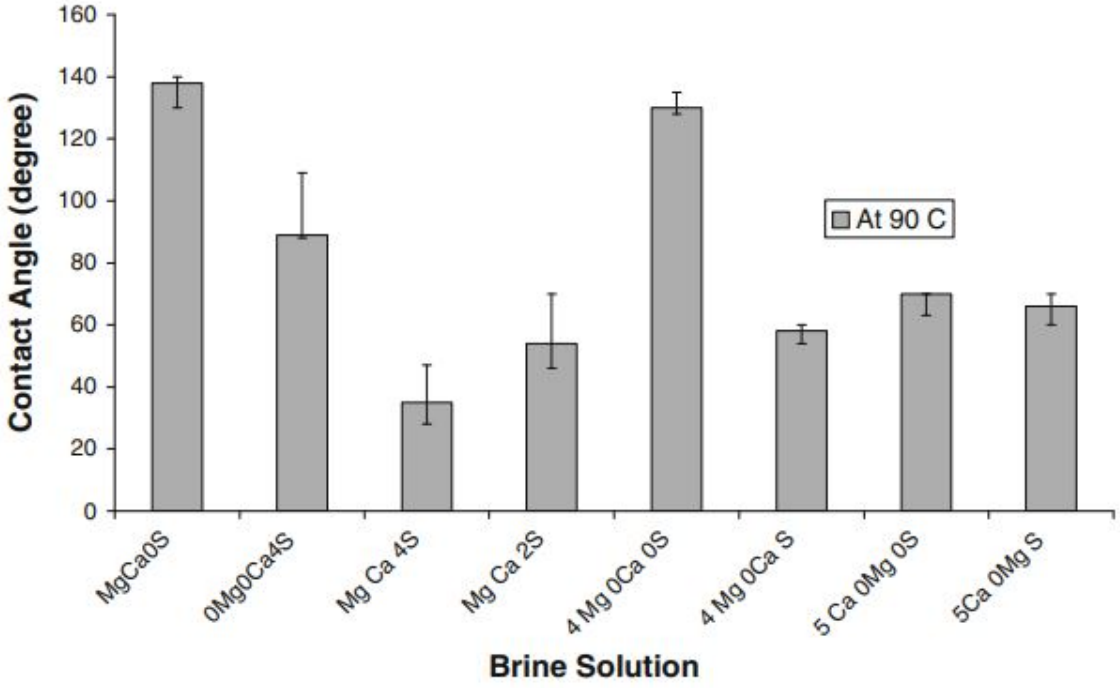

Figure 2.12: Effect of PDIs and their concentrations to wettability change at 90°C, and their inter-dependencies. (Gupta and Mohanty, 2011)

2.5.1 The sulfate ion, SO_4^{2-}

At nearly basic pH, (7-8), the sulfate ion is able to alter the **zeta potential** of a carbonate surface to negative (Zhang et al., 2006b; Nasralla et al., 2014). Using a NaCl solution, Zhang et al. (2006b) noticed that small increments of sulfate to the solution monotonically decreased the zeta potential of a chalk surface as shown in Figure 2.11(a). The same zeta potential trend was observed by Strand et al. (2006) in two parallel experiments. In one experiment they kept the $[Ca^{2+}] = 0.013$ mol/l, and in the second kept $[SO_4^{2-}] = 0.012$ mol/l. Both respective concentrations equal to those in SW. Discussing the SO_4^{2-} ion in wettability alteration process independent of either the Ca^{2+} or Mg^{2+} or both cations is practically impossible. At a pH = 8.4, Strand et al. (2006) observed that the relative concentration of Ca^{2+} and SO_4^{2-} dictates the charge at a chalk surface as seen in Figure 2.11c. However, Strand et al. (2006) argue that at zero potential, when $[SO_4^{2-}] = [Ca^{2+}]$, relative adsorption to chalk needs to be tested by using tiny amounts of the carbonate colloidal suspension so as as to have competition for places between the two ions. The zero potential does not necessarily imply that SO_4^{2-} and Ca^{2+} have the same affinity to a carbonate surface.

Contact angle measurements on calcite plates in NaCl solutions containing different SO_4^{2-} concentrations, indicate that the sulfate is able to improve the water wetting state (Gupta and Mohanty, 2011; Chandrasekhar, 2013). Gupta and Mohanty (2011) used polished-crude aged calcite plates and observed that at 90°C, the SO_4^{2-} was able to reduce the contact angle of an oil aged plate from bout ≈ 170°to about 80°as seen in the second peak in Figure 2.12 and better illustrated in Figure 2.13a. In presence of Ca^{2+} and Mg^{2+}, greater reductions in contact angle were observed as both $[SO_4^{2-}]$ and temperature increased, Figure 2.13a. They therefore concluded that even though SO_4^{2-} at elevated concentrations above that in SW is able to improve the water wetting state, it is more effective at both high temperature and in the presence

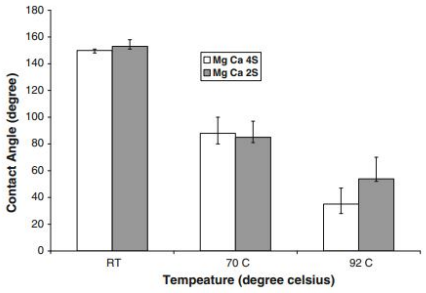

(a) $[SO_4^{2-}]$ and temperature effect on SO_4^{2-} activity during wettability change. Simultaneous increase in both improves the water wetting state visualised in contact angles (Gupta and Mohanty, 2011)

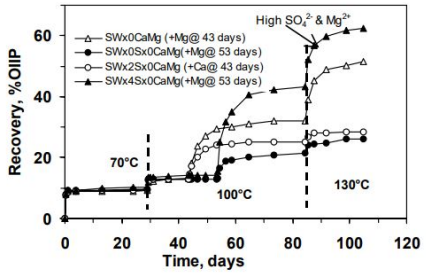

(b) A look at synergy between the three divalent ions on wettability alteration by comparing oil recoveries with main focus on the SO_4^{2-} ion. In the absence of Mg^{2+} and Mg^{2+}, the SO_4^{2-} ion does not alter wettability in carbonates (Tweheyo et al., 2006)

Figure 2.13: Dependence of a sulfate ion on temperature and presence of cationic PDIs in wettability alteration process

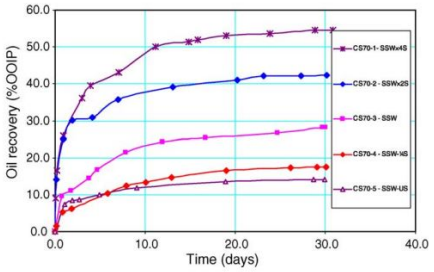

(a) Oil recoveries using cores with oil having AN=0.55mgKOH/g.

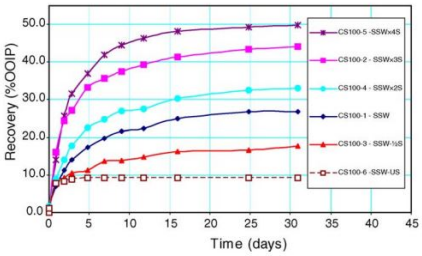

(b) Oil recoveries using cores with oil having AN=2.5mgKOH/g.

Figure 2.14: Comparison of the oil recoveries using core containing oil of different AN and imbibing brine having different $[SO_4^{2-}]$. Enriching imbibing brine with $[SO_4^{2-}]$ ions in the presence of cationic PDIs improves oil recoveries. An indicator of strong SI due to a better water wetting state initiated by SO_4^{2-} ions (Zhang et al., 2006b). Higher recoveries at 130°C than at 100°C also hints on the temperature dependence of SO_4^{2-} ions to initiate the wettability alteration process

of Ca^{2+} and Mg^{2+}.

Spontaneous imbibition experiments indicate that imbibing carbonate cores with brines of different $[SO_4^{2-}]$s is able to result in varying oil recoveries and recovery rates at different temperatures. The effectiveness of the sulfate in these experiments is more efficient in the presence of other PDIs (Zhang et al., 2006a; Zhang et al., 2007; Zhang et al., 2006b; Yu et al., 2008). The dependence of sulfate activity on other PDIs can be seen in Figure 2.13b as no improved oil recovery is seen when the imbibing brine has no Mg^{2+} or Ca^{2+} ions. Chandrasekhar (2013) say that it is only the Mg^{2+} ion that need to be available for the sulfate to alter wettability. This is contradicting and the negative results on the SO_4^{2-} with Ca^{2+} could be because the flooding experiment was only conducted at 100°C, during which anhydrite precipitate ($CaSO_4(s)$), precipitation might have come into play as was observed by Zhang et al. (2006a) and Yi et al. (2012).

Spontaneous imbibition experiments, Zhang et al. (2006b) tested the efficiency of SO_4^{2-} as

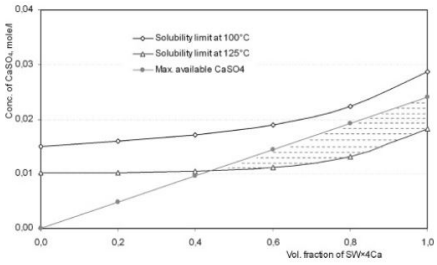

(a) $CaSO_4$(s) solubility at 100 °C and 125°C (Zhang et al., 2006a)

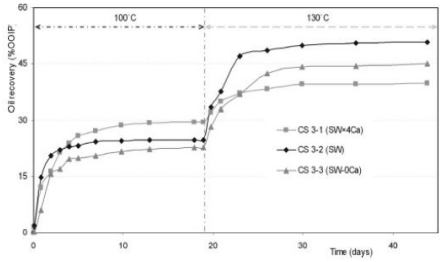

(b) The effect of $[Ca^{2+}]$ on oil recovery. At temeparatures below 100°C, increasing the $[Ca^{2+}]$ reuststs in increasing in recovery. At 130°C, the rise in $[Ca^{2+}$ has a negative impact on recovery due to] $CaSO_4$(s) precipitation (Zhang et al., 2006a)

Figure 2.15: Impact of $CaSO_4$(s) precipitation on SI and oil recovery in carbonate reservoirs and its dependence on temperature (Zhang et al., 2006a)

a PDI to a chalk surface in the presence of Ca^{2+} using synthetic seawater spiked or depleted in $[SO_4^{2-}]$. In these experiments, they kept $[Ca^{2+}]$ at 0.013mol/l, a concentration in the North-sea SW, and ran them at temperatures of 70°C, 100°C and 130°C. Based on the $[SO_4^{2-}]$ in the north-sea Ekofisk field sea water, the $[SO_4^{2-}]$ was altered by a factor of 0, 1, 2, 3 and 4. Zhang et al. (2006b) used two oils each having a unique AN, that were 2.07 and 0.55mgKOH/g. For identical cores containing the same oil, when they were imbibed at 70°C and 100°C using same brines, higher recoveries were attained from core sets having oil of lower AN than those with oil of high AN, Figure 2.14. The low recovery in the high AN oily core was attributed to the low water wetness caused by high volumes of adsorbed carboxylic groups and not to minimal SO_4^{2-} or PDIs activity in wettability alteration. The general trend of higher crude oil recoveries with increasing $[SO_4^{2-}]$ above that in SW in imbibing brine observed by Zhang et al. (2006b) at all test temperatures indicates the dependence of a SO_4^{2-} ion on its concentration in wettability alteration process in carbonate cores as shown in Figure 2.14. The highest recovery had quadruple $[SO_4^{2-}]$ in the imbibing brine. This was in line with what Yu et al. (2008) found on boundary-controlled outcrop chalk cores. Knowing that the solubility of $CaSO_4$(s) decreases with increasing temperature and ion concentration and theoretically reaches its limit at 125°C as seen in Figure 2.15, Zhang et al. (2006b) did not test the $[SO_4^{2-}]$ beyond that quadruple in SW.

when one oil with AN = 2.07mgKOH/g was used at 100°C and 130°C and using same imbibing brines with altered $[SO_4^{2-}]$, higher recovery and recovery rates were obtained at 130°C than at 100°C as seen in Figure 2.14. This confirmed that temperature influences the activity of SO_4^{2-} ions and they are more efficient at relatively high temperatures. Strand et al. (2006) through testing the efficiency of SO_4^{2-} at 110°C, also observed that increasing the SO_4^{2-} caused more recovery when SSW was flooded in the secondary mode. Though $CaSO_4$(s) precipitation needs to be taken into account at temperatures above 100°C as seen in Figure 2.15 (b). Zhang et al. (2006b) in addition observed that at relatively low temperatures, lower recovery could be compensated by raising the$[SO_4^{2-}]$ in the imbibing brine as shown in Figure 2.10 on all light green bars. It was also shown that when high imbibition temperatures are used then the $[SO_4^{2-}]$ in SSW is sufficient enough to obtain a recovery more less like that of synthetic seawater with 4x$[SO_4^{2-}]$ as depicted in Figure 2.10 middle and last bar pairs.

Wettability measurements by chromatographic tests by Zhang et al. (2006a) showed

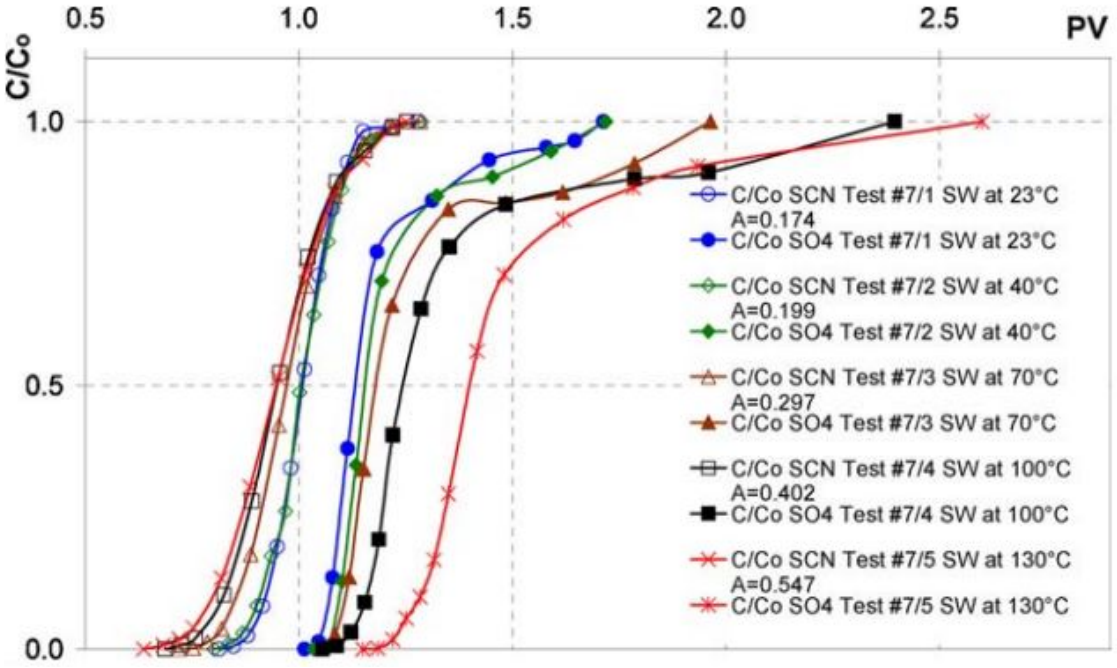

Figure 2.16: Increasing adsorption of SO_4^{2-} and its dispersion front to chalk with temperature (Strand et al., 2006)

that SO_4^{2-} in injected brine was able to able to adsorb A first step by the MIE mechanism for wettability alteration. In the experiment, chalk cores saturated with oil of AN 0.55mgKOH/g or 2.07KH/g were first flooded with FW containing no sulfate and the non-adsorbing tracer thiocyanate (SCN^-), and then flooded again in the tertiary mode with brine containing both SCN^- and SO_4^{2-}. The reference core was treated in the same manner but had n-heptane as the oil. N-heptane has no effect on carbonate rock wettability (Shariatpanahi et al., 2010). Ionic analysis on the effluent brine confirmed that the SO_4^{2-} in presence of Ca^{2+} is able to adsorb on the carbonate surface. The concentrations were normalised with concentrations from the reference core with the range between 0 and 1. 1 indicates completely water wet, 0.5 neutral and 0 completely oil wet. The value of 0.793, closer to 1, implying more water-wet, indicated that SO_4^{2-} adsorbs easily at the chalk surface, Zhang et al. (2006a).

Strand et al. (2006) conducted 19 tests on chalk surfaces to test the affinity of the SO_4^{2-} in presence of Ca^{2+} ions at 23, 70, 100 and 130°C. They conducted a chromatographic test by adjusting the $[Ca^{2+}]/[SO_4{}^{2-}]$ ratio between 0.135 and 1.6. Strand et al. (2006) observed that the area between SCN^- and SO_4^{2-} increased as both temperature and $[Ca^{2+}]/[SO_4{}^{2-}]$ increased as seen in Figure 2.16. Figure 2.17 compares the SO_4^{2-} adsorption areas at various $[Ca^{2+}]/[SO_4{}^{2-}]$ and temperatures and confirms the dependence of sulfate adsorption to temperature and other PDIs to a chalk surface At temperatures above 70°C, the SO_4^{2-} adsorbs more than at lower temperatures. This is due to increased activity of SO_4^{2-} in adsorption due to its desolvation as the hydrogen bonds between it and water molecules break (Strand et al., 2006). Increasing the the temperatures increases the dispersion front of the SO_4^{2-} ion and favours its adsorption . This phenomena too enhances the adsorption of other Ca^{2+} until a new equilibrium is made at the front as depicted in Figure 2.18.

Chromatographic wettability tests on **limestone core** have also shown that the SO_4^{2-} can

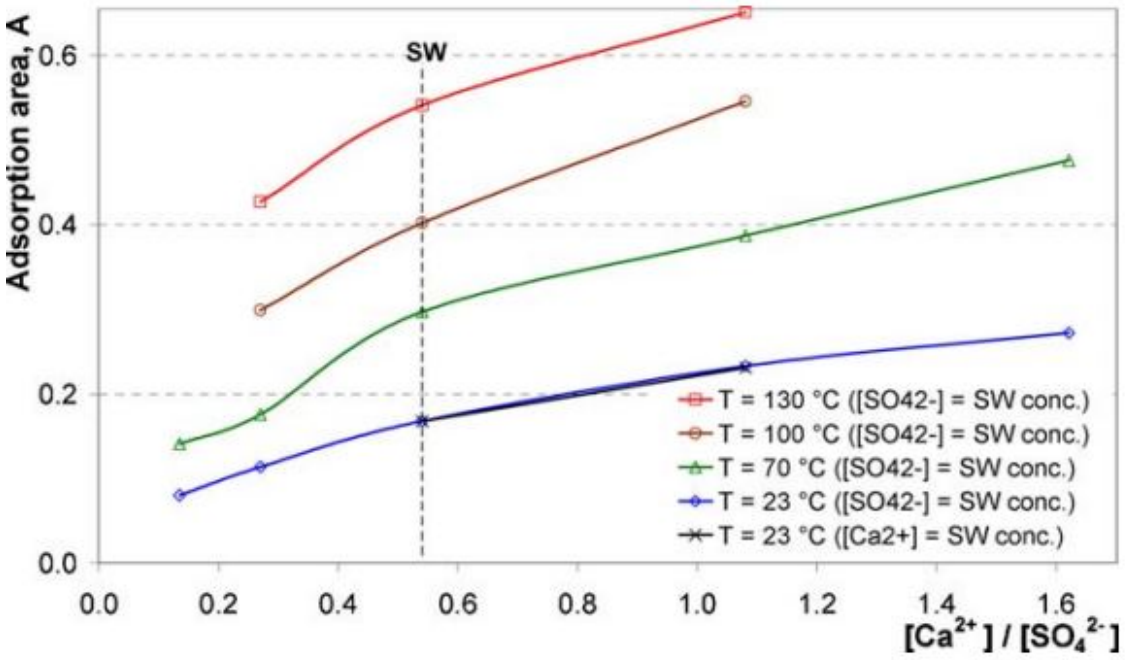

Figure 2.17: The adsorption area of SO_4^{2-} to chalk increases with temperature and and $[Ca^{2+}]$ at constant $[SO_4^{2-}]$ (Strand et al., 2006)

adsorb and make pore walls water well. Shariatpanahi et al. (2010) worked on actual limestone reservoir cores and conducted the chromatographic wettability test after mild cleaning of the plugs at room temperature. The area between the curves of SCN^- and SO_4^{2-} showed that the SO_4^{2-} can adsorb to a limestone surface in a similar way as in chalk. When the same experiment was repeated with SSW, an increase in the area of about 7% was observed. This indicated that more SO_4^{2-} from SSW adsorbed and made the plug more water-wet as seen in Figure 2.19. Adsorption of a SO_4^{2-} was also observed in another limestone cores from the middle east (Strand et al., 2008)

In **dolomite cores** , it has been shown that SW is not a smart EOR fluid. Through SI experiment with synthetic seawater, S. Shariatpanahi et al. (2016) observed low oil recovery rates and recoveries less than 8% at 70°C. The chromatography test at room temperature also showed minimal SO_4^{2-} adsorption as seen in Figure 2.20a. When the SI experiment was conducted with 10 times diluted SSW, the recovery rose to 25% . No extra recovery was obtained with 100 times diluted FW. This showed that the SO_4^{2-} ion and co-adsorption of Ca^{2+} in 10 times diluted SSW was still responsible for probable wettability alteration and extra 16% recovery, Figure 2.20b.

Therefore zeta potential measurements, wettability measurements by contact angle and chromatographic separation, and oil recovery from spontaneous imbibition all confirm that SO_4^{2-} is effective in altering wettability in limestone (Gupta and Mohanty, 2011; Strand et al., 2008; Chandrasekhar, 2013; Yi et al., 2012) and dolomite (Austad et al., 2015; S. Shariatpanahi et al., 2016), and it does so by altering the surface charge at the carbonate-Brine interface. Nasralla et al. (2014) explains how SO_4^{2-} makes the surface potential less positive.

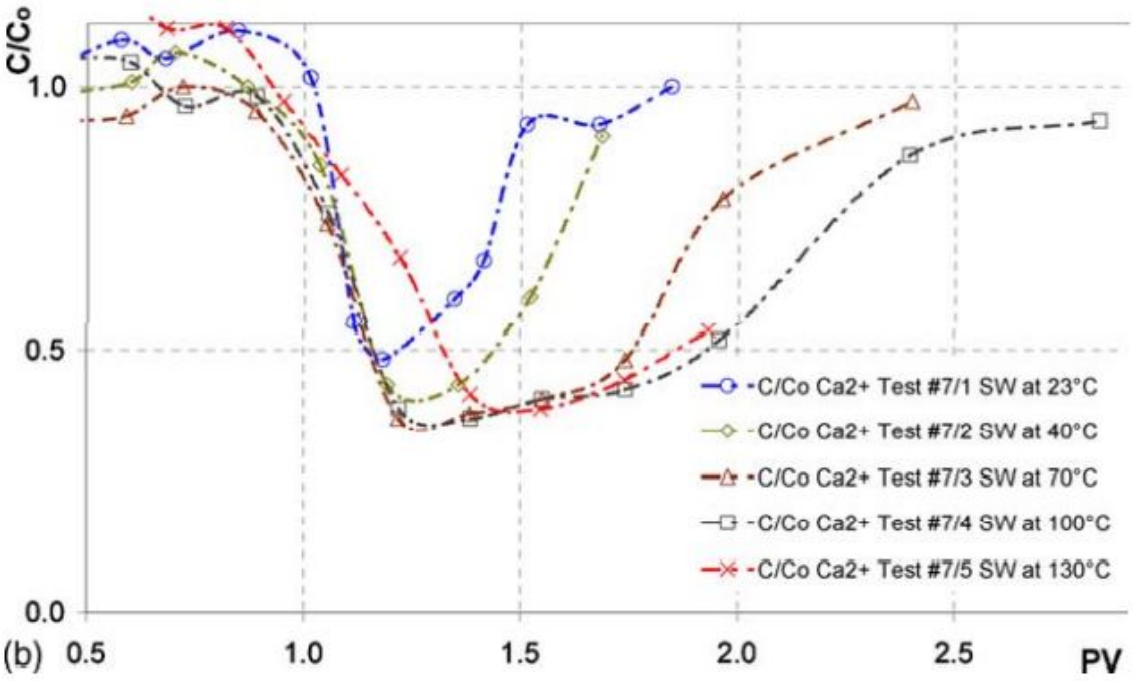

Figure 2.18: The dispersion front of SO_4^{2-} to chalk expands with temperature and enhance Ca^{2+} adsorption until new equilibrium is set (Strand et al., 2006)

2.5.2 The Calcium ion, Ca^{2+}

The calcium ion is a potential determining ion to a carbonate surface (Zhang et al., 2006b). Through **zeta potential measurements** on a chalk colloidal suspension, Zhang et al. (2006b) showed that a small increment in the $[Ca^{2+}]$ drastically and then linearly increases and makes the chalk surface potential more positive as seen in Figure 2.11 (a). With a fixed $[SO_4^{2-}]$ at 0.012mo/l in the NaCl solution, Zhang et al. (2006a) confirmed the relative adsorption of SO_4^{2-} and Ca^{2+} to a carbonate surface with the zero zeta potential when the concentrations are equal Figure 2.11b.

Contact measurements by Gupta and Mohanty (2011) showed that in absence of other PDIs, $[Ca^{2+}]$ raised by a factor of 5 above the concentration in SSW, was able to improve the water-wetness state from extremely oil-wet to mixed-wet as seen in Figure 2.12. The reactivity of Ca^{2+} ions seemed to be enhanced by presence of SO_4^{2-} ions at 90°C. Sodium chloride solutions without SO_4^{2-} but with equal amount of Mg^{2+} showed almost no activity in contact angle reduction at 90°C. Ionic substitution in a NaCl solution on limestone or calcite plates is expected to be absent at all temperatures (Strand et al., 2008). Therefore, Gupta and Mohanty (2011)'s work confirmed that wettability alteration by Mg^{2+} substitution for Ca^{2+} is limited in limestone and, if these ions are in equal concentrations, the activity of Ca^{2+} ions is limited in the absence of SO_4^{2-}.

Wettability measurement by the **chromatographic separation technique** indicate that the Ca^{2+} ion is able to adsorb on the carbonate surface and possibly act as a wettability modifier to carbonates at different temperatures chalk as seen in Figure 2.21a and for limestone in Figure 2.21b. Zhang et al. (2006a) showed that the Ca^{2+} ion in SSW is able to alter wettability if the process is initiated by the SO_4^{2-} ion. In this case, the SO_4^{2-} ions in the aqueous state adsorb at carbonate-brine interface and in so doing reduce the surface positive charge there.

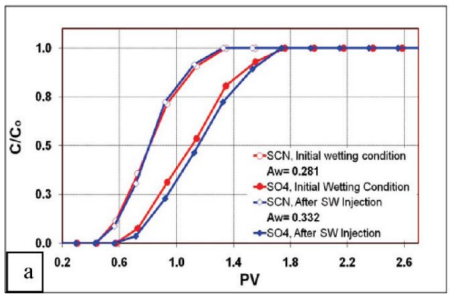

(a) Water wetting area both after mild cleaning and SI SSW.

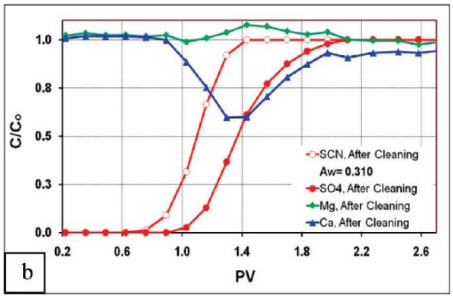

(b) calcium, magnesium, and sulphate relative concentrations in the effluent

Figure 2.19: Chromatographic wettability test on limestone reservoir cores at room temperature after mild cleaning with toluene, and SI withSSW (Shariatpanahi et al., 2010)

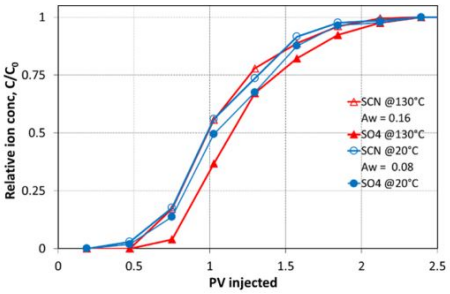

(a) Minimal SO_4^{2-} adsorption to a dolomite surface with temperature

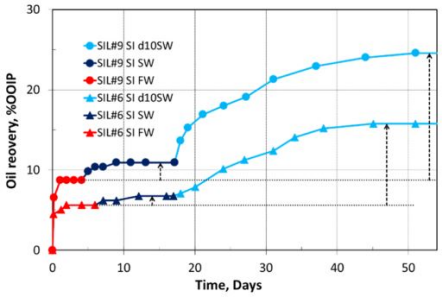

(b) Seawater is not a good smart water for EOR in dolomite

Figure 2.20: Among carbonates, dolomite has the least reactive surface to SW as an EOR fluid (S. Shariatpanahi et al., 2016)

More counter cations, Ca^{2+} ions, in the diffuse layer are attracted to the stern layer and end up forming forming complexes with and desorbing the carboxylic groups. A process that makes the rock site more water-wet.

In order to understand the impact of the Ca^{2+} ion in the wettability modification by **spontaneous imbibition analysis** , Zhang et al. (2006a) altered the $[Ca^{2+}]$ in both initial FW and in the imbibing brine. In all cases the $[SO_4^{2-}]$ was kept constant to the level present in sea water, 0.024mol/l. The $[Ca^{2+}]$ in initial FW had no impact on the initial wettability state but on SI, where higher $[Ca^{2+}]$ resulted in more SI and higher oil recoveries. Increasing the the $[Ca^{2+}]$ in the imbibing brine, especially at temperatures below 100°C, resulted in increase in oil recovery as seen in Figure 2.22. The temperature dependence of the Ca^{2+} ion on the wettability alteration process can be well seen in Figure 2.23. As already stated (Tweheyo et al., 2006) , the solubility of $CaSO_4$(s) in water, above 100°C, decreases with increasing temperature and theoretically reaches its threshold at 125°C. At higher temperatures the recoveries were low due to the initiation of $CaSO_4$(s) precipitation. However, the solubility of $CaSO_4$(s) at high temperatures in carbonate reservoir can be mitigated by introducing Mg^{2+} or altering the $[Mg^{2+}]$ ion in the imbibing brine. The phenomena behind this is discussed in Section 2.5.3.

In this study, the $[Ca^{2+}]$ was kept constant and equal to the the concentration in the North-Sea SW except in 0.1-SSW brine that was used in some contact angle measurements. It is important to note that keeping the $[Ca^{2+}]$ constant does not mean that the Ca^{2+} is inactive in the

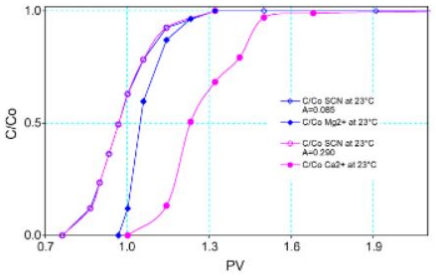

(a) Wettability measurement by Chromatographic separation technique. Area between SCN^- and the calcium at room temperature indicates that the Ca^{2+} ion adsorption (Zhang et al., 2007)

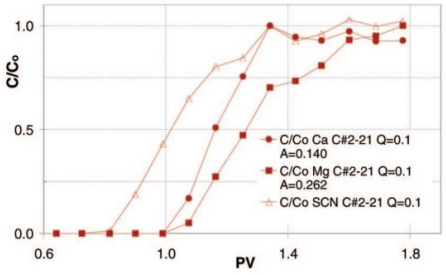

(b) calcium and magnesium, Wettability measurement. Comparing the adsorption areas at 100°C (Strand et al., 2008)

Figure 2.21: Adsorption of Ca^{2+} at room temperature of 23C and 100°C

wettability modification process.

2.5.3 The Magnesium ion, Mg^{2+}

The magnesium, ion is a very important ion in wettability modification process for carbonate reservoirs especially those at temperatures above 100°C (Yi et al., 2012; Chandrasekhar, 2013; Tweheyo et al., 2006; Zhang et al., 2007; Strand et al., 2008). Through **zeta potential** measurement, several literature show that the magnesium, ion is a potential determining ion to a carbonate surface (Zhang et al., 2007; Strand et al., 2008) and figure 2.24 (a). Studying advancing **contact angle measurements** on calcite plates aged at 80°C in SSW solutions containing different combinations of $[Mg^{2+}]$ with $[Ca^{2+}]$ and $[SO_4^{2-}]$, Chandrasekhar (2013) showed that varying by increasing the $[Mg^{2+}]$ in the brines, the contact angles at the calcite plates decreased. In NaCl solutions, the Mg^{2+} ion alone is not able to change the wetting state at the surface of a well polished calcite plate as depicted in Figure 2.12. However, in the presence of SO_4^{2-} or both SO_4^{2-} and Ca^{2+}, the Mg^{2+} is able to make the calcite plate more water-wet. The two observations were made by Gupta and Mohanty (2011) and (Chandrasekhar, 2013) in two different laboratory experiments.

In low salinity brine, calcite dissociates and releases a hydroxide ion among other products. The ^-OH group reduces the positive charge at the calcite surface (Nasralla et al., 2014). Karimi et al. (2016) observed that in such a case Mg^{2+} introduced in brine surrounding a calcite surface is attracted to the interface and form carboxylate complexes through ion pair formation. This process desorbs carboxylic groups and makes a calcite surface more water wet as seen in Figure 2.25a on the DB-M peak. Though more active in the presence of the SO_4^{2-} ion. The process of mineral dissolution itself makes the surface more water wet. Contact angle measurements in $MgCl.6H_2O$ solution at 23°C, 40°C, 70°C and 90°C by Karoussi et al. (2007) showed that the Mg^{2+} ion is able to make a calcite surface more water wet and it is more active at elevated temperatures.

Wettability measurements by the **chromatographic separation technique** was used by Zhang et al. (2007) to compare the relative affinity and adsorption of the Mg^{2+} and the Ca^{2+} ions to the chalk surface and the area difference for Mg^{2+} and SCN^- confirmed that the Mg^{2+} is able to adsorb on the chalk rock surface, Figure 2.21b(a), and possibly alter wettability. Zhang et al. (2007) says that the delay in the Ca^{2+} break through curves confirmed a stronger affinity

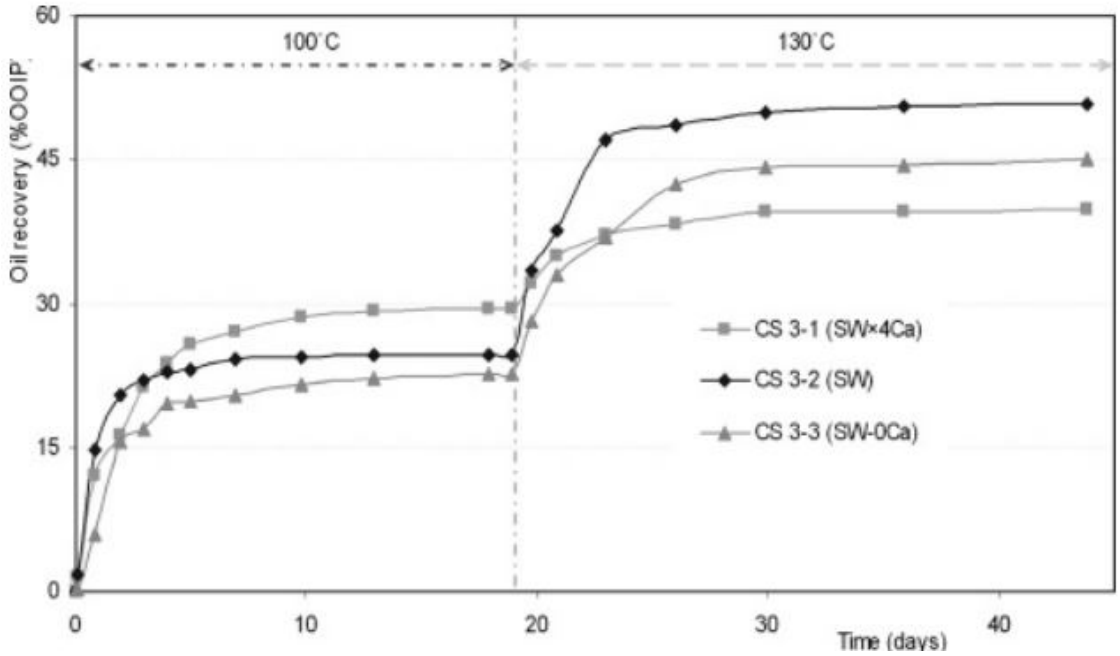

Figure 2.22: Oil recoveries as the [Ca^{2+}] in the imbibing brine is altered (Zhang et al., 2006a). Note the Swapping in the curve trends due to temperature (Solubility of $CaSO_4$(s))

of to a Ca^{2+} ion and the difference in the areas with the tracer SCN^- of 3.4 showed stronger adsorption by the Ca^{2+} ion. Wettability tests by Strand et al. (2008) and Figure 2.21b also show that the Mg^{2+} ion is able to adsorb to a limestone rock surface and the breakthrough points seemed to coincide which might hint on equal affinity of the two ions to a limestone surface.

Apart from adsorbing to the carbonate surface, at high temperatures above 100°C, the magnesium, ion can displace and substitute the calcium ion either in the rock crystal lattice at the surface or calcium ions to which the carboxylic groups are adsorbed as depicted in the normalised concentrations of the ions in Figure 2.24(b). A similar observation was made by Tweheyo et al. (2006). Strand et al. (2008) and Shariatpanahi et al. (2010) observed that in limestone, the presence of SO_4^{2-} in brine is key for the Mg^{2+} substitution and the process is initiated at temperatures above 80°C, quite higher than that in chalks (70°C) as seen in Figure 2.26, Figure 2.27b and Figure 2.27c. Either way the the wettability is modified and improves the water wetness state. This process also improves the solubility of $CaSO_4$(s) in brine (Zhang et al., 2007; Tweheyo et al., 2006). The structural strength of limestone or any other carbonate is also weakened when the Mg^{2+} substitutes for Ca^{2+} (Strand et al., 2008; Zhang et al., 2007). This is because the the Mg^{2+} ion is smaller than the Ca^{2+}. The extent of structural weakening is in the magnitude of about 2.7 for a chalk surface, (Zhang et al., 2007). This may also enable in the desorption of the carboxylic groups and hence improve the water wetness. The the substitution process is more prevalent at high temperature, above 100°C, than adsorption of the magnesium, ion, (Shariatpanahi et al., 2011; Zhang et al., 2007). Statistical results in another experiment by Shariatpanahi et al. (2011) indicates that the reduction in $[Mg^{2+}]$ is proportional with the increment in $[Ca^{2+}]$ and the substitution process is irreversible. The same observation was made by Shariatpanahi et al. (2010) on limestone reservoir cores.

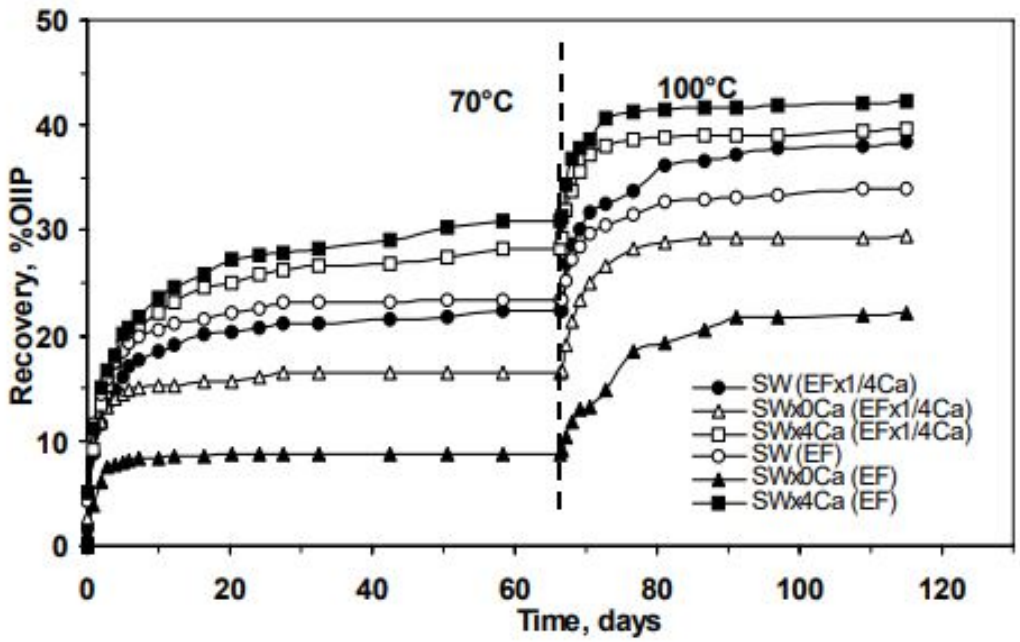

Figure 2.23: Effect of temperature on calcium ion activity during wettability modification

Spontaneous imbibition experiment by Karimi et al. (2016) at 75°C using 100 times diluted FW spiked in Mg^{2+} provided an incremental oil recovery of 8% . The increase in recovery was attributed to the activity of Mg^{2+} in wettability alteration to a more water wet state. prolonged SI experiments by Zhang et al. (2007) showed that the presence of the Mg^{2+} ion in modified SSW can improve the water wetting state of the rock-brine-crude oil system. At temperatures above 100°C, the Mg^{2+} is a better wettability modifier and results in a higher oil recovery than the Ca^{2+} ion, Figure 2.28a and Figure 2.28b. The observation was made using both oils of AN 0.55 and 2.07mgKOH/g to depict different initial oil wetting states. In both states the peak points for Mg^{2+}-containingSSW were higher than those for Ca^{2+} with a greater pronounced difference of about 12% in a more water wet initial state.

Shariatpanahi et al. (2011), Tweheyo et al. (2006) and Zhang et al. (2007) have shown that the presence of Mg^{2+} ion in SSW stabilises sea water . This makes it possible to inject SW or modified SW into reservoirs at temperatures above 100°C without worrying much about $CaSO_4(s)$ precipitation.

$$Mg^{2+}SO_4^{2-}(aq) \Longleftrightarrow Mg^{2+} + SO_4^{2-} \tag{2.4}$$

Zhang et al. (2007) showed that this is possible because of reduced activity of the SO_4^{2-} ion caused by aqueous ion formation with the Mg^{2+} ion, Equation (2.4). Zhang et al. (2007) say that at constant ionic strength, the equilibrium in Equation (2.4) shifts to the left as temperature increases.Therefore the aqueous ion pairing minimises the common ion effect and delays $CaSO_4(s)$ precipitation. In addition, the ion pair formation increases the $[Mg^{2+}]$ close to the carbonate surface, which enhances the role played by the Mg^{2+} in both surface brine-oil and substitution reactions at high temperatures above 100°C (Zhang et al., 2007). At constant temperature equilibrium in Equation (2.4) shifts to the right as the ionic strength increases. This might cause early precipitation of $CaSO_4(s)$ that damages rock permeability (Zhang et al., 2007).

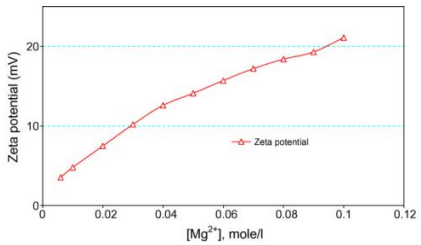

(a) The magnesium, ion is a PDI to a chalk-brine interface

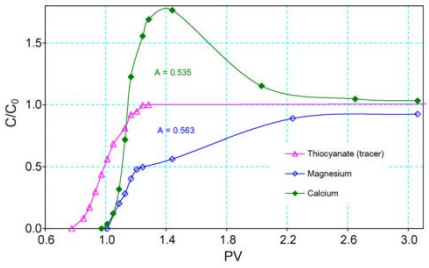

(b) relative concentrations in the effluent of Ca^{2+} and Mg^{2+} and the tracer in the NaCl solution

Figure 2.24: Comparison of the relative adsorption of Mg^{2+} and Ca^{2+} to the chalk surface (Zhang et al., 2007)

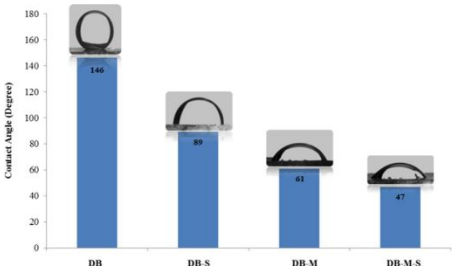

(a) Contact Angles on a calcite plate plate aged in 0.37mgKOH/g crude oil at 75°C and then aged in each brine for 48 hours at 75°

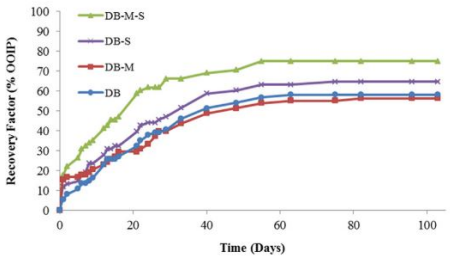

(b) Oil recovery by SI of FW and diluted FW spiked with either Mg^{2+} or SO_4^{2-} or both at 75°

Figure 2.25: Contact angle measurements and oi recoveries by SI process on calcite surface and Indiana limestone core respectively by Karimi et al. (2016)

2.5.4 Multi-Ion Exchange, MIE, mechanism: Focus on the Mg^{2+} ion

Wettability alteration by the MIE mechanism in an oil wet rock-crude oil-brines system is initiated in thin water films in water wet sites (Zhang et al., 2007). The process in carbonates is initiated by activation energy and effected by the sulfate ion adsorption on the carbonate surface, a process that ultimately lowers the net positive charge as the rock brine interface (Tweheyo et al., 2006). The activation energy window in carbonates is higher than in sandstones due to the stronger organo-metallic bond exhibited in carbonates (Strand et al., 2008). The activation energy in presence of calcium or magnesium, or both ions is achieved at temperatures between 40°C and 70°C (Tweheyo et al., 2006). The reduction in the positive charge due to SO_4^{2-} ion adsorption allows more calcium ions to be attracted and get co-adsorbed to the rock surface together with the sulfate ions (Zhang et al., 2006a; Tweheyo et al., 2006; Strand et al., 2008). The adsorbed Ca^{2+} ions form complexes together with the carboxylic groups and results in desorption of oil molecules as shown in Figure 2.29(a) according to

$$RCOO^- - Ca - Ca(CO_3)_2(s) + Ca^{2+}(ad) + SO_4^{2-}(ad) \\ \Longleftrightarrow RCOO^- - Ca^{2+}(aq) + Ca - Ca(CO_3)_2(s) + SO_4^{2-}(ad)$$

Active rock-fluid interface reactions at temperatures less than 100°C.

Revised version of equation by Azizov (2019)

(2.5)

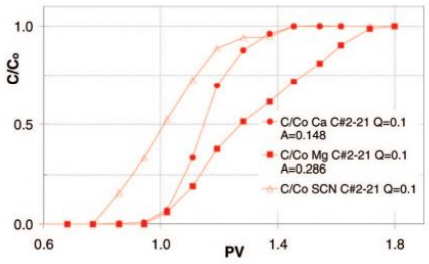

(a) The Mg^{2+} ion substitution is almost inactive in absence of SO_4^{2-} in NaCl solution at 130°C

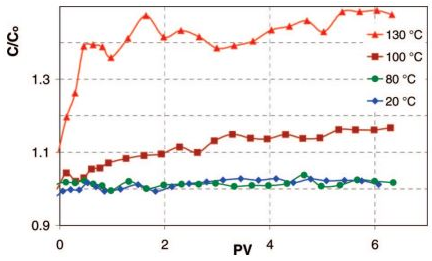

(b) Relative concentrations in the effluent of Ca^{2+} in NaCl solution with $[SO_4^{2-}]$=0.024m/l at different temperatures

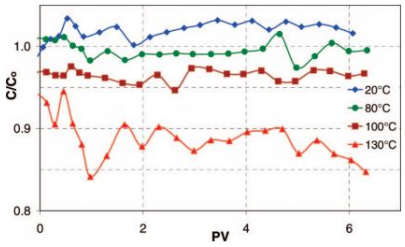

(c) Relative concentrations in the effluent of Mg^{2+} in NaCl solution with $[SO_4^{2-}]$=0.024m/l at different temperatures

Figure 2.26: A look at Mg^{2+} ion substitution in limestone cores at different temperatures (Strand et al., 2008)

Where:

- Where '$_{ad}$' and '$_{aq}$' ions or molecules adsorbed to a $CaCO_3$ surface and in solutionrespectively

At temperatures above 100°C, the Mg^{2+} ion plays the role that is played by Ca^{2+} at temperatures below 100°C in addition to the substitution effects as illustrated in 2.29(b) and

$$RCOO^- - Ca - Ca(CO_3)_2(s) + Mg^{2+}(ad) + SO_4^{2-}(ad) \\ \Longleftrightarrow RCOO^- - Ca^{2+}(aq) + Mg - Ca(CO_3)_2(s) + SO_4^{2-}(ad)$$

Active rock-fluid interface reactions at temperatures greater than 100°C.

Revised version of equation by Azizov (2019)

(2.6)

The relative proportions of all the three divalent ions in SW makes it possible to have all the processes present in different reservoirs at different temperatures. Zhang et al. (2006a) and Tweheyo et al. (2006) have shown through spontaneous imbibition and wettability measurement tests on chalk cores that this process is most dependant on temperature. Strand et al. (2008) also show the same temperature dependence in Limestone cores. Tweheyo et al. (2006) showed that at 40°C, (insufficient activation energy), the $[Ca^{2+}]$ in both initial FW and imbibing brine has no impact on spontaneous imbibition and recovery was mainly due to fluid expansion. However, at high temperatures, 70°C and above, the oil recoveries drastically increased with increase in temperature. Strand et al. (2008), Zhang et al. (2006a), Zhang et al. (2007) and Tweheyo et al. (2006) suggest that care needs to be taken at temperatures above 100°C in carbonate reservoirs as a $CaSO_4(s)$ precipitation may result in reduction of $[Ca^{2+}]$ and $[SO_4^{2-}]$ in solution required to alter wettability,Figure 2.22, and also block the flow path-

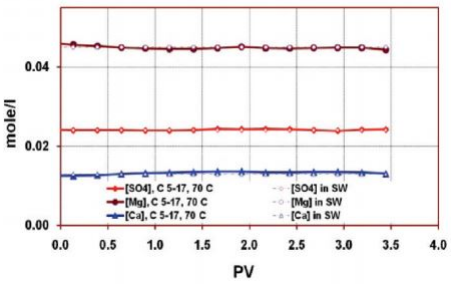

(a) No Mg-Ca substitution at 70°C

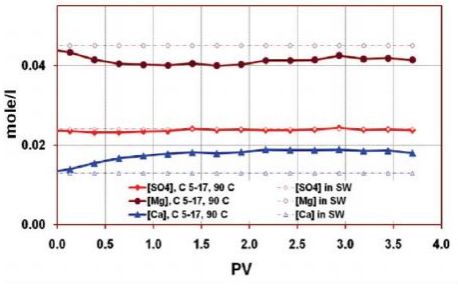

(b) On set of Mg-Ca substitution at 90°C. Observed from $[Mg^{2+}]$

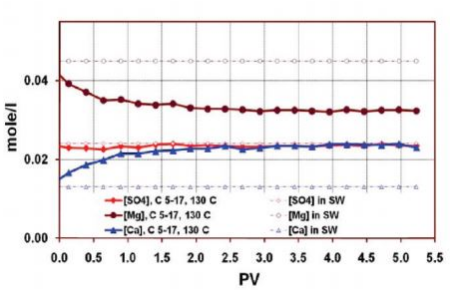

(c) Mg-Ca substitution process equal to $CaSO_4(s)$ precipitation from brine at 130°C

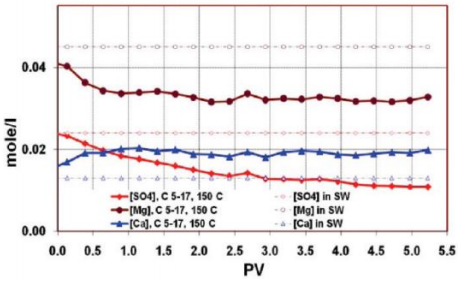

(d) $CaSO_4(s)$ dominating over Mg-Ca substitution at 150°C

Figure 2.27: The interplay of Mg-Ca substitution and anhydrite precipitation with temperature. Temperature windows for both processes (Shariatpanahi et al., 2010)

ways. Tweheyo et al. (2006) showed symbiotic action of the three divalent ions on wettability alteration and their dependence on temperature in carbonates by spontaneous imbibition of modified synthetic seawater. As was also observed by Zhang et al. (2007), Chandrasekhar (2013) the magnesium, ion is most effective at high temperatures and Tweheyo et al. (2006), Zhang et al. (2007) and Strand et al. (2008) suggest the temperature to be above 100°C. As already summarised in section Section 2.5.3 the Mg^{2+} ion plays 6 roles in two temperature windows

- Stabilizes sea water due to formation of an ion pair $Mg^{2+}SO_4^{2-}$(aq) which reduces$CaSO_4$(s) precipitation (Tweheyo et al., 2006)
- Substitutes for the calcium ion at the rock-brine interface increasing the $[Ca^{2+}]$
- Substitutes for the Ca^{2+} to which the carboxylic groups are adsorbed
- weakens the structural integrity of the rock-brine interface as the Mg^{2+} ion is smaller than the Ca^{2+} ion.
- The substitution reduces the common ion effect and then enhances $CaSO_4$(s) dissolution if the reservoir has anhydrite precipitate.

2.5.5 The effect of salinity on wettability alteration and the electric double layer (EDL) mechanism

Carbonate reservoirs have high saline salty waters with most having salinity well over 200000PPM. Therefore injecting sea water that has an average salinity of 35000 PPM introduces a great contrast in salinities. Yousef et al. (2010), Yousef et al. (2012(a)) showed that SSW and diluted versions of synthetic seawater can alter wettability in carbonates cores. Yousef et al. (2010) through series of core flooding - in the order of FW, SSW, twice diluted SSW, 10 times diluted

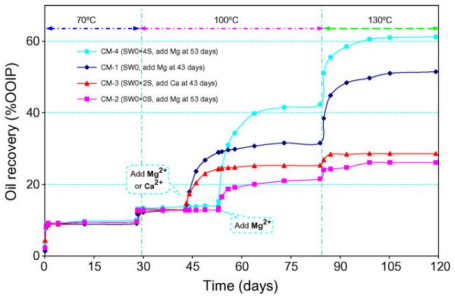

(a) The Mg^{2+} is a better wettability modifier than Ca^{2+} above 100°C in a more initial water wet system

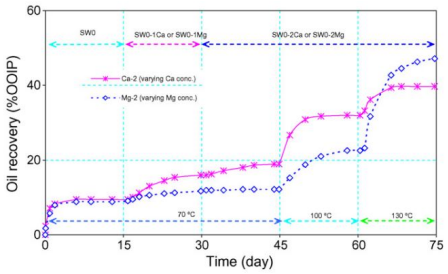

(b) The Mg^{2+} is a better wettability modifier than Ca^{2+} above 100°C in a less initial water wet system

Figure 2.28: SI results show that the Mg^{2+} ion is active in its wettability process at above 100°C in chalk cores (Zhang et al., 2007)

SSW, 20 times diluted SSW and 100 times diluted SSW - on two relatively identical composite cores observed that extra recovery was obtained with injected diluted SSW as seen in Figure 2.30a The greatest additional oil recovery was obtained with twice and ten times diluted SSW while 100 times gave no recovery.

Through repeated contact angle measurements, limestone chips exposed to FW, SSW and four versions of diluted SSW showed varying response to the measurement figure as depicted in 2.31 (a). Yousef et al. (2010) observed receding contact angles with increasing dilutions. Yousef et al. (2010)and Yousef et al. (2012(a)) did IFT measurements between the named brines with oil and found out there was no big difference in the diluted series after a drastic drop with SSW as observed on Figure 2.31 (b). Residual oil in reservoirs is controlled by capillary pressure which is a function of IFT and contact angle (wettability). Basing on this, Yousef et al. (2010) and Yousef et al. (2012(a)) were able to conclude that the extra oil oil recovered was due to wettability alteration to a more water wet observed with contact angle reduction and not to marginal IFT reduction.

Yousef et al. (2012(a)), Yousef et al. (2012(b)) and Yi et al. (2012) tested and confirmed that reducing the ionic strength of SW is sufficient enough and even more effective in wettability modification in Limestone reservoirs. It was observed that diluting the concentration of common ions Na^+ and Cl^- in both SSW and its diluted versions was effective. Yousef et al. (2012(a)), observed that the selective dilution provided even better wettability alteration through zeta potential measurement, Figure 2.30b . The argument was that even in diluted SSW, PDIs still play a role in wettability modification. Therefore reducing their concentration through salinity reduction by holistic dilution also limits their impact on wettability. This was in agreement with the later work by Yi et al. (2012) on Saudi Arabian carbonate core samples. However, the same observation could not be made by Shariatpanahi et al. (2010) in another set of limestone cores. In regards to temperature effects on the efficiency of LS-EOR in carbonates, Yi et al. (2012) argue that it is better to use diluted sea water in low temperature reservoirs, below 70°C, than increasing the $[SO_4^{2-}]$. In this case, dilution effects on wettability modification are more effective than those caused by PDIs. Through additional NMR measurements Yousef et al. (2010) and Yousef et al. (2012(a)) concluded that SSW and diluted SSW are able to alter wettability in two ways:

- Surface charge alterations that triggers the MIE mechanism that was suggested by Zhang et al. (2007)

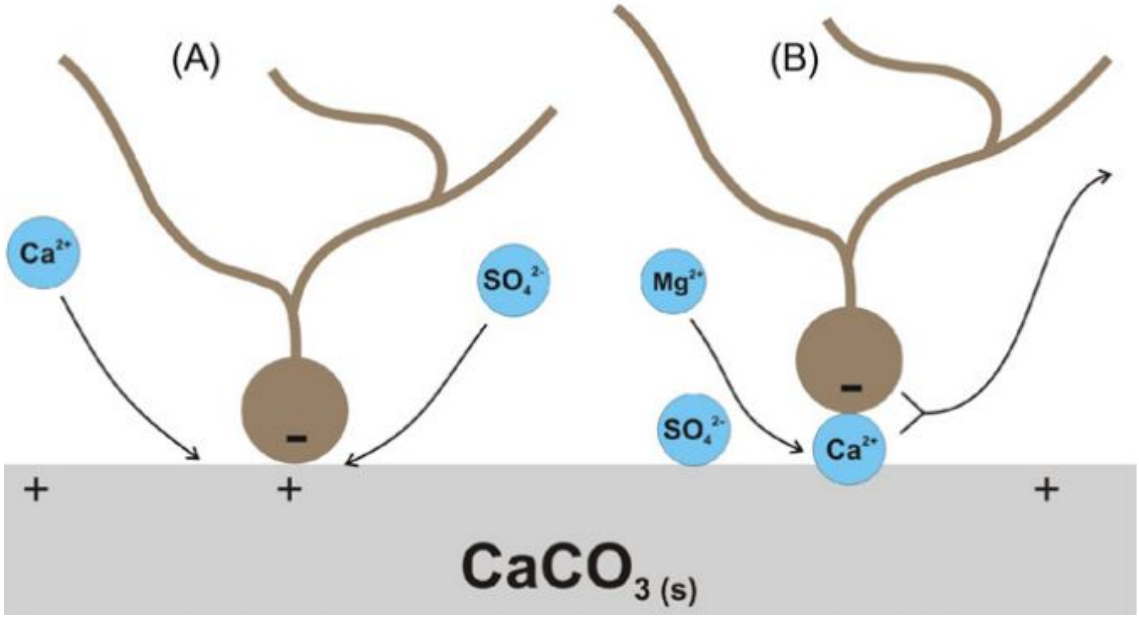

Figure 2.29: The schematic of the MIE wettability alteration mechanism as proposed by (Zhang et al., 2007) at both low and high temperatures in carbonate reservoirs

- Microscopic rock dissolution of both bulk carbonate rock and trace anhydrite usually present in carbonate reservoirs. The anhydrite provided an in situ source of sulfate ions. The rock dissolution also alters flow paths as pore throats are blocked due to fines migration.
- Electric double layer expansion of the thin water film between the rock and crude oil interfaces. This stabilises the thin water film and improves water wetness as the debye length increases due to reduced ionic strength.

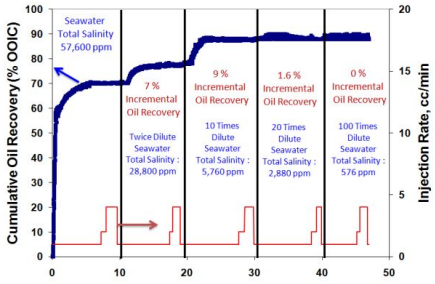

(a) Oil recoveries as the SSW and its diluted versions were flooded into composite cores (Yousef et al., 2010).

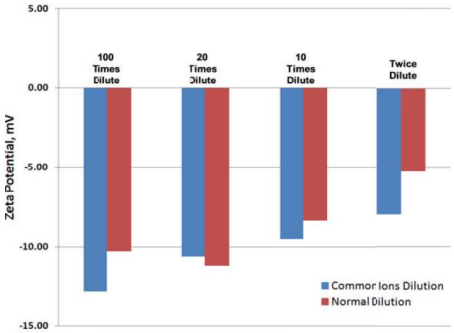

(b) Impact of Ionic strength dilution on wettability alteration on Saudi Arabian Carbonate reservoir (Yousef et al., 2012(a))

Figure 2.30: Scrutinizing the impact of holistic dilution on the wettability alteration process

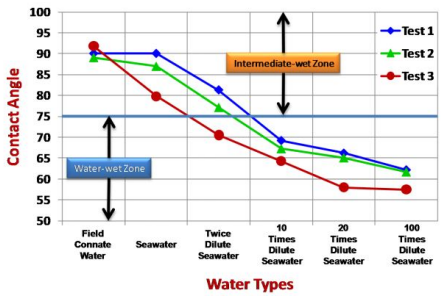

(a) Contact angle between oil and FW, SSW and diluted versions of SSW on limestone chips

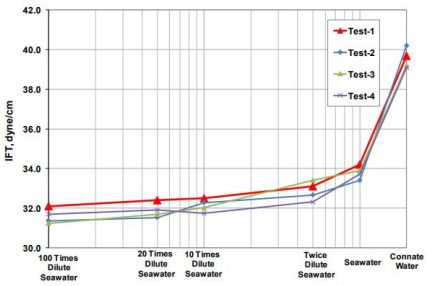

(b) IFT between oil and FW, SSW and diluted versions of SSW

Figure 2.31: Impact of SSW and diluted SSW on wettability modification in carbonates (Yousef et al., 2010)

Chapter 3

Theory

This chapter is about the theory of thin water films and surface energies and other supporting mathematical and physical models that determine the initial wetting state in oil reservoirs. It is in thin water films that double-layer expansion (DLE) hypothesis in the process of wettability modifications on a mineral surface is assumed to take place. The last part of the chapter also talks about the electric double layer (EDL) expansion mechanism and correlates it with the thin water film thickness as a key mechanism when discussing low salinity enhanced oil recovery (LS-EOR). The chapter has been written basing on the work that was done by Butt et al. (2013), Han (2002), Hirasaki et al. (1991), Nazari et al. (2020) and Tweheyo et al. (2006),

3.1 Interfaces,Surface charges, and Surface forces

The wetting of mineral surfaces by water or oil or both is described by models of surface forces caused by static charges at those surfaces and become important when the surfaces approach each other according the Derjaguin, Landau, Verwey, and Oberbeek (DLVO) theorem. The key surface forces that control the wettability state are Van der waals, electrostatic forces and structural forces sometimes called solvation forces - such as hydrogen bonds - when the thin water film is extremely thin or when shrinking within a threshold controlling thickness, Hirasaki et al. (1991).

In the original DLVO theorem, only Van der Waals and electrostatic forces were considered. These surfaces forces are expressed in form of disjoining pressure isotherms. Hirasaki et al. (1991) defines disjoining pressure as the energy change per unit area when a pair of interfaces approach each other from a large separation to a finite thickness at a 3-phase contact line. In terms of free Gibbs's energy, disjoining pressure can be defined as the change in Gibbs's free energy with distance, h, per unit area at constant cross-section area, temperature and volume (Han, 2002). Negative disjoining pressure causes attraction of the two interfaces whereas positive disjoining pressure causes the repulsion or separation of the two interfaces. In oil reservoirs, the interfaces are crude oil-brine interface and rock-fluid interface.

Stability of the thin water film occurs when the disjoining pressure is positive and of substantial magnitude. In that case, the thin water film is stable, thick and continuous and the surface is mostly water wet (Nazari et al., 2020). Hirasaki et al. (1991) says that the equilibrium condition for a 3-phase system with interfaces is a function of temperatures and chemical potentials among the phases and can be related through the augmented Young-Laplace equation, Equation (3.1). The wettability, defined by contact angle, can be obtained using the modified augmented Young-Laplace, Equation (3.2) assuming the film is brought from infinite

separation to an equilibrium stable thickness, h_{eq} (Nazari et al., 2020)

$$P_o - P_w = P_c = \Pi + 2H\delta_{ow} \tag{3.1}$$

where,

- P_o is pressure in the non-wetting phase, crude oi, P_w is pressure in the wetting phase, water, P_c capillary pressure, Π disjoining pressure, δ_{ow} as the IFT between crude oil, H define represents the curvature at the point of contact and water

$$Cos\theta - 1 = \frac{1}{\delta_{ow}} . \int_{h_{eq}}^{h_\infty} [\Pi(h) - \Pi_{eq}] dh \tag{3.2}$$

Where:

- θ is the contact angle at the 3-phase contact line

At the point of 3-phase contact, usually called the liquid meniscus, the interface separation is far larger than the thickness of the water film and in that case the disjoining pressure tends to zero and Equation (3.1) reduces to the common Young-Laplace equation. Also if the solid surface is flat and has a smooth texture, then the curvaure is zero and therefore $P_c = \Pi$.

The integral of disjoining pressure isotherm with respect to the thickness of the water film, h, gives specific interaction potential isotherms. The difference in energy states per unit area between position of minimum energy at equilibrium, h_{eq} and h gives the system's specific interaction potential according to, Equation (3.3) (Hirasaki et al., 1991).

The magnitude and sign of specific interaction potential determine the stability of the thin water films and the size of the contact angle angle at the meniscus. Just like disjoining pressure, when the specific interaction potential is positive, then the attractive forces are stronger than repulsive ones and the film shrinks. However, between two positions of equilibrium, there is always an intermediate thickness with an energy barrier that has to be overcome before the 3-phase system settles at a new stable or meta stable position (Hirasaki et al., 1991). Considering the film shrinking from a larger thickness, h_{eq} to a new thickness h_2, through h_1, the energy barrier at h_1 must be overcome before settling at h_2, Figure 3.1. The three positions, h_1, h_2, and h_{eq} must have a disjoining pressure equal to that at the initial position h_{eq}.

$$\Delta\omega = \int_{h}^{h_{eq}} [\Pi(h) - \Pi_{eq}] dh \tag{3.3}$$

Where

- $\Delta\omega$ is the specific interaction potential , and h is the film thickness

3.1.1 Disjoining pressure components

Total specific interaction potential of two interfaces consisting of a thin water film in between is a result of three inter-molecular or inter-atomic forces. Van der waals, electrostatic forces due to charges at the two interfaces and solvation forces, Figure 3.2. The first two forces are the main contributors and the last is when the film is in very close proximity (Hirasaki et al., 1991; Nazari et al., 2020). A number of models have been used to describe the contributions from the three forces and will be discussed next.

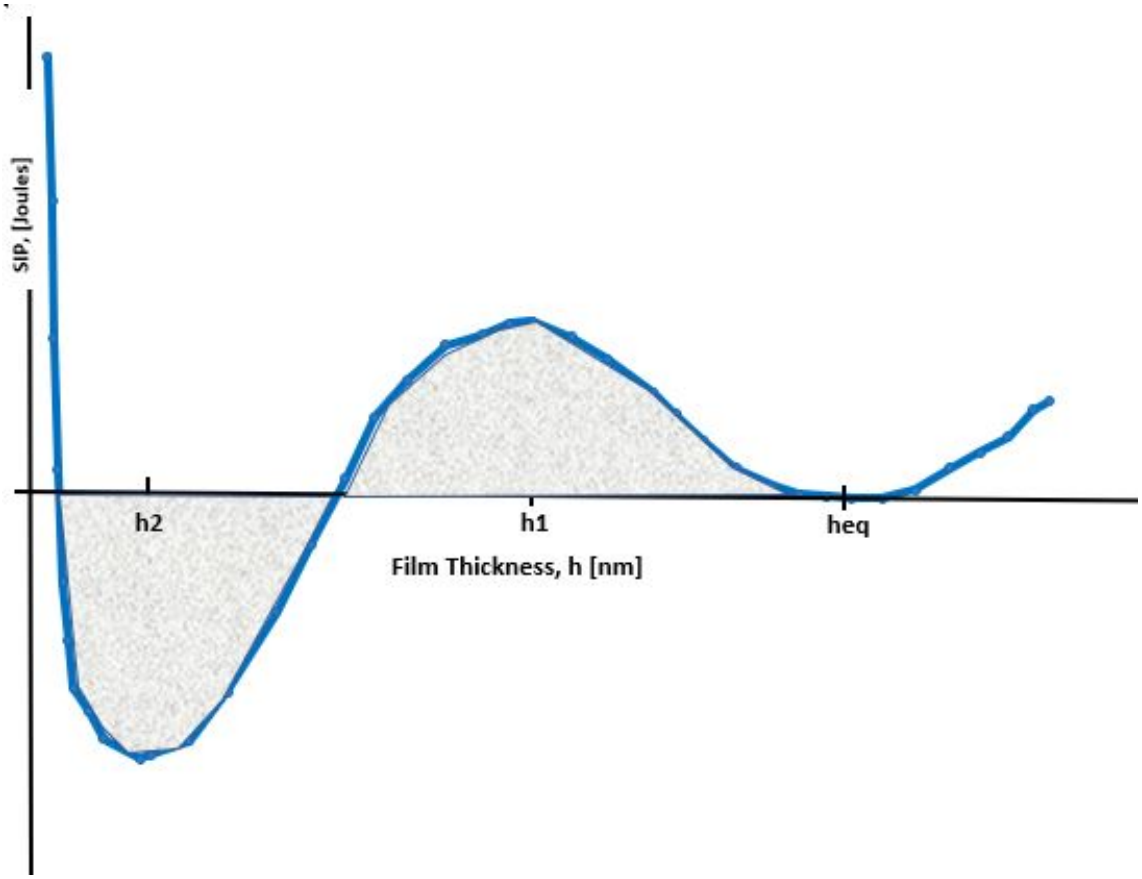

Figure 3.1: The dynamics of SIP during film shrinkage from h_eq to h_1. A reworked version of Hirasaki et al. (1991)

Van der waals force component

The Van der Waals force present among all objects in nature is caused by electron fluctuation around the the nucleus of neutral atoms. In Thin film studies, the Van der waals contribution is and based on the Hamaker theory. The Hamaker theory assumes that all objects in nature are pair-wise additive and independent of the intervening media and the interaction between two different media is a geometric mean of the interaction of each medium with itself. In this case the specific interaction potential contribution from Van der Waals is calculated from the Hamaker constant and the film thickness according to Equation (3.4) and Equation (3.5). These two equations assume a continuum in both bulk phases, (crude oil and the rock), and in the thin water film. It also assumes that the two interfaces are parallel and flat.

$$\omega(h) = (A/12\pi)h^{-2} \tag{3.4}$$

Where:

$$A = A_{v=0} + A_{v>0} \tag{3.5}$$

$$A_{v=0} = 3/4\kappa T[(\epsilon_1 - \epsilon_3)/(\epsilon_1 + \epsilon_3)][(\epsilon_2 - \epsilon_3)/(\epsilon_2 + \epsilon_3)] \tag{3.6}$$

$$A_{v>0} \approx \frac{3PV_e}{8^{0.5}} \frac{(\eta_1^2 - \eta_3^2)(\eta_2^2 - \eta_3^2)}{(\eta_1^2 + \eta_3^2)^{1/2}(\eta_2^2 + \eta_3^2)^{1/2}[(\eta_1^2 + \eta_3^2)^{1/2} + (\eta_2^2 + \eta_3^2)^{1/2}]} \tag{3.7}$$

where

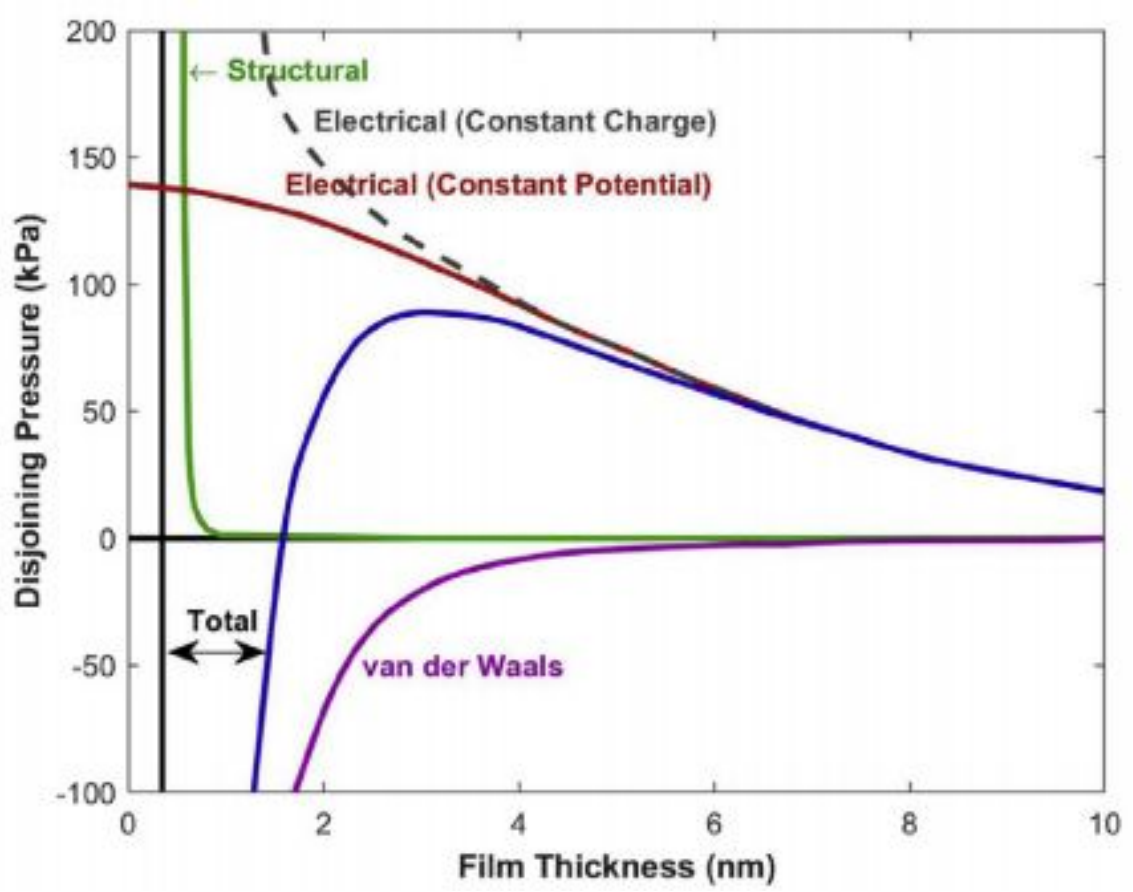

Figure 3.2: The disjoining pressure components. A reworked version of Hirasaki et al. (1991) by Nazari et al. (2020)

- ϵ_i (for i=1, 2, 3 are the crude oil phase, rock phase and thin water film phase respectively) is the zero-frequency dielectric constant for a phase i, η_i the refractive index in the visible part of the spectrum for a phase, V_e is the ionisation frequency, T absolute temperature, κ and P are Boltzmann's and Plank's constants for h

Butt et al. (2013) summarise in a table different values of ϵ_i, η_i and V_e for for various solids, liquids and polymers at 20°C. Hirasaki et al. (1991) reported that the Van der Waals contribution to specific interaction potential is negative or attractive when the Hamaker constant in Equation (3.5) is positive, and positive or repulsive when the Hamaker constant is negative.

In case of an adsorbed layer of finite thickness, δ, at the rock surface contributes to the thickness, h, of the thin water film, then a modified Hamaker constant needs to be used that incorporates the layer of adsorption. The Hamaker assumptions of pair-wise interaction and geometric mean interaction between dissimilar media still apply. Equation (3.8) is used.

$$\omega(h) = \frac{1}{12\pi}\left[\frac{\left(A_{11}^{1/2} - A_{44}^{1/2}\right)\left(A_{22}^{1/2} - A_{33}^{1/2}\right)}{(\delta + h)^2} + \frac{\left(A_{44}^{1/2} - A_{33}^{1/2}\right)\left(A_{22}^{1/2} - A_{33}^{1/2}\right)}{h^2}\right] \tag{3.8}$$

where

- i=4 stands for the fourth phase cause by the adsorbed layer

Hirasaki et al. (1991) says that when δ«<h, then Equation (3.8) reduces to Equation (3.4) of the 3-phase system. When δ »>h, then Equation (3.4)is also opted for but the Hamaker properties for the thin film are those of the adsorbed layer. Hirasaki also noted that this physical state in the thin water film can affect the sign of the specific interaction potential which define the contact angle or wettability.

In the recent review by Nazari et al. (2020), they suggest that the Israelachvili approximation, Equation (3.9) gives better results of the Van der Waals forces. In that case the Hamaker constant for the crude oil-brine-rock system is about 7.1x10^{-21} J and it is independent of the brine concentration the thin film phase.

$$\omega(h) = \frac{-A}{12\pi h^3} \tag{3.9}$$

And A is the total Hamaker constant given by Equation (3.10),

$$A = \left[(\sqrt{A_{11}} - \sqrt{A_{33}}).(\sqrt{A_{22}} - \sqrt{A_{33}})\right] \tag{3.10}$$

Where:

- A_{11}, A_{22}, A_{33} refer to the Hamaker constant involving single component pairwise interactions for oil-oil, carbonate -carbonate, and brine-brine, respectively

Electrostatic force component

Coulomb's law governs the interaction of static charges in a vacuum. In an oil reservoir, static charges are at the rock-fluid interface and at the crude oil-brine interface and the medium between them in case of a water at the time of crude oil accumulation is a thin water film enriched in monovalent Na^+ and Cl^- ions. In carbonate reservoirs, the brine is also rich in Ca^{2+} ions. These ions in the thin water film complicate the interaction of the two interfaces (Nazari et al., 2020). Hirasaki et al. (1991) note that the electrofield near a charged surface decays exponentially with the decay length called Debye length. The Debye length is inversely proportion with the concentration of the electrolyte. Specific interaction potential (SIP) contribution of electrostatic charges at interfaces is approximated on the assumptions of either constant surface potential or constant surface charge using Hogg, Healy and Fuerstenau (1966) and Usui (1973) analytical models respectively.

$$\omega_D = 1/2\left[\pm\left(1 + F_{\Phi e}^2\right)(cothh_D - 1) + 2F_{\Phi e} cosechh_D\right] \tag{3.11}$$

where

- $F_{\Phi e}$= Φ_{eo2}/Φ_{eo1}; h_D=κh; and κ= $\left(e^2\Sigma\left(C_i^o z_i^2\right)/(\epsilon_o \epsilon \kappa T)\right)$. : with Φ_{eoi} as the surface electrical potential of surface i at infinite separation, C_i is the electrolyte concentration, and z_i accounting for electrolyte charge

Hirasaki et al. (1991) notes that for total Specific interaction potential (SIP) calculated using the constant surface charge is always positive when both charges have the same sign. However, the SIP calculated using constant potential can be negative at very small separation when the separation nears the molecular length.

More accurate measurements of the electrostatic contribution to SIP are obtained using the linear Poisson-Boltzmann (P-B) equation, see Section 3.2, by assuming constant but unequal

potentials at the two interfaces, Equation (3.12). Surface potentials ψ, are obtained from zeta potential measurements at the two interfaces using Equation (3.13).

$$\omega(h) = \frac{\epsilon_o \epsilon \kappa \left[2\psi_1\psi_2 - (\psi_1^2 + \psi_2^2)e^{-\kappa h}\right]}{e^{+\kappa h} - e^{-\kappa h}} \tag{3.12}$$

$$\psi_i = \frac{e\zeta_i}{\kappa_B T} \tag{3.13}$$

Where:

- κ^{-1} is the Debye length (defined in Section 3.2), ψ_i surface potential at either interfaces, ζ_i zeta potential, κ_B as Boltzmann constant, T temperature.

Solvation force component

The contribution from solvation forces such as hydrogen bonds and other forces due to the finite nature of the ions is very minute and can be ignored except in very thin films, Figure 3.2 (Nazari et al., 2020). At this film thickness, these forces are strongly repulsive and therefore always positive and try to resist any further film shrinkage. Hirasaki et al. (1991) noted that for disjoining pressure isotherms of film with different concentrations of electrolytes, the maximum disjoining pressure decreases with increasing electrolyte concentration.

3.1.2 Stability of a water-wetting film

According to Hirasaki et al. (1991), a thick wetting film will always be stable if there exist adequate energy barrier between a thick wetting film with zero or small contact angle (completely water wetting) and a thin film with a significant contact angle. Also in the case of zero P_c a stable film can also be established when the sum of electrostatic and van der walls SIP has a maximum in the the thick film region. In other-words when the total disjoining pressure is positive.

Hirasaki et al. (1991) asserts that when the P_c increases, then the energy barrier between a thick metabstable film and a smaller thickness reduces and hence a new equilibrium is set at a smaller thickness which results in a thinner film. The stability of the thin water film is also dependant on the texture of the solid surface (Nazari et al., 2020). When the surface has protrusions, the the disjoining pressure according to Equation (3.1) is less than the capillary pressure and hence small film thickness than when the surface is flat and smooth. Nazari et al. (2020) say that when the thickness of the film is much larger than the surface protrusions, then the surface appears to be flat and can be assumed so,

3.2 The Electric Double layer theory

Thin water films in oil reservoirs and electric double layer theorems have something in common, and that is the solid-fluid interface. Butt et al. (2013) defines an interface as an area that separates two phases from each others. Interfaces are unique to systems containing them because such systems are controlled mainly by the interface properties. This is because the interface to volume ratio is so large that forces like gravity are negligible.

Most solid surfaces in a water solution are charged (Han, 2002), and this is because water has a dielectric or relative permitivity for ions in solution. Butt et al. (2013) and Han (2002)

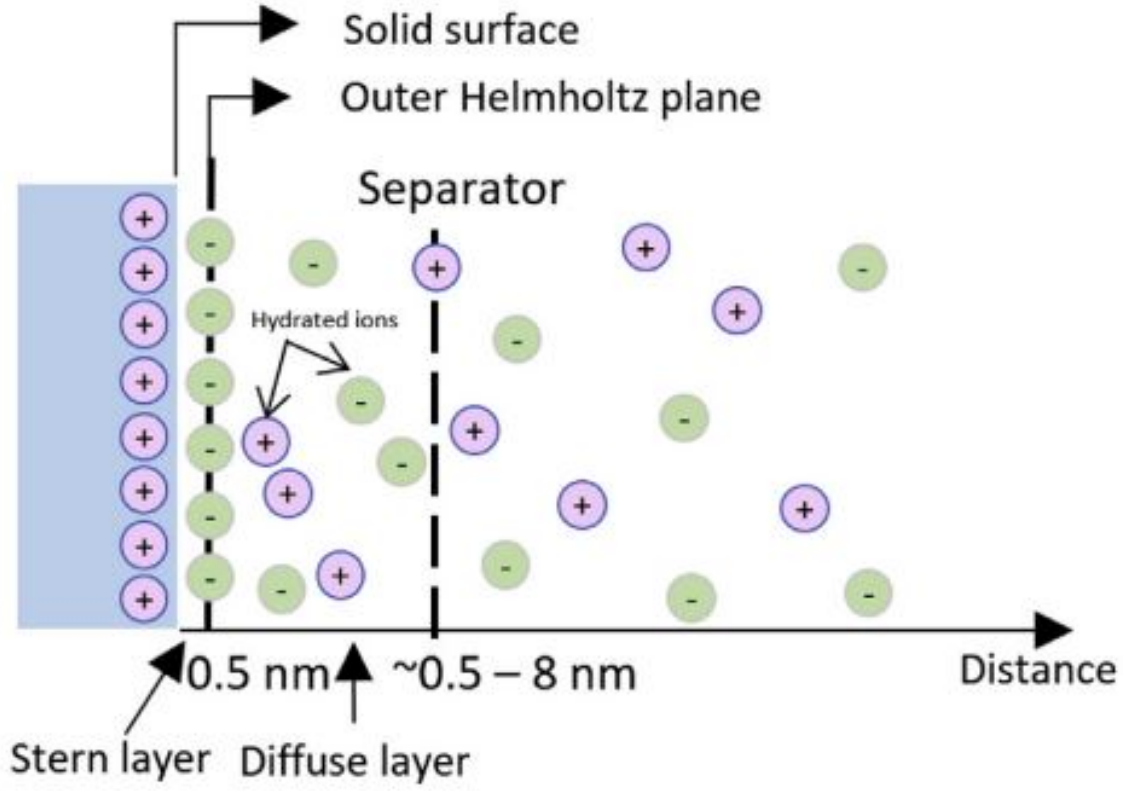

Figure 3.3: Illustration of the electric double layer based on the Gouy-Chapman model (Nazari et al., 2020)

summarise a number of processes that can lead to the solid surface getting charged. As a result, the surface charge creates an electric field which attracts counter ions in solution that strongly adsorb to the surface in the process of creating electro-neutrality (Han, 2002). This process creates an electric double layer.

One layer contains charges in the solid phase and the other contains adsorbed charges in the liquid phase. Therefore, an electric double layer is a layer of surface charges and counter ions adsorbed to it. Two models in literature are used to describe the electric double layer (EDL) theorem. In the Helmholtz model, the electric field generated by the surface charge is limited by the molecular size, and counter ions bond directly to the surface charge and neutralise the surface charge. Whereas in the Gouy-Chapman model thermal fluctuations tend to drive counter ions away from the surface and led to the formation of the diffuse layer, which is more extended than the molecular layer (Butt et al., 2013), and Figure 3.3.

The Poisson-Boltzmann theory and surface potential

Hirasaki et al. (1991) noted that the contact angle or wettability at a 3-phase contact line is controlled by the Specific interaction potential at the solid-fluid interface. The potential of a charged surface in a brine solution is function of the distance normal to the surface. Considering a charged solid surface with a uniform charge density, δ_o. The surface charge generates a surface potential, ψ_o at X=0, for X=[x, y, z]. The local charge density, ρ_e and

electric potential ψ as a function of X are related by the Poisson equation as in Equation (3.14).

$$\nabla^2\psi = \frac{\delta^2\psi}{\delta x^2} + \frac{\delta^2\psi}{\delta y^2} + \frac{\delta^2\psi}{\delta z^2} = \frac{\rho_e}{\epsilon\epsilon_o} \tag{3.14}$$

Where:

- ϵ is the dielectric constant for the liquid bulk phase and ϵ_o vacuum dielectric constant

With known spacial distribution of ions in solution, C_i, provided by the Boltzmann equation, Equation (3.15), and known spacial surface charge distribution, the potential distribution in a EDL can be calculated.

$$C_i = C_i^o.e^{-\omega_i/\kappa_B T} \tag{3.15}$$

Where:

- ω_i is the work done to bring an ion from a bulk solution at infinite distance to a certain position closer to the solid surface, C_i^o local surface ion concentration, κ_B and T as Boltzmann constant and Temperature respectively. ,

Butt et al. (2013) says that the local ion concentration (C_i), depends on the local electric potential within the EDL. If the local potentials at a certain location is positive, then there is a high like-hood of finding more anions at that locations than cations. The local [cation] and [anion] are related to the the local potential ω by Boltzmann factors as in Equation (4.11 and 4.12).

$$C^+ = C_o.e^{-\omega_i/\kappa_B T} \tag{3.16}$$

$$C^- = C_o.e^{+\omega_i/\kappa_B T} \tag{3.17}$$

Where:

- C_o is the bulk electrolyte concentration.

Therefore at any position X, the local charge density, ρ_e, is related to the two local [ion] through Equation (3.18).

$$\rho_e = e(C^+ - C^-) = C_0 e.\left[e^{-\frac{e\psi}{\kappa_B T}} - e^{\frac{e\psi}{\kappa_B T}}\right] \tag{3.18}$$

$$\nabla^2\psi = \frac{C_o e}{\epsilon\epsilon_o}.\left[e^{-\frac{e\psi}{\kappa_B T}} - e^{\frac{e\psi}{\kappa_B T}}\right] \tag{3.19}$$

Combining Equation (3.18)and Equation (3.14) gives the Poisson-Boltzmann equation, Equation (3.19). With known boundary conditions which are; ψ (X=o)=ψ_o ans ψ_o(X≈∞=0, the second order differential equation can be solved numerically for ψ(x) at X>0. In case of low potentials, $\kappa_B T$»$|e\psi|$, and infinitely long planar surface in x direction, (y,z=0), and Taylor expanding the exponential terms, Equation (3.19) reduces to Equation (3.20) which when solved analytically and applying the listed boundary conditions gives ψ(x) as in Equation (3.21). From this eqaution, it can be seen that the potential at a position other than the surface is a function of potential at the source and a constant k.

$$\frac{d^2\psi}{dx^2} = \frac{2C_o e^2}{\epsilon\epsilon_o\kappa_B T}.\psi \tag{3.20}$$

$$\psi(x) = \psi_o.e^{-kx} \tag{3.21}$$

$$k = \sqrt{\frac{2C_o e^2}{\epsilon\epsilon_o\kappa_B T}} \tag{3.22}$$

Where:

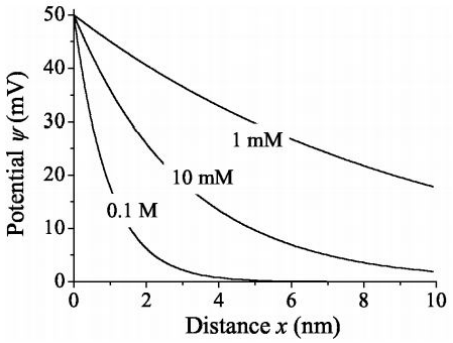

(a) Linear solution of potential for a surface with ψ_o=50mV at 25°C in salts of varying concentration

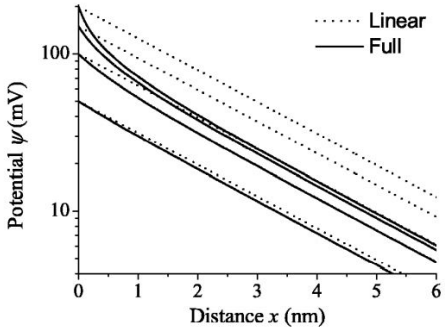

(b) Comparison of linear and full solution of the Poisson-Boltzmann equation

Figure 3.4: Analytical solution of potential vs normal distance x for surface of different potentials in a 20mM NaCl solution and λ_D=2.15nm (Butt et al., 2013)

- The k^{-1}=λ_D is the Debye length

Butt et al. (2013) defines Debye length, λ_D, as the length along which the potential in an EDL system exponentially decays to zero. From Equation (3.22), the Debye length decreases with increase in salt concentration as shown in Figure 3.4a. In divalent and multivalent salts, Butt et al. (2013) defines another expression for the Debye length which is a function of ion valence and local surface ion concentration. Even though the low potential linear solution is a good approximation to ψ(x), it introduces in errors at higher surface potentials as illustrated in Figure 3.4b. using same boundary conditions as for a low potential case, and dimensionless potentials and for a monovalent salt solution, the Equation (3.21) can be solved for a general case including cases of ψ_o>50mV. Butt et al. (2013) worked out expression and it is showed in Equation (3.23)

$$e^{y/2} = \frac{e^{y_o/2} + 1 + (e^{y_o/2} - 1).e^{-\kappa x}}{e^{y_o/2} + 1 - (e^{y_o/2} - 1).e^{-\kappa x}} \tag{3.23}$$

Where:

- y_o=$\frac{e\psi_o}{\kappa_B T}$, y= $\frac{e\psi}{\kappa_B T}$ and they are all dimensionless potential terms

There exists a relationship between surface potential, ψ_o and local surface charge density δ_o. This is provided through the Grahame equation, Equation (3.24). For low potential surface, following the same criteria as in Equation (3.21), relationship is provided by Equation (3.25). The relationship work on the principle of electroneutrality of total charge in the system. That is the sum of surface charge and the charge in the bulk should equate to zero.

$$\delta_o = \sqrt{8C_0\epsilon\epsilon_o\kappa_B T}.sinh(\frac{e\psi_o}{2\kappa_B T} \tag{3.24}$$

$$\delta_o = \frac{\epsilon\epsilon_o\psi_o}{\lambda_D} \tag{3.25}$$

The Stern layer, diffuse layer and Zeta Potential

The electric double layer (EDL) can be split into two parts. The inner part called the stern layer and the outer part called the diffuse or Gouy-Chapman layer. In the stern layer, ions are directly adsorbed to the solid surface and are immobile, whereas the diffuse layer consists of

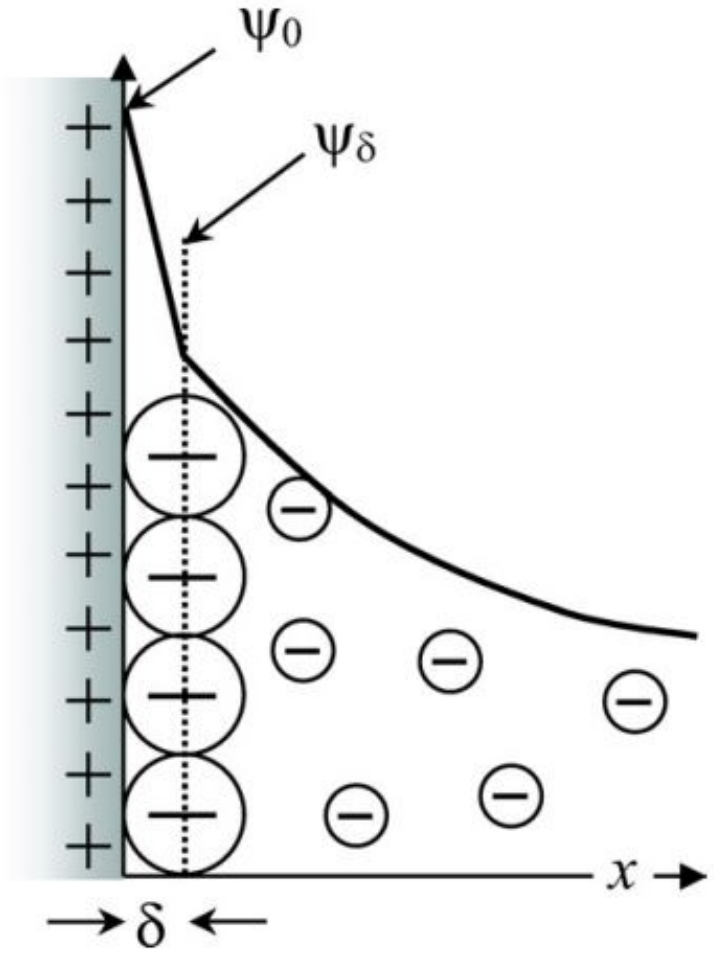

Figure 3.5: Illustration of the Stern layer in an EDL system

immobile ions. The stern layer can be described by the size of counter ions. These ions get adsorbed to the surface within a distance of their hydration shell sizes. This distance between the surface and the center of these adsorbed ions is called the Helmholtz plane. This plane separates the stern layer from the diffuse layer as shown in Figure 3.5. The Helmholtz can also be subdivided into two. The inner Helmholtz consisting of strongly adsorbed counter ions and the outer Helmholtz with hydrated counter ions loosely adsorbed to the surface.

The potential at the point where the stern layer ends and the diffuse layer begins is called zeta potential. It is therefore a potential at a point where ions start to have the freedom to move around in solution. When the potential at this point is zero, then the concentration of potential determining ion (PDI) ions is called the isoelectric point. Zeta potential is easier to measure than surface potential.

Chapter 4

Materials and Methods

In this chapter, the **Materials** section describes rock and fluid materials used to conduct different experiments. Methods for the spontaneous imbibition experiments are described in the **Spontaneous Imbibition methodology** section. The new dynamic aging set up is described in the **Dynamic Aging methodology** section. Sections **Routine Core Analysis (RCA)** and **Special Core Analysis (SCAL)** describe methods used in core analysis. The spontaneous imbibition experiments are described and summarised in **Spontaneous Imbibition Experiments** section. The last part of this chapter is the **Experimental set-up units** section that briefly describes key experimental set up units used in all experiments and reasons for choosing them.

4.1 Materials

In this section, description of rock and fluid samples used to conduct different experiments is given.

4.1.1 Core Material

A limestone rock material was used in rock-fluid experimental studies. Whole cores were provided by Equinor AS, and were all outcrop cores obtained from different places. Ainsa whole core was drilled from an outcrop in Spain, while the Angola core was drilled from an outcrop in Angola. The Ainsa core material was more homogeneous when compared with that from Angola that is shown in Figure 4.1. The Angola core material was more representative of an off-shore reservoir operated by Equinor AS in Brazil. Ainsa core plugs used in this experimental study had been used before by Azizov (2019).

4.1.2 Crude Oil

Dead crude oil was used in the experiment and was provided by Equinor AS. It was tapped from a surface flow line after the final stage separator in 2012. The oil had an acid number (AN) of 3.3mgKOH/g, and base number of 1.2 mgKOH/g. The crude oil was from an off-shore field operated by Equinor AS in the Norwegian sea. Its physical and chemical properties are summarised in Table 4.1. Before any use, the oil was filtered through a 5 μm filter paper to remove wax, pollen, sand particles, precipitates and any other particulate matter that could plug pore space and affect absolute permeability of in test core plugs.

Figure 4.1: Angola Core plugs were dry drilled from this whole core in a direction parallel to the bedding. Deep vugs on the left of the core and the general rough texture hint on the extent of heterogeneity

Temperature (°C)	Density (g/cm^3)	Viscosity (cP)	AN (mgKOH/g)	BN (mgKOH/g)
23	0.886	7.30	3.30	1.20
96	-	5.93	-	-

Table 4.1: Crude oil properties

4.1.3 Brines and brine preparation

A total of 6 brines were used. Five brines were used in spontaneous imbibition experiment. Formation water (FW) had the same composition as formation water in the Ekofisk field. Synthetic seawater (SSW) had the same composition as the North-sea sea water. Synthetic seawater varieties included 10 times NaCl-diluted SSW with $[Mg^{2+}]$ and $[SO_4^{2-}]$ respectively 4 and and 2 times above that in SSW (SSW-2S4Mg), 10 times NaCl-diluted SSW with $[Mg^{2+}]$ and $[SO_4^{2-}]$ respectively 8 and and 2 times above that in SSW (SSW-2S8Mg), 10x-NaCl-diluted synthetic seawater (0.1-NaCl-SSW), and ten times diluted SSW (0.1-SSW). 0.1-SSW was only used in contact angle and zeta potential measurements. Physical properties of the brines used are summarised in Table 4.2. The concentrations of salts in brines are summarised in Table 4.3. All brines were synthetically prepared in the laboratory and the preparatory procedure is described in below.

Brine	Density [g/cm^3]	TDS [g/l]	Conductivity [μS/cm]	Salinity [%]
FW	1.120	247.793	4510	24.00
SSW	0.972	34.82	1053	3.00
SSW-2S4Mg	0.967	32.46	934	2.00
SSW-2S8Mg	0.990	52.945	1406	5.00
0.1-NaCl-SSW	0.960	-	-	-
0.1-SSW	0.900	-	-	-

Table 4.2: Physical properties of the brines

Brine **Salt**	FW [g/l]	SSW [g/l]	SSW-2S4Mg [g/l]	SSW-2S8Mg [g/l]	0.1-NaCl-SSW [g/l]	0.1-SSW [g/l]
NaCl	148.52	23.741	2.374	2.374	2.374	2.734
$NaHCO_3$	-	0.194	0.194	0.194	0.194	0.019
$NaSO_4$	-	3.976	7.952	7.952	3.976	0.398
KCl	5.51	0.755	0.755	0.755	0.755	0.076
$MgCl.6H_2O$	22.93	10.696	85.568	85.568	10.696	1.069
$CaCl.2H_2O$	99.47	1.500	1.500	1.500	1.500	0.150
$SrCl.6H_2O$	13.34	0.024	0.024	0.024	0.024	0.002
Ionic srength, [mol/l]	5.13	0.691	0.883	2.298	0.320	-

Table 4.3: Salt concentrations

Brine Preparation

All brines were prepared at 23°C before loading each in two 550ml-brine reservoirs and eventually placed in the oven. Salts used in brine preparation were at least 99.3% pure and were outsourced from VWR BDH Chemicals-Belgium, Figure 4.2b. Brines were prepared in batches of 2000ml. 1100ml of each brine for spontaneous imbibition and 900ml for any other measurements such as contact angle and zeta potential measurements. During brine preparation, 2000ml of deionised water was placed in a 2000ml beaker and filled up to the mark. Weighed volume of each salt as shown in Table 4.3 was then gently placed in the 2000ml of deionised water.

To minimise errors especially for small weights, the flat glass plate holding weighed salt was briefly dipped in the beaker to completely dissolve away all the weighed salt to the beaker. The beaker was then placed on a magnetic stirrer shown in Figure 4.2a, and its contents stirred for about 5 minutes at 23°C. Afterwards, the stirred solution was transferred to a small-outlet 2000ml flask and stirred further for 2 hours while degassing the brine at same temperature. Degassed brine was then quickly transferred to its respective reservoirs and sealed. When all brine reservoirs were clamped vertically on a stand, they were transferred to the oven. At this point the brines in the reservoirs were ready for use.

4.2 Spontaneous Imbibition methodology

This sections contains a description of an improved experimental design, set up and procedure for spontaneous imbibition (SI) experiments at 96°C . The set up is designed to be an almost closed system with pressure balancing units. The set-up components inside the oven are isolated and not tampered with throughout the experimental time with an uninterrupted SI process. The purpose of the set up is to test the impact of potential determining ions (PDIs),

(a) Magnetic stirrers at RT were used to thoroughly mix and degass brines contained in the two containers shown

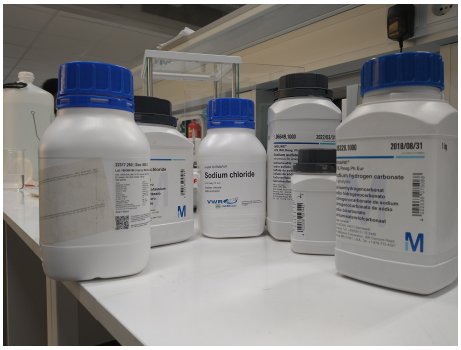

(b) Salts used in brine preparation

Figure 4.2: Synthetic brine preparation process

witrh focus on magnesium, (Mg^{2+}) ion in a sulfate-enriched synthetic seawater (SSW) selectively depleted 10 times in NaCl content, on wettability alteration. This was done by SI of test brines in crude oil-saturated cores plugs. The outcome of the experiment was visualised by improved oil recoveries based on the volume of oil initially in the core (OIIC). The set up also tested the effect of core aging process on crude oil-aged cores by the same methodology.

To achieve these goals, two spontaneous imbibition rig designs were made. The outcome of each design as shown in Figure 4.3 and Figure 4.4 was to allow an uninterrupted SI process, and each will be discussed discretely. Both set ups were utilised in wettability study whereas only the first step configuration was used in core aging studies. Each setup allows for safe decommissioning and any other safety measures reported in Appendix C.3.

Though the new SI set up as a whole is an improved version of the work reported by Azizov (2019), the set up designs and modes of operation are distinctly different as the whole operation is done external to the heating chamber. The procedure allows for SI of brine into crude oil-containing cores without opening the oven when changing from one brine type to another in a serial approach. The new SI set up design is meant to allow the following processes to be carried out when operating it at 96°C . All of the steps were successfully implemented.

1. Degassing and initiating spontaneous imbibition process set-up.
2. Set-up for switch between brines from brine of a higher density or salinity to light brine or brine of lower salinity.
3. Set-up for switch between brines of relatively similar densities or from brine of lower density to a heavier brine.

In all steps, brines are pre-heated in the same rig except for the degassing.

The two set-ups shown in Figure 4.3 and Section 4.2.3 and their modes of operation address most of experimental errors and challenges that were reported by Azizov (2019). The the degassing procedure and pre-heated brines help to eliminate gas from the system. The pumping fluid, Exxsol D60 (D-60) was not degassed before use. Cumulative crude oil production as a result of SI is made inside the Amott cells. This minimised crude oil spreading and sticking on plastic PTFE lines that could otherwise introduce errors on the already small production from the cores. In addition, the set ups guarantees seemingly static conditions when replacing one brine type for another at 96°C . Cumulative produced crude oil with previous brines does not

need to be flushed out, and therefore the spontaneous imbibition process continuously takes place at 96°C without any interruption. The valve network allows external operation of the entire operation without need to open the oven at 96°C that can pose a safety concern to the operator. Pressure build up in the system was eliminated by installation of 2 bar pressure relief valves at the base of the Amott cells and with the brine columns in the external production system.

Before conducting the main wettability experiments, the set ups were first tested to confirm that they safe and operational. The procedure and results of the testing round are not reported in this work. The test was conducted at both room temperature of 23C and at 96°C for all the listed steps. Results of the test run were used to fine tune the designs.

With the design shown in Figure 4.3 and for operations in steps 1 and 2 listed above, three brines were used; formation water (FW), sea water (SW), and 10 times NaCl-diluted SSW with $[Mg^{2+}]$ and $[SO_4^{2-}]$ respectively 4 and and 2 times above that in SSW (SSW-2S4Mg). And in the second design shown in Section 4.2.3 when switching from brine of low salinity to brine of higher salinity, SSW-2S4Mg was used as the crossover brine whereas 10 times NaCl-diluted SSW with $[Mg^{2+}]$ and $[SO_4^{2-}]$ respectively 8 and and 2 times above that in SSW (SSW-2S8Mg) was the new and last test brine in the series. The properties of brines used are summarised in Table 4.2.

4.2.1 System degassing, Leakage test, Initiating Spontaneous Imbibition process

This step removes air from the flow components. It also tests whether all the connection points are tight enough and not leaking. The first test brine, FW, is used to achieve these two points as it simultaneously fills up the Amott cells. The schematic shown in Figure 4.3 was followed. At this stage there is freedom to open the oven for all actions are done at room temperature. Before degassing, all system components internal and external to the oven from the D-60 reservoir to the outside production end are connected. All three way T-valves, from T1 to T8, are in closed positions. The flow systems connected to the two Amott cells are degassed and filled with the first brine one at a time. The full operational procedure for this step can be found in Appendix C.2. Knowing the total volume of the Amott cell and all flow components connected to it to be less than 400ml, and the net volume of each brine reservoir as 550ml, up to 450ml of the first brine is pumped and ensures that the entire systems is free of gas. The test brine in burette outside the oven and the pressure relief valves help to pressure balance the system.

When the system has been successfully degassed, tested for leakages, and stabilised, the oven is closed and set to a temperature of 96°C for 100 days. Temperature starts to rise and reaches 96°C within 30 minutes. No liquid boiling was observed nor any production within this period. After about 2 hours a thin layer of produced crude oil forms at the top of brine in the Amott cell necks. The liquid level rises but is constantly maintained at one level by slowly opening valves T4 and T3 to effluent for less than 1 minute. Cumulative production readings were made in the the neck of the Amott cell after every 24 hours and recorded. With a controlled liquid level, measurement were recorded until when production plateaued and instigated need for change of brine. Though most brines plateaued with in 4 days, 7 days were allotted to each test brine to confirm no further production caused by the brine the system.

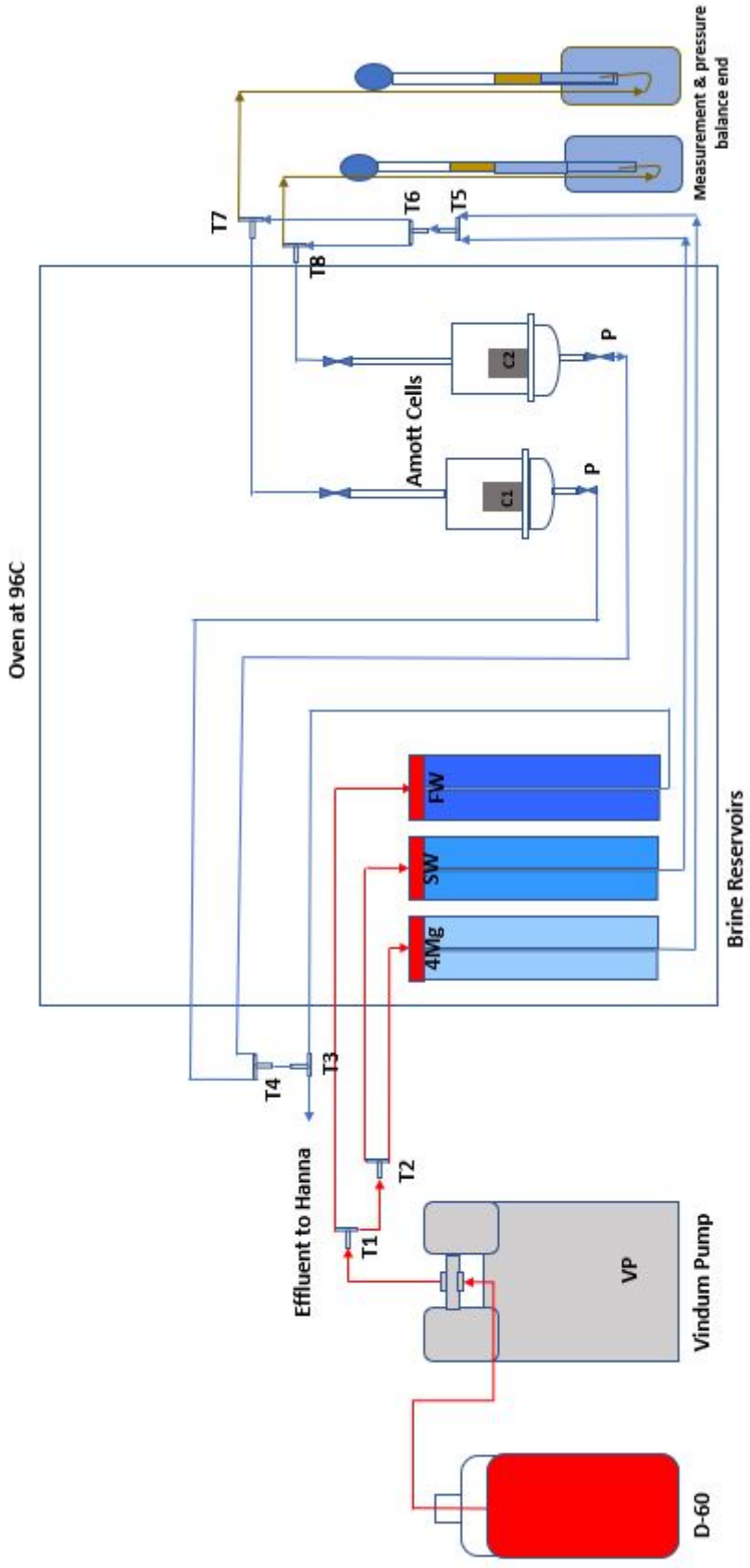

Figure 4.3: Schematic of the spontaneous imbibition setup for replacing a fluid by a lighter fluid. The setup includes system degassing, SI at static conditions and change of brine from dense to light brine at 96°C

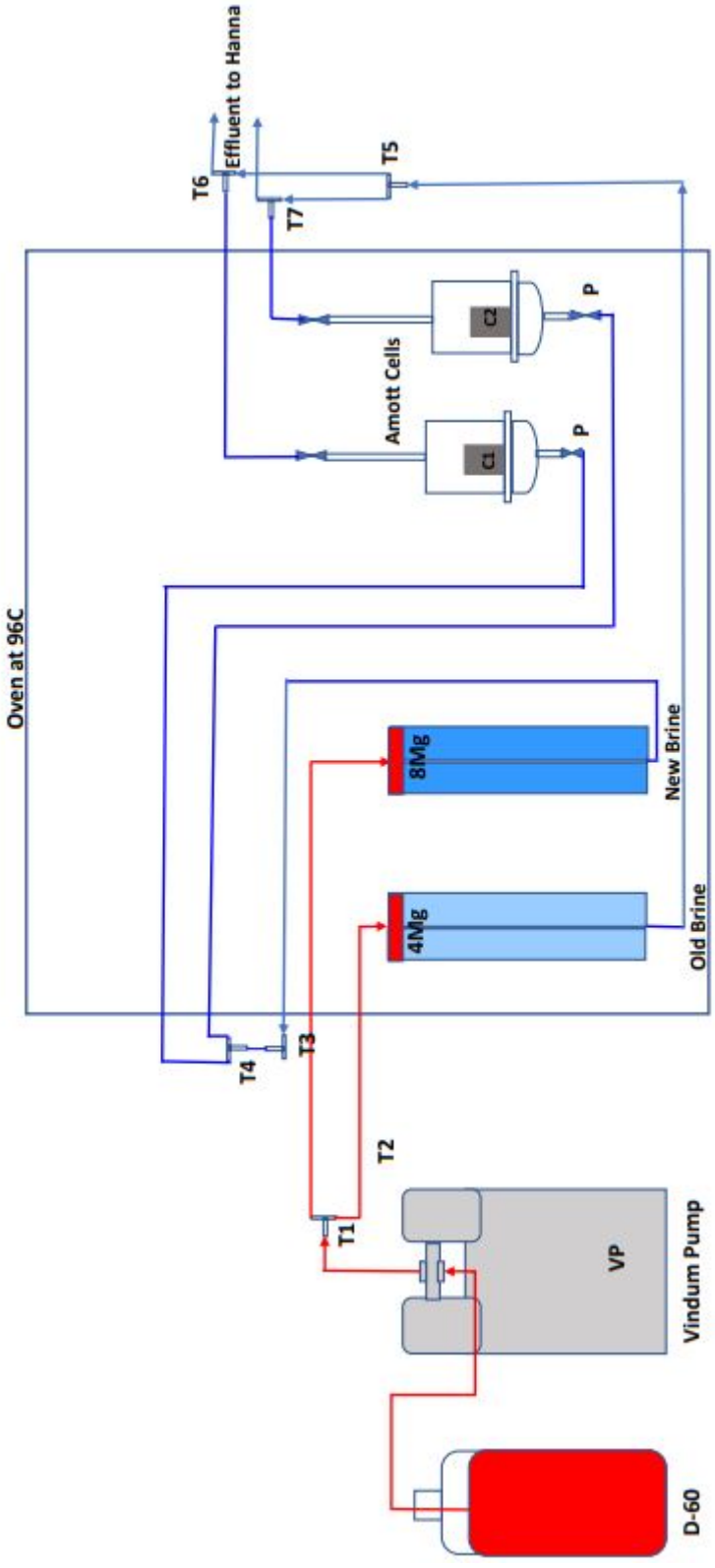

Figure 4.4: Schematic of spontaneous imbibition for changing light brine or brine of lower salinity to a brine of a higher salinity. The setup is inside a heating chamber at 96°C

Figure 4.5:
The piston-like displacement in the right Amott cell. The brine on top is SW while FW at the bottom. A contrast can be made with static conditions in the left Amott cell

4.2.2 Switch from heavy brine to new light brine

When the new brine is lighter than the current brine in the system, the replacement of the current brine by the new brine was done counter-current from the top of the Amott cell. Azizov (2019) showed that at a low rate, a dense brine can be piston-like displaced by a light brine with marginal mixing at the front at 96°C. The same observation was made when the two brines had contrasting salinities, with the incoming of lower salinity. The replacement test was repeated and confirmed the piston displacement.

In this study, FW was replaced by SW, which in turn was replaced by SSW-2S4Mg, and Figure 4.3 shows the configuration. Change of brine is done for each Amott cell system one at a time. During change of brine, both the current brine and new brine are at 96°C. A full operational procedure for this step can also be found in Appendix C.2. During the change, a piston-like displacement could be observed in the cell as depicted in Figure 4.5 in 5 minutes. The layer of produced crude oil in the Amott cell neck shields the brine below from any form of disturbance, which prevents production during the change. A complete change of brine was noticed by keeping track of salinity of the effluent after pumping in about 300ml of D-60. For FW and SW, the salinity changed from 2.4 to 0.3, Table 4.2, after about 350ml. After successful change of brines, productions readings were recorded every 24 hours until 3 days after plateauing.

4.2.3 Switching when new and old brines are of relatively similar density or New brine of higher density/salinity than old brine

This set-up was used when changing from SSW-2S4Mg to SSW-2S8Mg. Brine SSW-2S4Mg is of a lower salinity and density in comparison with Table 4.2. Azizov (2019) observed and concluded that pumping from the base of the Amott cell would result in minimal mixing of

the two brines. The configuration shown in Figure 4.3 is meant for this kind of change of brine. During change of brine, cumulative production from the previous round is flushed out at 10ml/minute before cooling down the oven. The pumped out crude oil is collected in a burette and its volume confirmed with the cumulative volume in the Amott cell neck noted before pumping. The oven is then cooled down and the procedure in Appendix C.2 followed. Brine SSW-2S4Mg is tested over 24 hours before introducing SSW-2S8Mg to confirm no further production with it.

4.3 Dynamic Aging Methodology

An experimental configuration for dynamic aging at temperatures of up to to 96°C and pressures as high as 35 bars was set up. Conditions above these were not tested. The set up is shown in Figure 4.6 and is designed to achieve injection of dead crude oil into a core or cores placed inside a steel hassler core holder under confining pressure of up to 35 bars. The experimental procedure can be found in Appendix C.1. With all connected flow components, confining pressure is activated and set at 35 bars. In the case of Ainsa core plugs, sleeve pressure was not used. All T-valves from T1 to T5 were opened and the Isco pump (which was later replaced with a a Vindum pump for visualisation reasons), set at a rate of 1.5ml/hour. The back pressure regulator was activated to 2 bars. The oven temperature was set at 96°C and time set to infinity. With the piston placed inside the crude oil reservoir, D-60 pushed out and injected crude oil into the the core inside the core holder. Angola core plugs were tight with permeabilities between 0.3 and 11mD. Each core plug was placed in a separate core holder. For every moment in time, a new batch of crude oil with probable surface active components flows through the core. Fernø et al. (2010) says that dynamic aging becomes effective when aging lasts for at least 3 days. In the current study, Ainsa and Angola cores were respectively aged for 90 and 28 days.

4.4 Routine Core Analysis (RCA)

A number of measurements were made and description of procedures followed for each measurement is given in this section. These methods were meant to prepare each core plug for further special core analysis and and later be utilised in wettability tests.

4.4.1 Core drilling

Ainsa core plugs were drilled by Azizov (2019) while Angola core plugs were drilled from the whole core at the Thin section Laboratory. Considering that the rock material was a salt, drilling it required a lot of attention. First the drill bit coolant had to be compatible with the rock to successfully ensure no salt dissolution and tampering of the rock material. Pressurised dry air was used as a coolant to the drill bit. A diamond toothed drill bit was used for drilling but at a lower RPM. This made it possible not to create any cracks in drilled plugs. Drilling was done in the direction apparent to be the direction of bedding, figure 4.1 and this preserved intrinsic physical features in each plug.

4.4.2 Core cleaning and drying

Core cleaning process depicted in Figure 4.7 was done to restore, though difficult to achieve, a complete core water wetting state. The cleaning process removed all fluids and the particulate matter including dust that were probably residing in pore spaces. Before cleaning and

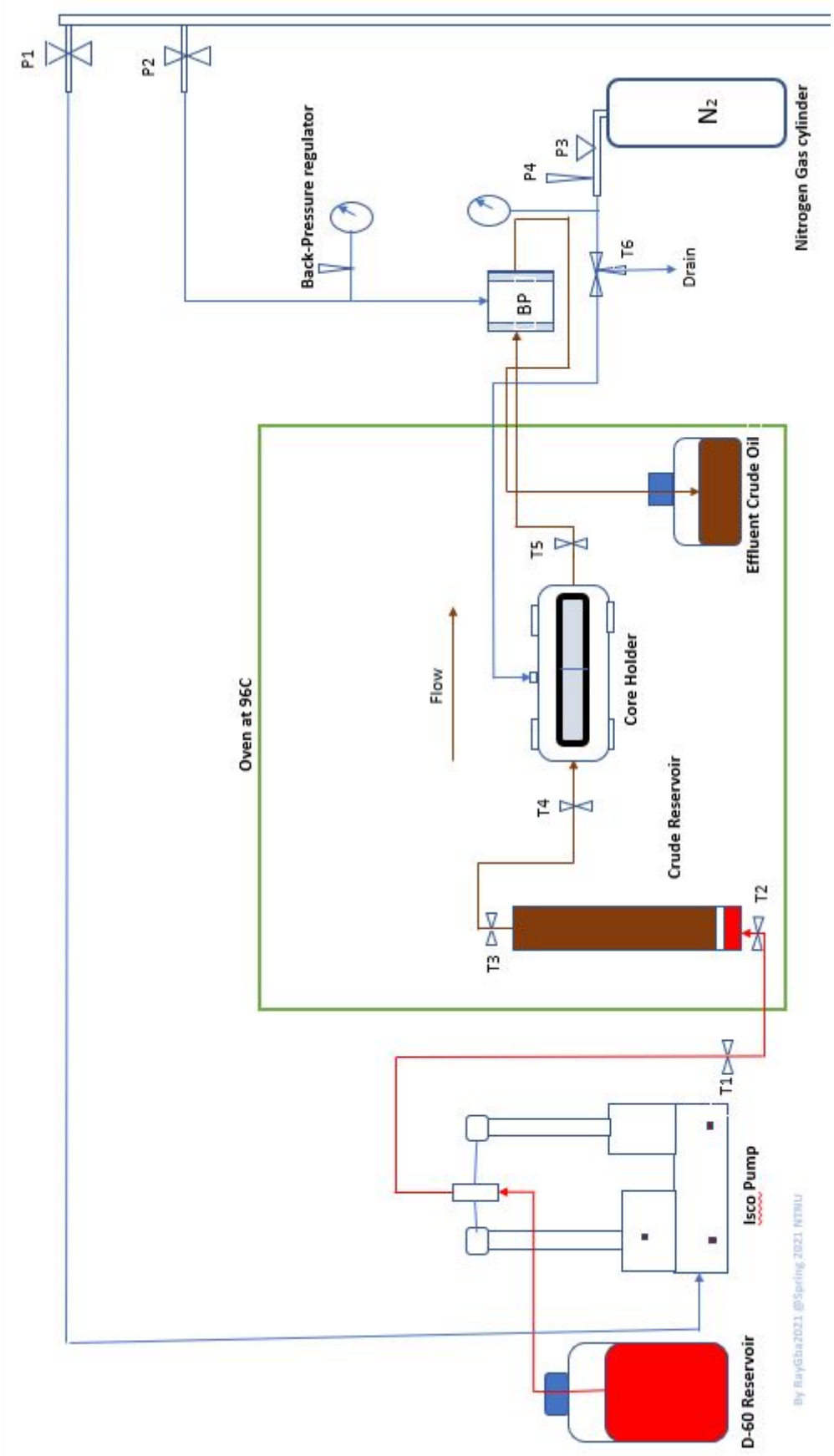

Figure 4.6: Schematic for the new experimental set up for dynamic aging at high temperature and high pressure of less than 35 bars

after drying, weight of each cores was recorded to note any weight difference due to displaced matter in the core. Eleven cores were cleaned. Two Ainsa core plugs, (B5 and B6), and all 5 Angola plugs were cleaned in methanol for one day and the apparent no change in the colour of methanol did call for no further cleaning in Toluene.

After cleaning, they were immediately placed in a drying oven at 60°C for 5 days. The remaining 4 Ainsa core plugs, (B1, B2, B3 and B8), were cleaned in Toluene for 5 days. In the first 3 days, dirty Toluene in the Soxhlet reservoirs was changed and replaced with clean toluene. On the last 2 days, the colour of toluene remained clear which indicated that the cores were free of any organic matter. After cleaning in toluene, the 4 Ainsa plugs were immediately placed in the drying oven and dried for 5 days.

Figure 4.7: Core cleaning by Soxhlet. Methanol and Toluene were used as cleaning solvents

4.4.3 Core storage

At all times uncleaned dry cores plugs were always wrapped in aluminium foil whereas those saturated with crude oil were kept in sealed containers and still submerged in crude. All cleaned core were kept at room temperature and at all times wrapped in aluminium foil. All this was done to minimise the impact of ambient conditions on the core material. For example Angola plugs had patches of rust on their surface and so the extent of rusting had to be minimised by wrapping in aluminium foil to cut off moisture and air supply.

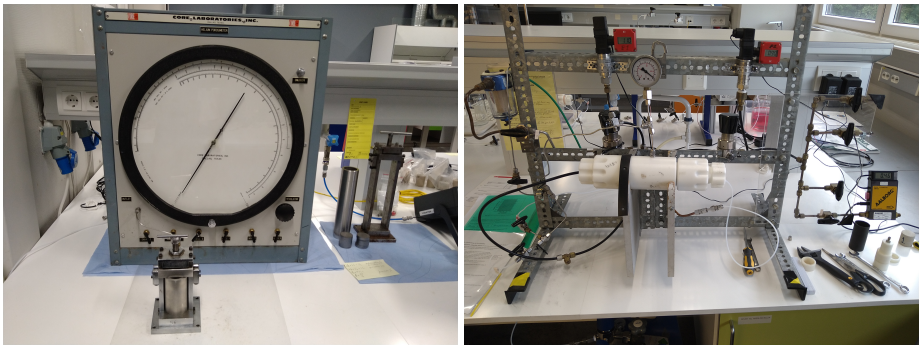

(a) Porosity measurement setup **(b)** Permeability measurement set up

Figure 4.8: Porosity and air permeability set ups

4.4.4 Porosity Measurements

Porosity measurements of all cores were made using a helium porosimeter, Figure 4.8a, and bulk volume measurements. From the helium porosimeter experiment, grain volume V_2 of each core was determined while respective bulk volumes V_b were calculated from using average core diameter and length measurements. Core diameter, D and length, L were measured using a digital vernier caliper. For each dimension, 4 measurements were made and their average calculated and recorded.

Porosities of core plugs B1, B2, B3 and B8 were determined using the liquid saturation method. With known dry weight of each core and FW density, wet weight of each core was determined after saturating the cores in FW by a vacuum pump method described in Torsæter and Abtahi (2003). Before making wet weight measurement, the core was shaken for 10 seconds to minimize weight errors due to surface volumes. Care had to be taken on Angola plugs that were vugy.

4.4.5 Permeability Measurements

A constant head permeameter was used to measure permeability, Figure 4.8b and Figure 4.9. Gas permeabilities were measured from which Klinkenberg-corrected liquid permeabilities were obtained from a plot of reciprocal mean pressure versus gas permeability. During the experiment, a core was placed in a hassler core holder and surrounded with a rubber sleeve. A confining pressure of 10 bars was applied on the sleeve. At least 4 gas rate measurements were made. Using the Darcy equation, (Equation (4.1)), gas permeability for each rate and pressure drop was measured and recorded.

$$Q = \frac{Ak(P_1^2 - P_2^2)}{2\mu L P_{atm}} \tag{4.1}$$

Where:

- Q is the recorded steady gas flow rate, A is crossection area of the core, k gas permeability to be calculated, P_1 and P_2 upstream and downstream pressures, *mu* gas viscosity, L length of the core, P_{atm} atmospheric pressure

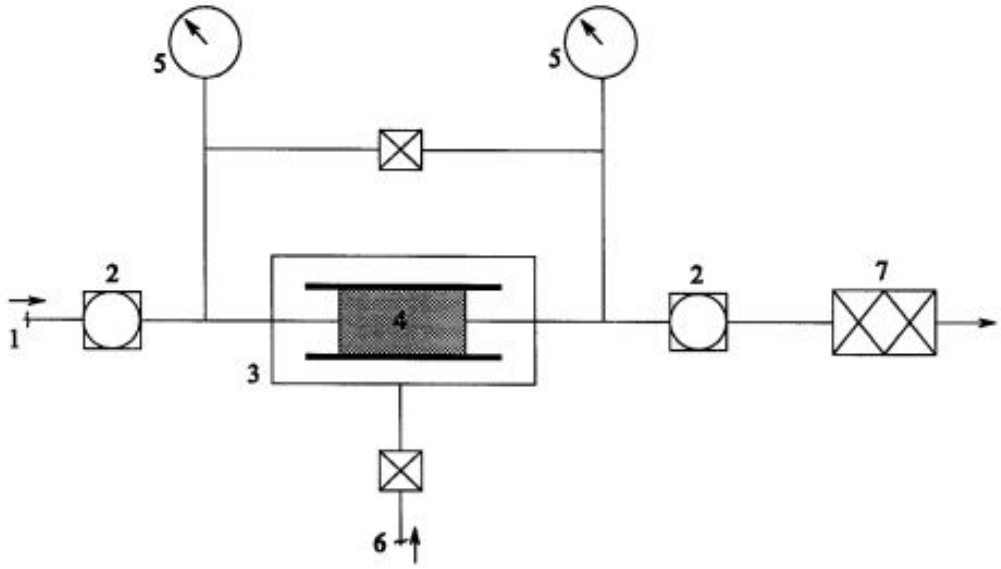

Figure 4.9: Schematic of a constant head permeameter. 1-air supply, 2-reduction valves, 3-core holder, 4-core sample, 5-manometers, 6-sleeve pressure, 7-Gas volume meter (Torsæter and Abtahi, 2003)

4.4.6 Density measurements

All brine and oil densities were measured by weighing a knowing volume of each fluid placed in a graduated cylinder. To mute out the cylinder weight, the scale was tared after placing an empty dry cylinder on top of it. In each density measurement, 4 measurements were made and an average of the 4 was considered the liquid density. The core material grain density, ρ_g, was calculated according to Equation (4.2) using core plug dry weight from Section 4.4.2, and the grain volume from helium porosity measurement.

$$\rho_g = \frac{W_{dry}}{V_g} \tag{4.2}$$

Where:

- W_{dry} is the core plug dry weight, and V_g grain volume

4.4.7 Formation water saturation (100%)

Fully 100% formation water saturated cores were prepared according to the saturation procedure suggested by Standnes and T. Austad (2000). Five Angola and 6 Ainsa cores were saturated in formation water (FW), using the vacuum pump, figure Figure 4.10. The weight of a clean dry core and its weight after FW saturation were recorded. The difference between the two weights was used to calculated the porosity of each core plug.

The vacuum pump was first activated with the core inside to ensure that a good vacuum was created inside and stabilised at 0.1 bar on the pump meter. After a stable pump reading, formation water was let into the core from above the evacuator to the beaker containing the core plug until when the core was fully submerged. The vacuum pump was run for 2 hours and during this time FW in the beaker could be seen boiling which confirmed a good evacuation procedure. To minimise air from being introduced and sacked into the core, about 100 ml of

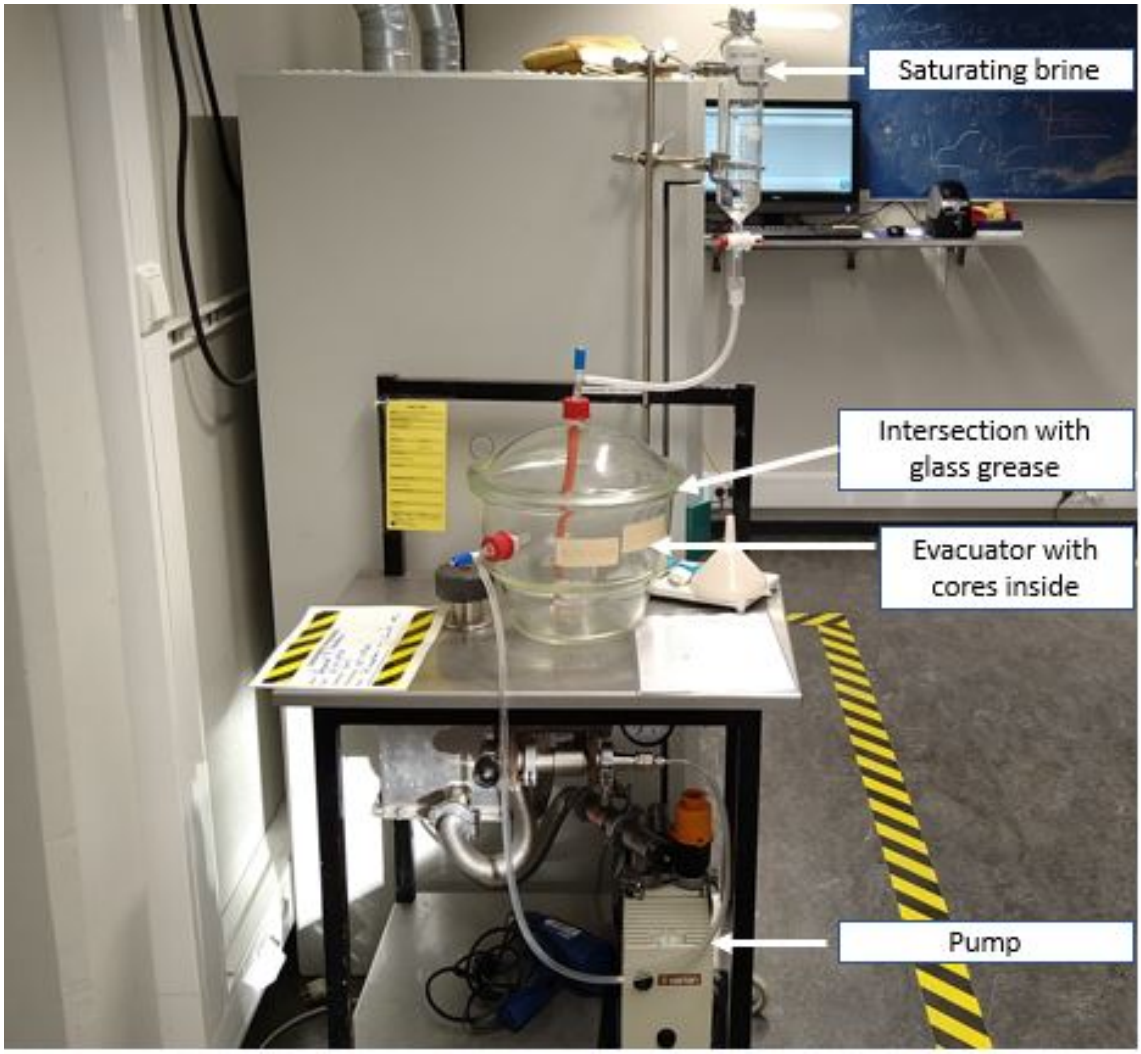

Figure 4.10: FW Saturation of all core plugs in the vacuum pump

FW was left left inside the reservoir. The core plugs were then removed from the evacuator and aged in the same brine and weighed again after 2 hours. They were then aged in the same brine for a period of 5 days at 23°C . A second wet weight measurement was done and for all core, the two wet weight were similar with a percentage difference of between 1-0.3% . The larger variation was in Angola cores due to their vugy surfaces.

4.4.8 Core aging

Angola core plugs C1, C2, and C3 were dynamically aged under sleeve pressure at 96°C according to the procedure described in Section 4.3 and Appendix C.1. Ainsa cores except B8 were aged in the same way but without confining pressure. Core plug B8 was aged statically in a steel glass cell a the same temperature and in the same oven.

4.4.9 Viscosity measurements

Crude oil viscosity measurements were done using a Brookfield viscometer DV-11+ Pro, Figure 4.11. Its a rotational type viscometer with a bob and spindle set up. Viscosity measurements

Figure 4.11: Viscosity measurements set up. The heating chamber, with red digits, made it possible to make measurements are 96°C

were done at both 23°C and 96°with 20ml 31-spindle and 10ml 18-spindle, respectively. For accuracy reasons,the torque was kept with in 24% at RPM of 100, 120 and 160.

4.5 Special Core Analysis (SCAL)

This section describes procedures that were used to study the chemistry of the pore surface , back-scatter electron imaging (SEM) analysis, and procedure for establishing irreducible water saturation (Swi).

4.5.1 Contact angle measurements

Contact angle measurements were made with the goniometer KSV CAM200. This goniometer has a reported accuracy of ±1°and uses curve fitting image analysis algorithms to determine contact angle measurements at the 3-phase contact in a liquid-solid system. All brines described in section Section 4.1.3 were used in contact angle measurements except 0.1-SSW. Only static contact angles were made. Two well polished, 35mm diameter chips, cut from the solid end caps of the Angola core material were used in the measurements. Chip 1 and chip 2.

decision to cut these end caps was based on CT images which revealed that these sites were indeed solid and impermeable. End caps were shaped, sized and polished at both diameter ends into chips at the Thin Section Laboratory at the Department. Polishing made the two end of the chips even more solid and impermeable. To ensure exposure to same conditions, the 2

Figure 4.12: SI rig internal arrangement. The 6 white cylinders clamped on blue stands are the brine reservoirs. They are connected with white PTFE lines to the two Amott cells on the right. Not the pressure relief valves installed at the base of each Amott cell.

polished chips were statically aged in crude oil in one steel aging cell for 20 days.

In all contact angle measurements on each chip, measurements were done using only one polished side and on an area about $\frac{1}{4}$ of the surface. Before measurements were made, the chip was rested on two short nuts placed inside a transparent glass box. The chip was then submerged in a test brine. Using a hook-shaped needle, an oil droplet was gently placed on underneath side of the chip. It was done so because all brines used were denser than crude oil. At this stage the glass box was closed, and with a fitted adjustable screw at its top tightened to firmly grip the chip in position during measurements. After every round of measurement, the chip was gently cleaned of all crude oil by pressing it between soft tissue and then gently rubbed with a Nitrile surgical glove before exposure to the next test brine. Four sets of contact angle measurements were done.

First Contact angle measurements

In this set only one oil droplet on chip 2 was used and was sequentially exposed to FW, SW, SSW-2S4Mg, and SSW-2S8Mg at 23°C. Contact angle measurements were made every 30 minutes for 2 hours in each brine. Change from one brine to another was achieved with the use of a peristaltic pump that delivered or sucked out 75ml of brine in 8 minutes. The procedure was based on the piston-like displacement described in Section 4.2.2. Measurements in FW revealed that the surface was completely oil wet. Further measurements in other brines

revealed no significant change in measured contact angles.

Second Contact angle measurements

Measurements in this case were done to test the impact of potential determining ion (PDI)s in wettability alteration with focus on Mg^{2+} and SO_4^{2-}. Chip 2 was used in this set of measurements. Before exposure to the first brine, formation water, the chip was rinsed in deionised water and dried to get rid of all residual SSW-2S8Mg from the 1^{st} test. Chip 2 was then sequentially aged in each test brine at 96°C for 24 hours. After aging, the chip was cooled down and contact angles measured in same brine at 6 different sites using 6 oil droplets. FW was used first followed by SW, SSW-2S4Mg and then SSW-2S8Mg last. After SSW-2S8Mg, the chip was again aged in FW to test if the observed trend in angles could be reversed to the initial state at the start of the sequence. To minimise errors due to mineral heterogeneity, all measurements were made at the same sites on the chip in all brines.

(a) The used polished ends of the 2 chips

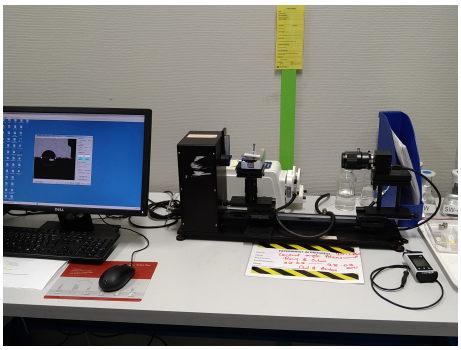

(b) The goniometer set up for contact angle measurements. Including the pump for the 1^{st} category

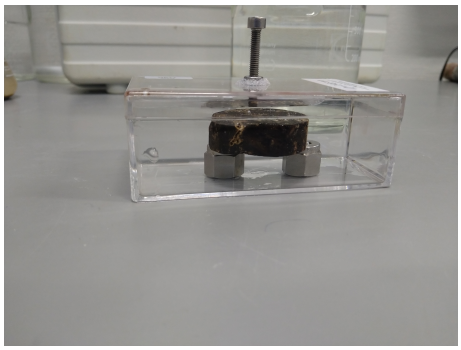

(c) A fabricated transparent glass box with a fitted screw to hold the chip in position as it rests on th two nuts.

Figure 4.13: Contact measurement angle set up

Third Contact angle measurements

In the third case, FW, SW, and 0.1-NaCl-SSW were test brines. The objective of this category was to test the effect of selective dilution of NaCl in SW has on the activity of PDIs during wettability alteration. The chip 1 aged in each test brine for 3 days at 96°C was used. Measurements in each in brine were made after every 24 hours.

Fourth Contact angle measurements

The purpose of this category was to test the impact of temperature on activity of PDIs during wettability alteration. The same procedure described in 2^{nd} category was followed except that chip 2 was aged in each brine at 23°C. After treatment in the 2^{nd} category, the chip was hard cleaned in toluene and methanol for 3 days and then dried at 60°C for 2 days. It was then re-aged statically in crude oil at 96°C for 15 days.

4.5.2 Zeta Potential measurements

Zeta potential measurements were done using the Zetasizer Nano ZS. All 6 brines described in Section 4.1.3 were used in ZP measurements at either 25°C or 70°C. Measurements could not be conducted at 96°C due to a temperature limitation of the instrument with its upper limit at 70°C. ZP measurements were done on a 5% wt limestone rock powder suspended in a 95% wt test brine. The powder was was obtained from the end rock craps of the Angola core material and was prepared using a diamond grinder at the Thin Section Laboratory. The particles in the powder were filtered and at least 85% of them were 8μm or less in diameter. Measurements were done at pH values summarised in Table 4.4.

Temperature 23(°C)	FW	SW	SSW-2S4Mg	SSW-2S8Mg	0.1-NaCl-SSW	0.1-SSW
Fresh powder	6.74	8.28	7.86	7.75	8.11	8.40
Crude oil aged powder	7.14	8.3	7.91	7.74	8.1	9.16

Table 4.4: Brine suspension pH condition at test point

Two categories of measurements were done. The objective of the first category was to test relative adsorption of PDIs in sea water or sea water varieties. The rock powder was suspended in each brine test brine in a glass vial. The mixture was gently stirred for 48 hours until equilibrium was established. A small sample of each mixture was then loaded in a folded capillary cell DTS1070 of the Zetasizer Nano ZS. ZP measurements were done at 25°C and then 70°C on the same loaded sample. Though some degree of particles settling out of solution was observed, Figure 4.14, majority of them stayed in suspension and therefore reliable measurements were done.

In the second category, measurements were made on a powder aged first at 96°C in crude oil. The procedure for powder preparation before mixing it in each test brine is given in Appendix B.2.1. The test pH conditions are summarised in Table 4.4. The second category experiment was then conducted like in the first category. The objective of this test was to study the adhesion effect of surface active components in crude on the activity of PDIs during wettability alteration. The ZP experiment in its entirety also looks at the DLE mechanism in relation to surface charge. In all zeta potential runs, 15 measurements were made and an average value was spit out for recording per round of a run.

4.5.3 Centrifugal irreducible water saturation

All core plugs used in this study were driven to irreducible water saturation using a centrifuge. The Beckman centrifuge, *Beckman Coulter Optima L-80 XP Ultracentrifuge* was used. Before placing core plugs into the centrifuge, core holders (cups) and cores were thoroughly prepared to ensure good and safe centrifuging. The weight difference among cups, with their

(a) Particles uniformly distributed in suspension in a DTS1070 Zetasizer cell before loading in a Zetasizer

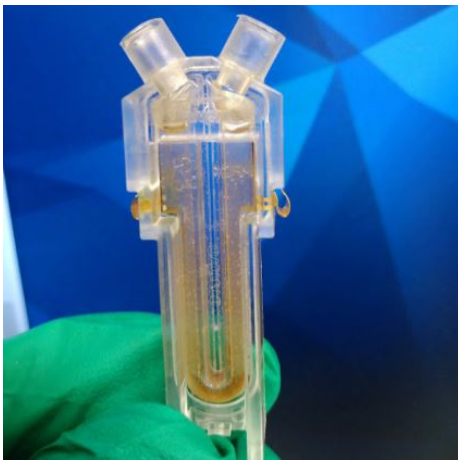

(b) Particles settling out of suspension in a DTS1070 Zetasizer cell after unloading from a Zetasizer

Figure 4.14: Particle distribution in a DTS1070 Zetasizer cell

contents, was kept with in ±0.05g. This guaranteed safe swirling. The centrifuge, connected to a control computer, was reconfigured using a Weatherford source Centas Optima application. Reconfiguring involved setting parameters such as RPM to 5000 for Ainsa core plugs, centrifuging time to 10 hours, temperature to 24°C, rotor acceleration and deceleration to maximum and activating the vacuum. Figure 4.15(a) and (b) respectively show cup preparation before loading into the centrifuge and a schematic of the drainage process.

Before centrifuging core plugs classified as Angola, plugs C1, C2, C4 and C5, centrifuge parameters especially the RPM and centrifuging time needed to be adjusted to higher values. This was because the the Angola core material was different from its Ainsa counterpart. The Angola core material was more vugy, heterogeneous and tight, Section 4.1.1. The petrophysical properties of the Angola material were analogous to the material that was used by Yi et al. (2012). Short core plugs C4 and C5 were used in a short centrifuging test run at an RPM of 8000 and 10 hours. The run was to test whether a low Swi within 10-20% could be archived at that RPM while keeping the mechanical and structural integrity of the core plug intact.

After a successful test run, plugs C1, C2 and C3 were set for a centrifuging run at RPM=8000 and 10 hours. Core plugs were checked whether they were submerged in crude both before and after the run in order to ensure that no air infiltrated into the system. Care was taken in tightening the different components of the centrifuge cups so as to ensure no mass loss to leaking. The cups with their contents inside were weighed before and after to provide another check for mass conservation.

The crude oil used in centrifuging, and the rest of the experiments, was filtered though a 5μm filter paper. Filtration was done to remove all the wax, precipitates, sand particles, pollen and any other particulate matter that could potentially damage porosity and permeability of the core plugs

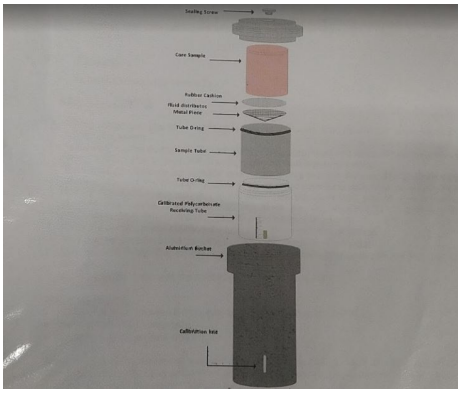

(a) Arrangement of different components of centrifuge cups (Coulter, 2006)

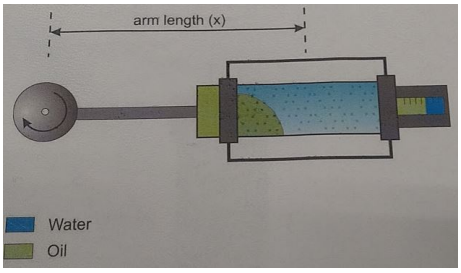

(b) Illustration of the drainage process during centrifuging (Coulter, 2006)

(c) Preparing different components of the centrifuge cup before centrifuging

Figure 4.15: Key steps in the centrifuging process

4.5.4 Back-Scatter Electron imaging, SEM

Back scatter electron imaging was done on Angola limestone thin sections. Thin sections were prepared from the end caps of core plugs C1 and C2 at the Thin Section Laboratory. The immersion fluid used was an epoxy resin. The thin sections were qualitatively analysed for elemental composition which hinted on the mineralogical composition of the Angola core material. X-ray diffraction had already been done on Ainsa core plugs by Azizov (2019) and were already known to be at least 98% limestone with no anhydrite precipitate.

4.6 Spontaneous Imbibition Experiments

All previously described methods and materials in this chapter were prerequisite steps to the the main spontaneous imbibition experiment about wettability alteration in limestone cores. According to the third objective outlined in Chapter 1, a high temperature spontaneous imbibition rig was set up, Figure 4.12 and used in all SI experiments.

The first application was done on testing the role played by potential determining ions in wettability alteration of a limestone surface from an oil wet state to a more water wet state with main focus on Mg^{2+} in a sulfate-enriched sea water depleted in NaCl content, objective 1 and 2 in Chapter 1. Two runs of these experiments were successfully made according to the procedure described in Section 4.2 and Section 4.2.3. All experiments were conducted at 96°C.

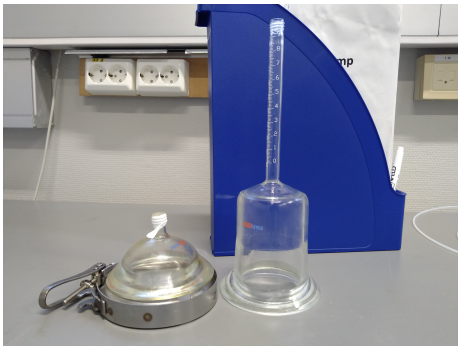

(a) The high temperature Amott cell used

(b) An oil-saturated core standing vertically on a perforated copper stand placed on the conical end of the Amott cell

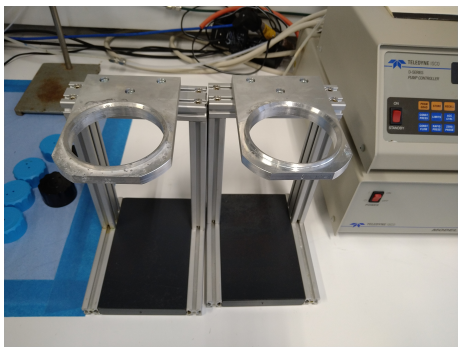

(c) Weight at the base of the stand held to keep the Amott cell stable and safe from any tripping due to weight burden

Figure 4.16: The Amott cell and its extra components

In the first run brines formation water (FW), sea water (SW), 10 times NaCl-diluted SSW with $[Mg^{2+}]$ and $[SO_4^{2-}]$ respectively 4 and and 2 times above that in SSW (SSW-2S4Mg) and 10 times NaCl-diluted SSW with $[Mg^{2+}]$ and $[SO_4^{2-}]$ respectively 8 and and 2 times above that in SSW (SSW-2S8Mg) were tested. According to Tweheyo et al. (2006), Zhang et al. (2007) and Strand et al. (2008), the Mg^{2+} ion begins to be active in wettability alteration processes in limestone at about 80°C and in the presence of SO_4^{2-}. The sequence of brines in this run was testing these two ions. Each brine was tested for 7 days and crude oil recoveries in that period were made and recorded. Characteristic of the production trend was also observed with the biggest response at switch from FW to SW and prolonged production from SSW-2S4Mg to SSW-2S8Mg.

In the second run, the effect of selective dilution of SW with respect to NaCl was tested. Four brines, FW, SW, 0.1-NaCl-SSW and SSW-2S4Mg, were used sequentially in that order. The difference between SW and 0.1-NaCl-SSW was the NaCl content with it being 10 times less in 0.1-NaCl-SSW. Each brine was also tested for 7 days, except FW for 3 days, and crude oil recoveries in those periods were made and recorded. SSW-2S4Mg was considered to test and confirm that selective dilution of monovalent ions Na^+ and Cl^- improves the activity of PDIs during wettability alteration at high temperatures.

The 4^{th} objective in Chapter 1 was to study the best aging process for restoring a representative initial oil-wetting state suitable for wettability studies. After a successful dynamic rig set up, core B1 and B8 respectively aged dynamically and statically were used in the 3^{rd} spon-

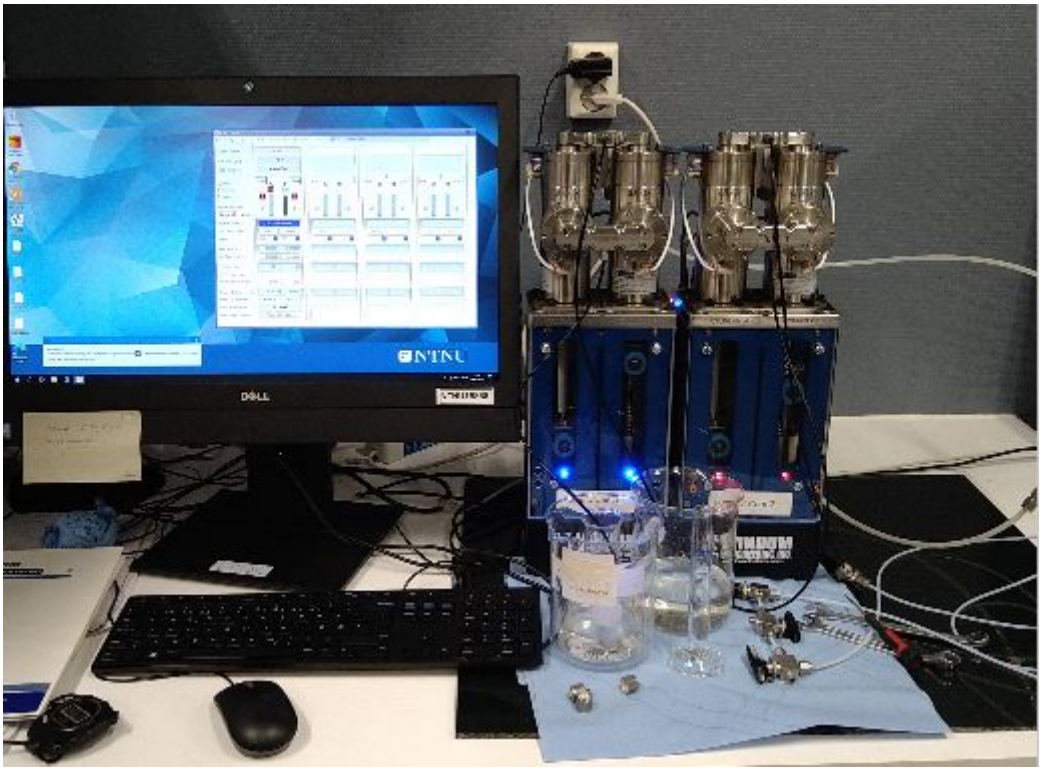

Figure 4.17: The vindum pump

taneous imbibition experiment to study this effect. The experiment compared the crude oil wetting states in both plugs. Two brines FW and SW were used. Each brine was allotted 7 days and in that period crude oil recoveries and recovery rates were observed and recorded.

4.7 Experimental set-up units

4.7.1 Amott Cell and Core Stand

High temperature Amott cells designed for spontaneous imbibition of core plugs surrounded by a test brine were used. The cell material can withstand a temperature as high as 120°C and pressure of 2 bars. To keep pressure in the system below 2 bars, a 2-bar pressure relief valves was installed at the base of teach Amott cell. The Amott cell is designed in such a way that any produced oil can be collected and read from the cell's 10ml-graduated neck and it was what was used. The bottom end of the end is conical and therefore not good to keep a core plug in a vertical position. To keep the plug vertical, perforated copper core stands were utilised. The perforated base allows imbibing brine to also penetrate the core from its base. The sides and top of the core are free and left in direct contact with test brine. An extra weight at the base of the core stand, , helped to keep the Amott cell in position. This minimised any chance of the Amott cell breaking due to tripping caused by loaded weights inside it. The whole set up is shown in Figure 4.16.

4.7.2 Pumps

In both SI and dynamic aging process, a dual-piston high-pressure metering vindum pump provided by Vindum Engineering Inc. was used. The pump can deliver ultra-precise, pulse-

Figure 4.18: Brine reservoirs held in vertical position with steel stands. PTFE lines are connected to the reservoirs

free, continuous flow in either constant-pressure or constant-rate modes, and has a good visual interface, Figure 4.17. It can deliver at a minimum rate of 0.1μl/minute and maximum of 29ml/minute. During change of brines in SI set-ups, a rate of 10ml/minute was used. For dynamic aging, the pump was set to deliver crude oil at a rate of 1.5ml/hour. The pump can pump fluids at 160°C. In order to preserve the integrity of the pump, D-60 at 23°C was used by the pump to pump fluid in reservoirs at 96°C. Before using the pump, a safety pressure had to be defined. When pressure in the system rises above the safety pressure, the pump automatically stops pumping. In order to protect the most vulnerable components in the setup from bursting, (PTFE flow lines), a safety pressure of 27 bars was used.

4.7.3 Brine Reservoirs, Flow lines and Stands

High temperature plastic brines reservoirs made of reinforced Teflon were used to hold pre-heated degassed brines. Flow between components was achieved with high temperature poly-tetrafluoroethylene (PTFE) flow lines. The lines have an inner diameter of 1.5mm and can withstand pressure as high as 35 bars. A safety pressure of 27 bars set with the Vindum pump was far below PTFE line threshold bursting pressure. In order to keep brines reservoirs vertically placed, and their bottom ends at the same height with the lower outlet of the Amott cells, short steel stands were used. All the three components are shown in Figure 4.18

4.7.4 Flow Controls and External Production Network

In spontaneous imbibition experiment, flow was controlled outside the oven by manually operating appropriate 3-way T-valves. In the external production network, valves T7 and T8 were utilised to switch between communication between brine reservoirs and Amott cells, and

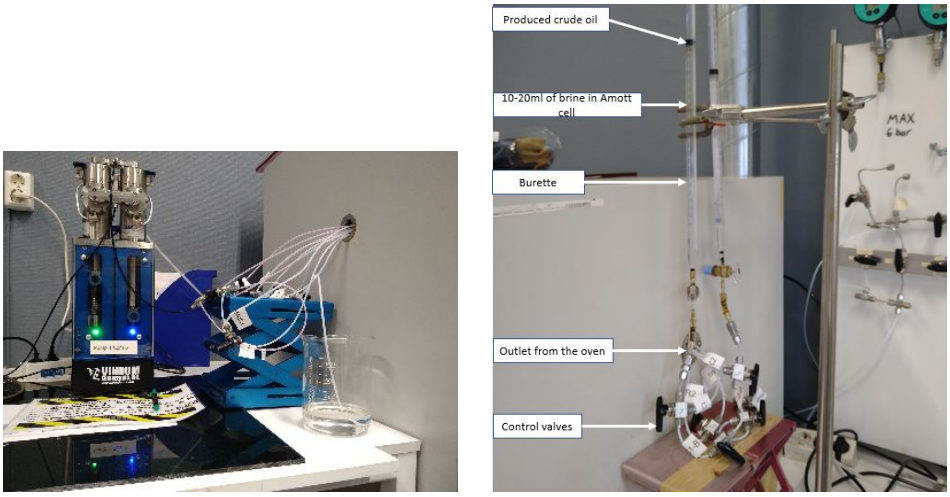

(a) Injection end of the oven **(b)** External production end of the oven

Figure 4.19: Flow control with T-valves and internal production measurement made it possible to not open the oven during SI process

between burettes and Amott cells. The burettes were kept at 23°C and were used to confirm cumulative production collected in the graduated necks of Amott cells, Figure 4.19. The burette set up allowed gas in the system to exit to the atmosphere and therefore prevented a pressure build up in Amott cells.

4.7.5 Hassler Core Holder, and Crude oil Reservoirs

In the dynamic aging set up, a steel hassler core holder was used, Figure 4.20a. The core holder had a 4mm-thick rubber sleeve inside it. With applied confining pressure of 35 bars, the rubber sleeve would hold tightly against the core and force flow through the core in one direction. Care was taken when applying sleeve pressure, and recommended procedure and safety measures are in the risk analysis report Appendix C.3. End pieces of the core holder in contact with the core were grooved to increase surface area and also provide a good contact between injected crude oil and the core inside, Figure 4.20b. Capillary end effects were also minimised with the grooves. To avoid plastic from reacting with crude oil, and thus changing its chemistry, high temperature 500ml-steel reservoirs were used to hold pre-heated crude oil. A piston was placed inside each reservoir and separated the pushing D-60 from mixing with crude oil since both are miscible.

4.7.6 Pressure Sources

Confining pressure during dynamic aging was sourced from a 300-bar nitrogen gas (N_2) cylinder. Gas pressure before exiting the cylinder was choked and regulated to 35 bars with a 65-bar regulator. Applied back pressure was sourced from a wall pressure line in the laboratory and was regulated at 2 bars using a back pressure regulator shown in Figure 4.20c. Safety pressure defined for the vindum pump was also sourced from the wall pressure line. Safety measures concerning handling these pressure sources can be found in Appendix C.3.

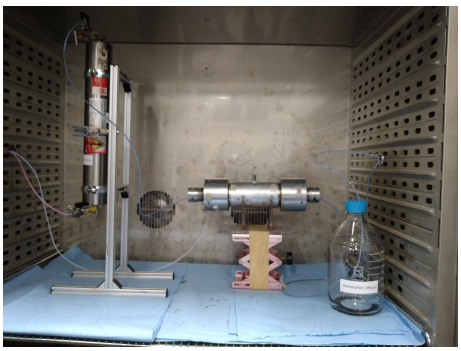

(a) A steel Hassler core holder at 96°C and a crude oil reservoir. The glass flask (front right) was for the effluent crude oil.

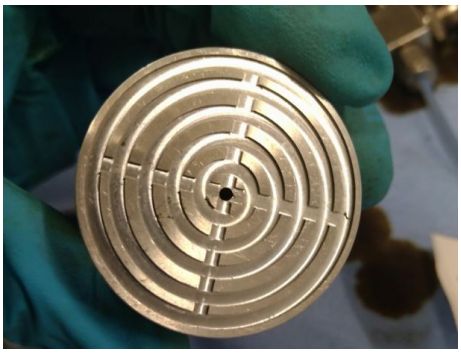

(b) Grooved end piece in contact with the core improved core-core holder end-piece contact

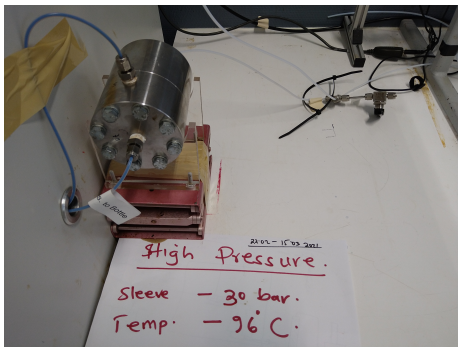

(c) A steel back pressure regulator

Figure 4.20: Key components of the dynamic aging setup

Chapter 5

Results and Discussion

In this section a record of experimental results that were observed or calculated is given. A detailed discussion follows each set of results. Results and discussion on RCA and SCAL is a revised version of my Chapter 5 that I had in the specialisation project in the preceding semester. Results on oil recoveries from spontaneous imbibition are expressed as percentages of the oil initially in the core (OIIC) for every core plug.

5.1 Porosity measurements

As already stated in Section 4.4.4, Helium porosity measurements were made on all cores and porosities were calculated using Equation (5.1) and data summarised in Table 5.1.

$$\Phi = \frac{(Vb - V2)}{Vb} \tag{5.1}$$

- where Vb is the bulk Volume, V2 the grain volume

$$Vb = \pi * \frac{D^2}{4} * L \tag{5.2}$$

- where D is the averaged core diameter, and L the averaged core length

For Ainsa cores, that were restored after cleaning, had similar porosity values just like had been calculated by Azizov (2019). For core plugs that had been previously used (B1, B2, B3 and B8), showed small reduction in porosity within a range of 1 to 5% . This showed that the cleaning process was efficient with all oil and brine inside the cores driven out by Toluene and Methanol. The Liquid Saturation method on (B1,B2, B3 and B8) also showed relatively similar but higher porosity values. The deviation was in the range of 0.1 and 1% . The relatively higher liquid porosity values can only be attributed to the excess fluid on the surface of the cores during wet weight measurements.

5.2 Permeability Measurements

Results of nitrogen gas liquid permeability experiment for Angola and Ainsa core are summarised in Table 5.3 and were obtained according to the procedure described in Section 4.4.5. Air permeabilities were plotted vs respective mean pressures and the resultant curve was extrapolated to infinite mean pressure to get the liquid permeability value according to the procedure described by Torsæter and Abtahi (2003). Due to small measurements made during production, its is important for cores involved in SI experiments to have substantial pore volume and

Core ID	Diameter	Length	Bulk Volume	Matrix Volume	Pore Volume
	D [cm]	L [cm]	Vb [cm^3]	Vm [cm^3]	Vp [cm^3]
Angola					
C1	3.73	4.52	49.52	41.50	8.02
C2	3.76	4.49	49.96	42.60	7.36
C3	3.77	4.59	51.26	45.30	5.96
C4	3.77	3.13	34.86	32.90	1.96
C5	3.76	2.61	29.10	27.90	1.20
Aisa					
B1	3.80	4.62	52.33	41.45	10.88
B2	3.81	4.59	52.43	41.80	10.63
B3	3.82	4.61	52.68	41.90	10.78
B5	3.71	4.60	49.75	43.10	6.63
B6	3.80	4.42	50.15	40.90	9.25
B8	3.81	4.56	52.03	42.00	10.03

Table 5.1: Core description

permeability for those small productions to be observable and recordable. From Table 5.3, all Ainsa cores have favourable pore volumes and liquid permeabilities. The similarity in pore volume and permeability for B1, B2 and B3 tells more about the homogeneity of the core material.

The Angola core material, as discussed in Section 4.1.1, was more heterogeneous than the

Core-ID	Initial FW-Cup	Total FW-Cup	Total FW-Cup	Prod.FW	Prod. FW	OOIC	Swirr
Ainsa	[g]	[cm^3]	[g]	[g]	[cm^3]	[cm^3]	[%]
B1	8.00	14.20	15.90	7.90	8.85	8.85	15.23
B2	8.00	14.50	16.24	8.24	9.23	9.23	9.88
B3	8.00	14.40	16.13	8.13	9.10	9.10	12.02

Table 5.2: Parameters used in irreducible water saturation calculations

Ainsa core material. Permeability and pore volume measurements as observed in Table 5.3 vary significantly from plug to plug. Permeability for example varies in order of x10 between the most and least permeable plug, (C1 and C4). Due to the vugy nature and fractures across matrix blocks, there was no observable correlation between porosity and permeability as seen in Table 5.3. However, basing on pore volume, core plug C1, C2 and C3 have substantial pore volume that can be producible during SI experiments. Work that was done by Yi et al. (2012) showed that SI is also possible in very tight cores. In that case, Yi et al. (2012) used cores that had liquid permeability of 0.53 mD. C2 and C3 even though they have low permeabilities can still be used in SI experiment. The low permeabilities, pore volumes, and porosity values of C4 and C5 make it impractical for them to be used in core plug SI experiments in the laboratory.

5.3 Back-Scatter Electron Imaging Results

Qualitative back-scatter electron imaging (SEM) results on the two thin sections prepared from the Angola core showed that the rock is mostly limestone. However, peaks of magnesium

Core ID	Liquid permeability	Pore Volume
AINSA	Kl [mD]	[cm^3]
B1	35.544	10.430
B2	30.241	10.430
B3	42.658	10.380
B5	89.583	6.630
B6	19.158	9.250
B8	48.352	9.730
ANGOLA		
C1	15.378	8.020
C2	1.730	7.360
C3	0.998	5.960
C4	0.302	1.960
C5	14.235	1.200

Table 5.3: Klinkenberg-corrected liquid permeabilities in milidarcy (mD) for all drilled cores

in the rock were also observed. This showed some traces of dolomitization, but it could not be quantifiable to define the rock as dolomite. A substantial amount of iron (Fe), was also recorded. Therefore, rusty patches on the surface of the Angola core could have stemmed from Fe oxidation. The presence of iron in the core could have stemmed from the fact the rock was sourced from an outcrop. Weathering products from run-offs and other atmospheric condition could have introduced iron into the rock. This explained residual Fe observed in some pore Walls but could not be used to infer on that observed elsewhere. The presence of Fe has an effect on wettability in outcrop cores but was not studied in this work. In conclusion

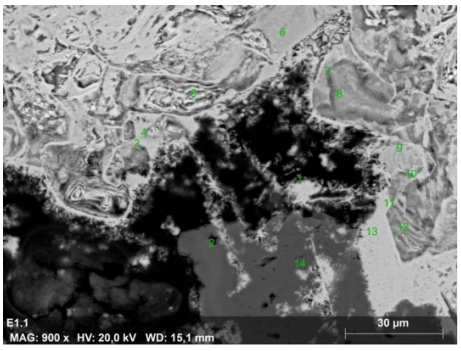

(a) Some Fe deposits in the pore space of thin section E1

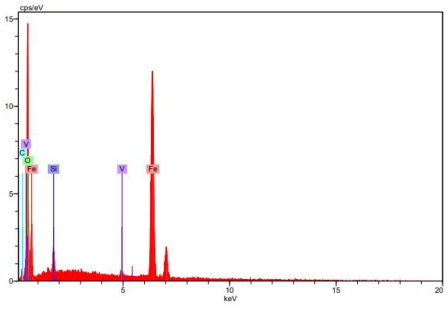

(b) The rock has almost no silicification

Figure 5.1: SEM analysis if thin section E1

the rock was confirmed to be limestone. It is therefore mineralogical representative to the oil reservoir in the Brazilian off-shore field under study.

5.4 Brines chemistry

As described in Section 4.1.3, brines were synthesised deionised water and with re-agent in the laboratory. Ionic compositions of brines brines are summarised in Table 5.4. Ionic strength

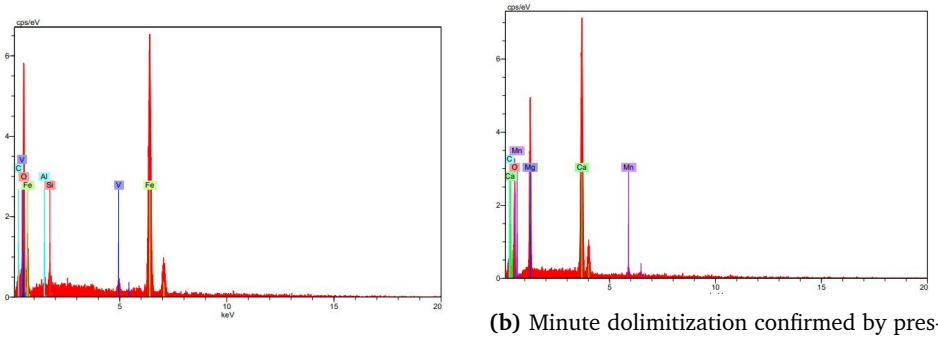

(a) Some Fe deposits in the matrix of E3

(b) Minute dolimitization confirmed by presence of Mg^{2+}

Figure 5.2: SEM analysis of thin section E3

of each brine was calculated basing on its ionic content.

BRINES IONS	FW [mol/l]	SSW [mol/l]	SSW-2S4Mg [mol/l]	SSW-2S8Mg [mol/l]	0.1-NaCl-SSW [mol/l]
Na^+	2.541	0.464	0.155	0.155	0.099
Cl^-	4.294	0.542	0.492	0.913	0.177
K^+	0.073	0.010	0.010	0.010	0.010
HCO_3^-	0.000	0.002	0.002	0.002	0.002
SO_4^{2-}	0.000	0.028	0.056	0.056	0.028
Mg^{2+}	0.113	0.053	0.0210	0.421	0.053
Ca^{2+}	0.677	0.010	0.010	0.010	0.010
Sr^{2+}	5E-02	9E-05	9E-05	9E-05	9E-05
TDS, [g/l]	247.793	34.822	32.459	52.495	13.455
Ionic stregth	5.13	0.69	0.88	1.515	0.323

Table 5.4: Ionic composition of brines used in SI experiments

5.5 Irreducible water saturation, Swi

The results of irreducible water saturation (Swi) from the centrifuging process are summarised in Table 5.5. Swi calculations were obtained from mass balance and volume calculations according to Equation (5.3)

$$Swi = \left[\frac{W_w - W_o}{\rho_o}\right]/PV \tag{5.3}$$

$$W_w - W_o = M_t - M_l \tag{5.4}$$

- Where W_w is the weight of a 100% formation water saturated core, W_o weight of a core at Swi, ρ_o as density of oil in the core, and PV the core pore volume.
- M_t is the total mass of FW after centrifuging and M_l is the mass of FW loaded into the cup, (8g)

The centrifuging round for the Ainsa was smooth and mass, as discussed in Section 4.5.3, was conserved. Even though the test result for the Angola core material was smooth (C4 and C5), centrifuging plugs C1, C2 and C3, (Angola), was quite challenging. Mass was conserved in centrifuge cups containing plug C2, and Swi calculations from both mass balance and volumetric balance calculations were similar with an acceptable error bound of about 5%. Just like for Ainsa core plugs.

CORE ID	PV [Cm^3]	Porosity [%]	Permeability [mD]	Swir [%]
B1	10.430	19.931	35.544	15.229
B2	10.430	19.893	30.241	9.884
B3	10.380	19.703	42.658	12.022
B8	9.730	18.701	48.352	9.450
C1	8.020	16.192	15.378	23.699
C2	7.360	14.723	1.730	40.100

Table 5.5: Summary of the key physical properties for cores used in spontaneous imbibition experiments

CORE ID AInsa	PV [Cm^3]	Porosity [%]	Permeability [mD]	Swi [%]	Aging Type [-]	Aging Time [Days]	Ultimate oil RF [%]
B1	10.44	19.96	35.544	15.23	Dynamic	90	28.25
B8	9.64	18.52	48.352	9.45	Static	90	33.26

Table 5.6: Comparing SI results of Static and dynamic aging. Results obtained at 96°C

After centrifuging plugs C1 and C2, the mass of formation water (FW) from respective cups was less than the 8g that were loaded in each cup before the run. Noticeable salt deposits and oil spills were found inside the centrifuge. When the centrifuge plastic cups, FW holder, were analysed, linear macro cracks were seen at their bases. These cracks also contained a brownish lining which clearly looked like crude oil stains. The cleavage on the centrifuge cup holder also had salt deposits. All these were indicators of massive leakages from centrifuge cups containing C1 and C3, Figure 5.3

The explanation for the cause that led to centrifuge plastic cups cracking was not straight forward. This is because the *Beckman Coulter Optima L-80 XP Ultracentrifuge* centrifuge has custom made plastic cups that should be able to withstand an RPM of up to 12000. Therefore, cracking due to high RPM and long run period was ruled out. The cause was rather that the mechanical strength of the cups was tampered with due to cleaning fluids that were used in the past. They had previously been cleaned with toluene rather than iso-propane. All, past runs were done at RPMs lower than 5000 and for periods less than 2 hours. Therefore, when the cups were exposed to an RPM of 5000, the centrifugal force generated was stronger than their current elastic limit. The cups had to rupture to release stress which in turn led to loss of fluid.

With an already tampered drainage process during centrifuging, Cups C2 and C3 were reloaded again, together with a dummy core, in a centrifuge for another run. This time round there was no leakages. Weights of C1 and C3 with unknown Swi fraction and their weights when fully saturated with formation water were used to calculate the irreducible water saturation in these two cores. The calculated values, that were later used in SI experiments are quite unreliable with an error margin of between 10-15% . Surface volumes from vugy sections of these plugs exacerbate these errors. Therefore, quantitative SI results for C1 might be questionable, though its qualitative response to test brine in the later discussed spontaneous imbibition results might not.

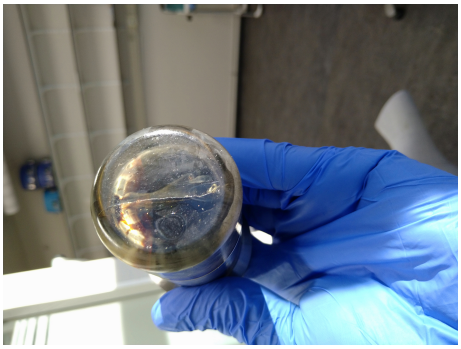

(a) Cracks in plastic cups permitted leaking

(b) Salt deposits due to leaking

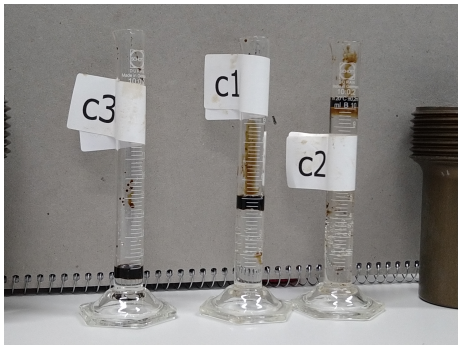

(c) Fluid loss was confirmed during measurements

Figure 5.3: Challenging centrifuging round for tight Angola cores

5.6 Core aging results: Dynamic vs Static efficiency comparison

As described in Section 4.4.8, two cores B1 and B8, were aged dynamically and statically respectively. The results of the two mechanisms are summarised in Table 5.6 and Figure 5.4. The degree of spontaneous imbibition (SI) of either FW or SSW in terms of ultimate oil recovery factor show that plug B1 was more oil wet than plug B8. A greater response to FW by B8 indicates that the rock material in this core was more water wet than in B1. As discussed by Fernø et al. (2010), static aging seems to leave most of the outcrop core material water wet with positive capillary forces. A greater initial response to FW was as expected in B8. Strand et al. (2008) and Fernø et al. (2010) argue that for divalent ions in SSW to have a big and recognisable impact on wettability alteration, majority of pore walls need to be originally oil wet. Therefore as observed in Figure 5.4 when SSW was introduced on the 4^{th} day, a sudden rise in recovery of 8% was observed in B1 compared with 3% in B8. B1 plateaued with additional recovery of 12% and B8 4% . This implies that that there was a more oil wetting state in B1. The recovery rate, which directly relates to induction time, was also high in the Amott cell containing B1 when SSW was introduced. All these factors indicate that the original wetting state was restored better with dynamic aging making B1 more oil wet than B8.

It is important to note that in the dynamic aging experimental setup, the core used was not under sleeve pressure. The set up was a bit different from what Fernø et al. (2010) used. The injection rate of 15 ml/hr, (limited by the peristatic pump), was also 5 times greater than the optimum rate (3 ml/hr), that was observed and suggested by Fernø et al. (2010). The core plug not being put under confining pressure, implies the annulus between the core plug and the core holder provided the easiest route for oil to flow through to the outlet rather than

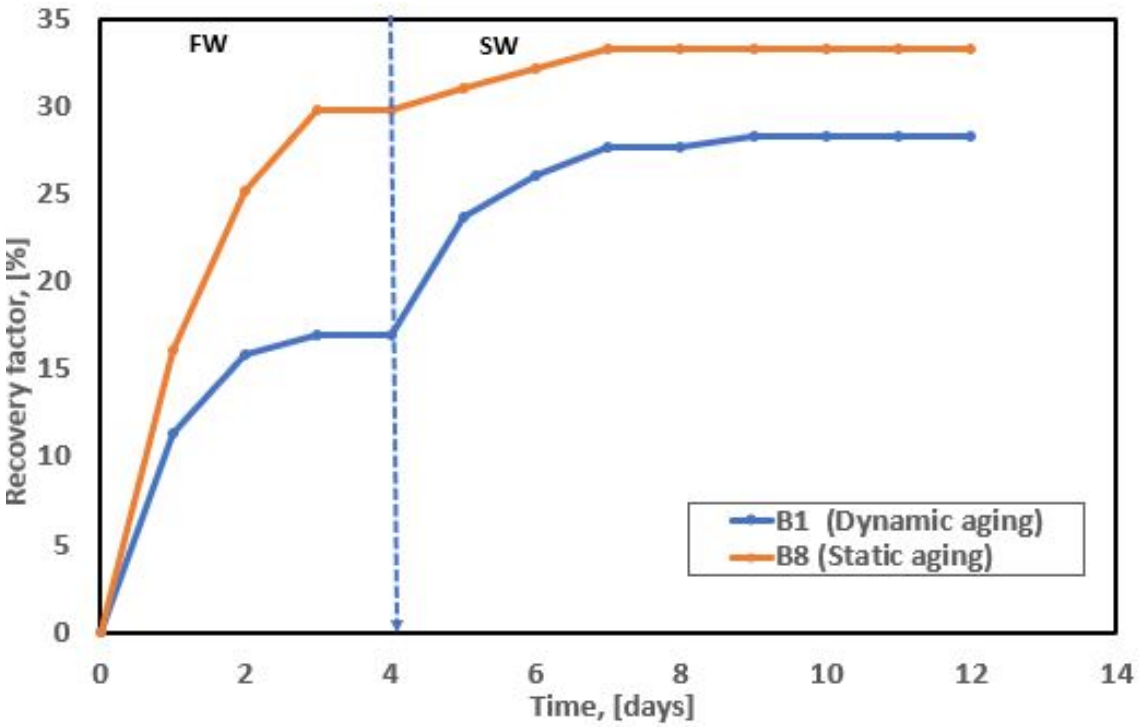

Figure 5.4: Comparing SI results of Static and dynamic aging. Results obtained at 90°C . Crude oil recovery expressed as percentage of OIIC

the core. The only mechanism that could explain the difference in wetting state is diffusion. Transport by diffusion enabled surface active components in crude oil to continuously adsorb and establish equilibrium between crude in the annulus with that in the inner parts of the core at any moment in time. With an injection rate of 1.5 ml/hour, it is possible to calculate the corresponding rate of diffusion.

According to Standnes and T. Austad (2000), chromatographic separation of different components in crude oil implies that the lighter components, $<C_7$, that are non reactive or adsorbent to a solid surface diffuse fastest into the inner parts of the core. Whereas heavy and slow components such as asphaltenes and resins stay relatively retarded to the surface or a few inches into the core. Carboxylic groups in these components get attracted to the positively charged pore surfaces and strongly adsorb there. The low recovery in B8 with SSW hints on this observation with limited oil wet sate inside the core after a significant recovery from areas closer to the outer diameter of the core. However, Standnes and T. Austad (2000) say that over sufficient aging time, chemicals equilibrium for all components is set with in the core and this improves the oil wetting state whether the core is under confining pressure or not. The strong wetting state in core B1 over B8 upon introduction of SSW during spontaneous imbibition is in agreement with what Standnes and T. Austad (2000) observed.

The internal length of the core and the injection rate play an important role. This is because for equilibrium to be set, the retention time for crude inside the core holder needs to be sufficient for the diffusion rate to transfer active components inside the core. It is still expected though that better results could be obtained when the core under confining pressure is flushed with crude at a much slower rate than 15ml/hour.

5.7 Static Contact angle measurements

Contact angle measurements as described in Section 4.5.1 were static. The algorithms used on the goniometer KSV CAM200 to make measurements were Young-Laplace and circle. Only measurements with Young-Laplace, and left angles, except for the 3^{rd} category, have been reported. The difference between the left and right angles was with 0.5-8°units. The difference could be due to heterogeneity on surface mineralogy but also it could be due to mechanical errors due to hand placement of the droplet. And on most droplets the right angle was bigger than the left angle. It was also observed that larger droplets smeared more than smaller droplets and medium sized droplets were opted for.

Measurements made on a single crude oil droplet and monitored over time showed no significant change in the subsequent angles over the period of 24 hours. The values varied sporadically from brine to brine and there was no consistent trend observed as seen in Figure 5.5. Measurements in this category showed that the chip surface was strongly oil wet with contact angles between 170°-171°, Figure 5.12a. The crude oil wetting state, low temperature (23°C) in addition to less reactive limestone surface as described by Strand et al. (2008) implied PDIs in all test brines were not active enough to change the wetting state over the course of 2 hours.

When the same chip, chip 2, was aged in each brine and measurements made after 24 hours as described in the 2^{nd} category in Section 4.5.1, monotonic reduction in angles was observed as brines were sequentially changed from FW, SSW, SSW-2S4Mg to SSW-2S8Mg, Figure 5.6 . No observable difference in contact angles was made with aging in FW when compared with values in the 1^{st} category. Even though this brine is rich in cationic PDIs, Mg^{2+} and Ca^{2+}, the absence of SO_4^{2-} implies that the two cations faced a strong electrostatic repulsion and were not able to adsorb or form carboxylate complexes that would desorb crude oil components from the solid surface and improve the water wetting state. This is in line with the symbiotic synergy of the 3 PDIs during wettability alteration suggested by Zhang et al. (2006a). Upon aging in SSW, contact angles decreased on average by 43°from $\approx$ 171°. The large response with SSW was catalysed by the presence of SO_4^{2-} ions which according to the MIE mechanism by Zhang et al. (2006a) activate Mg^{2+} and Ca^{2+} to alter wettability. When test brines were sequentially changed from SSW, SSW-2S4Mg to SSW-2S8Mg, contact angles reduced by not more than 10°and the surface remained mixed wet but with an improved water wettingness, Figure 5.12(b-d). Aging in FW after SSW-2S8Mg showed no change in angles from those made in SSW-2S8Mg. This confirmed that the wettability alteration process is irreversible.

Measurements made in the 3^{rd} category in Section 4.5.1 with chip 1 showed the same trend from FW to SSW and same discussion as for the 2^{nd} category holds. Values of 170°+ in FW showed that the initial oil wetting state of this chip was similar to that of chip 2 which showed uniformity in conditions during aging in crude oil, and also some degree of homogeneity of the polished surfaces of the two chips. However, the prolonged exposure of the chip to PDIs in SSW, 3 days, provided a better water wetting state than in the 2^{nd} category with an average value of 100-110°, Figure 5.12e. This, together with observations of the 1^{st} category showed that PDIs' activity is also dependant on exposure time. When the chip was aged in 0.1-NaCl-SSW, all angles measured were in the water wetting range suggested by Anderson et al. (1986) with values lying between 50-70°, Figure 5.7 and Figure 5.12f. The difference between this brine and SSW is the NaCl content which is 10 times less in 0.1-NaCl-SSW. Therefore a reduction in contact angles of about 60°is huge to be accredited to exposure time. It is rather the impact of selective dilution of NaCl content in SSW that reduces the the $[Na^+]$ and $[Cl^-]$

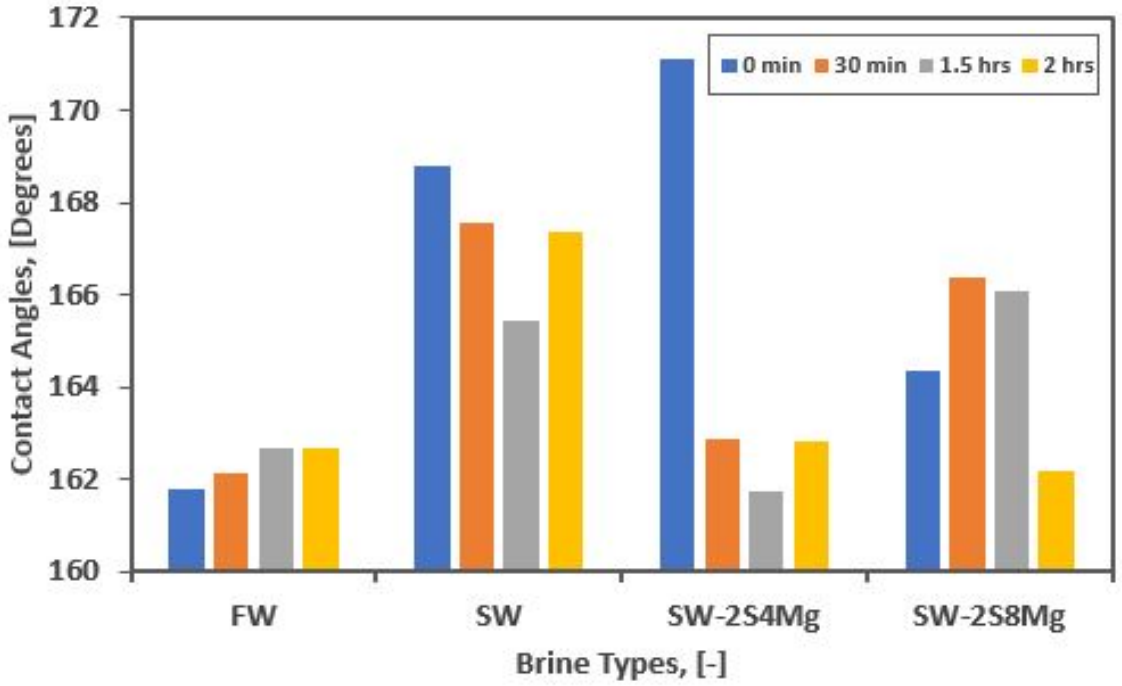

Figure 5.5: 2 hour contact angle analysis on one crude oil droplet at C

that would otherwise hinder the activity of PDIs to wettability alteration. This experiment was done basing on the recommendations made by Yousef et al. (2012(a)).

In the 4^{th} category as described in Section 4.5.1, contact angles in FW, about 135°, showed that chip 1 was not restored to a better oil wetting state as was observed in the 3^{rd} category, Figure 5.8. Even though measurements were made at room temperature of 23C, a better trend in reduction in contact angles from FW to SSW-2S8Mg was observed with the difference between the two brines as 65°. This trend was expected but not to this magnitude. Considering that there is a better initial water-wetting state, more sites are available for PDIs to evade the solid surface and ultimately desorb the carboxylic groups. This explains the trend and why with increased $[Mg^{2+}]$ and SO_4^{2-}, from SSW to SSW-2S8Mg, the water wetting state improves.

5.8 Zeta potentials

As described in Section 4.5.2, two categories of measurements were made. In the 1^{st} category, Table 5.7, and at 25°C an average measurement of 5.66 mV in FW indicated that the Angola limestone surface may not have a large positive charge in comparison with its Ainsa (20 mV) counterpart that was done by Azizov (2019). Increase in ZP from measurements made in SSW, SSW-2S4Mg to SSW-2S8Mg, indicates an increased adsorption of cationic ions. According to Zhang et al. (2006b), adsorption of PDIs to a carbonate surface depends on relative concentration of these ions. In SSW, SSW-2S4Mg and SSW-2S8Mg the $[Mg^{2+}]$ is highest and it is therefore expected to have preference to a carbonate surface. At 70°C, 11.5mV in SSW-2S8Mg still showed preference of the Mg^{2+} ion. In FW, the surface charge is even more positive and the high $[Mg^{2+}]$ and $[Ca^{2+}]$ is the reason.

Measurements in 0.1-NaCl-SSW and 0.1-SSW both at 25°C and 70°C gave the lowest ZP

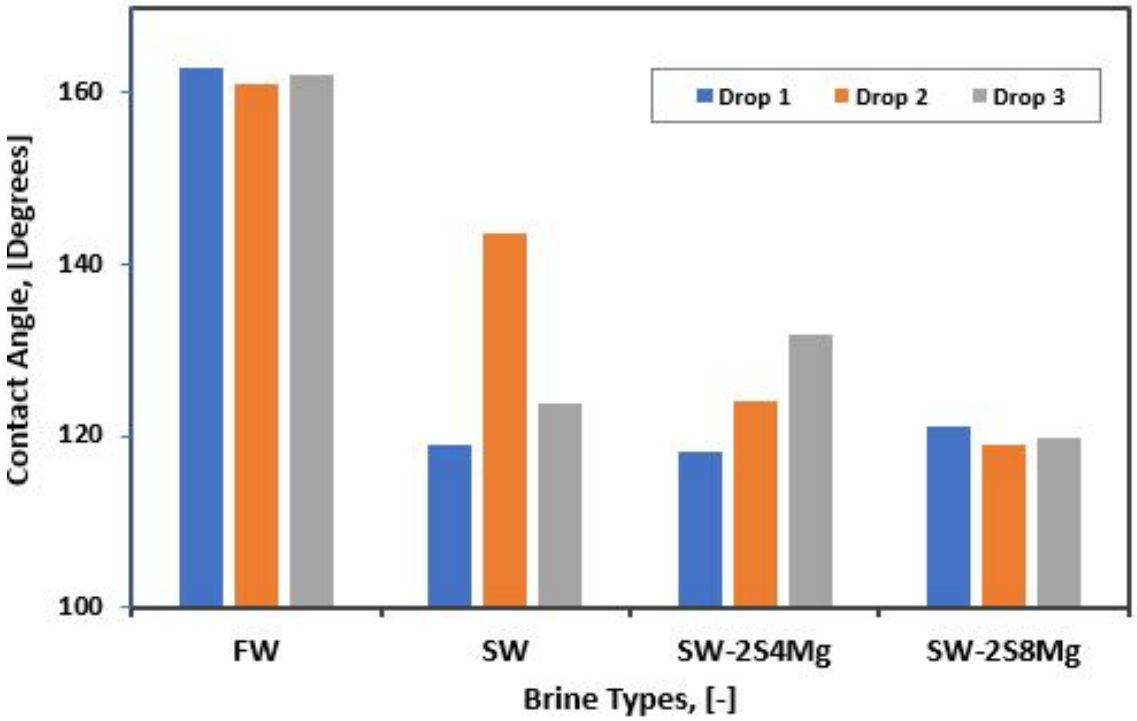

Figure 5.6: Crude oil droplet contact angles on chip 2 aged in each brine at 96°C for 24 hours. Measurements made at RT.

Brine	ZP, [mV]	at	at 25°C		ZP, [mV]	at	70°C	
FW	5.94	5.96	5.08	5.66	6.22	9.15	6.77	7.38
SSW	5.32	6.81	6.25	6.53	5.53	7.12	3.07	5.24
SSW-2S4Mg	7.76	6.7	6.06	9.84	3.67	5.46	8.51	5.88
SSW-2S8Mg	9.11	9.90	10.10	9.90	11.50	10.40	7.76	11.50
0.1-NaCl-SSW	4.64	5.04	5.26	4.98	5.21	5.03	5.10	4.45
0.1-SSW	5.49	4.85	5.14	5.16	4.06	5.41	4.38	4.04

Table 5.7: zeta potential (ZP) of the Angola limestone rock powder suspended in test brine at 25°C and 70°C

values. This shows that both holistic and selective dilution of SSW with respect to NaCl reduces the positive charge of a limestone surface. This highlights the activity of the SO_4^{2-} ion.

In the 2^{nd} category of measurements with the powder aged in crude oil, Table 5.8, all FW values at both 25°C and 70°C were relatively higher than in the 1^{st} category. This was unexpected because aging in crude oil should make surface active components in crude oil adsorb to and reduce the positive charge at the limestone surface. Considering that toluene dissolves all hydrocarbon molecules, then its possible that the toluene content in a 50% n-heptane-toluene mixture was not effective in doing powder cleaning and therefore washed away most of the hydrocarbon molecules adsorbed to powder surface. ZP values in SSW at both temperatures were lower than in FW. This was expected as the SO_4^{2-} ions in SSW reduce the positive charge at the limestone surface. With the reduced positive charge, quadrupling in $[Mg^{2+}]$ in SSW and with the selective dilution effects, should increase the Mg^{2+} ion adsorption and make the surface more positive as seen Table 5.8. The same trend was expected for SSW-2S8Mg but it was not the case and values of 1.6 and 4.79 at 25°C and 70°C were far below those for SSW-2S4Mg. Ion pair formation between the Mg^{2+} and SO_4^{2-} ions as suggested by Zhang et al. (2007) and

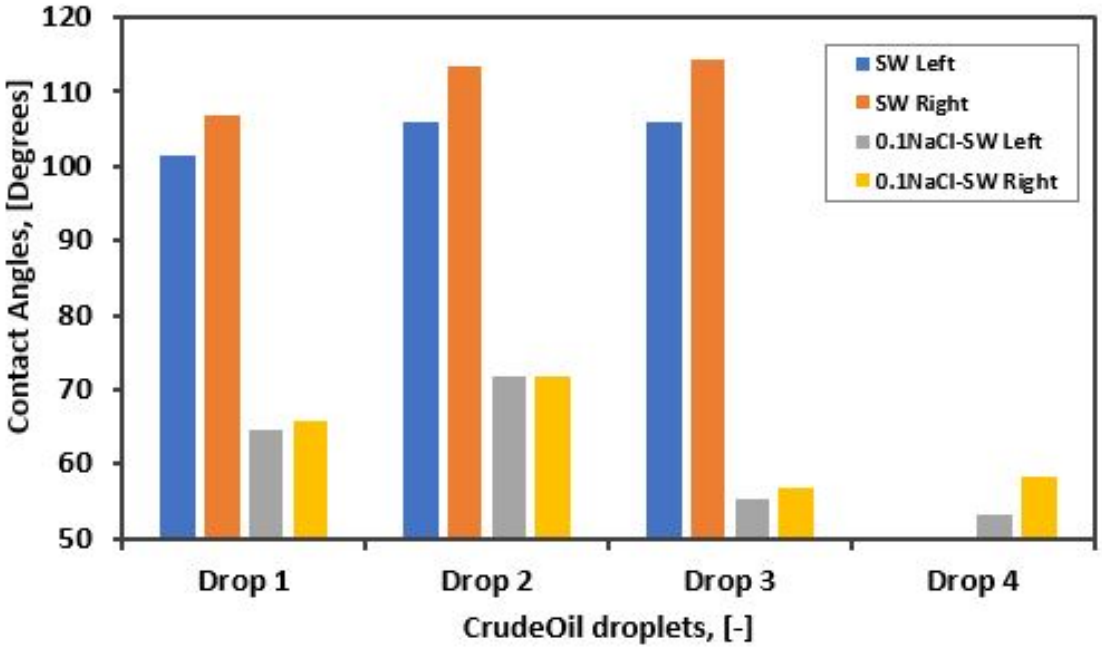

Figure 5.7: 3-day crude oil contact angles on chip 1 aged in each brine at 96°C

Karimi et al. (2016) was the plausible explanation behind this. This implies that with increased temperature beyond 70°C, the surface could be more positive through availability of Mg^{2+} ions in ion pairs.

Measurements in 0.1-NaCl-SSW and 0.1-SSW at both 25°C and 70°C were negative, Table 5.8.

Brine	ZP, [mV]	at	25°C		ZP, [mV]	at	70°C	
FW	10.08	7.78	8.08	8.89	5.7	7.38	7.83	7.00
SSW	7.10	6.21	9.97	6.76	3.85	4.05	1.05	2.98
SSW-2S4Mg	10.20	8.73	7.02	8.65	11.10	12.80	9.18	11.00
SSW-2S8Mg	1.27	1.45	2.09	1.60	7.74	2.65	3.99	4.79
0.1-NaCl-SSW	-1.78	-1.87	-1.49	-1.71	-0.67	-0.188	-0.512	-0.678
0.1-SSW	-2.17	-2.15	-1.92	-2.08	-0.319	-0.076	-0.059	-0.151

Table 5.8: zeta potential (ZP) of the Angola limestone rock powder aged first in crude oil for 20 days and then suspended in test brine at 25°C and 70°C

However, values at 70°c were less negative than those at 25°C. In the DLE mechanism described in Chapter 3, reducing the ionic strength of brine through either selective or holistic dilution increases the Debye length (Firoozabadi et al., 2015; Nazari et al., 2020). This increases electrostatic repulsion of the two interfaces and positive disjoining pressure which might result in detachment of adsorbed carboxylic group. However, the increase in the positivity of ZP at 70°C also hints on the activity of the cationic PDIs that are responsible for the MIE mechanism described by Zhang et al. (2005), Strand et al. (2008) and Tweheyo et al. (2006) and Yousef et al. (2012(a)).

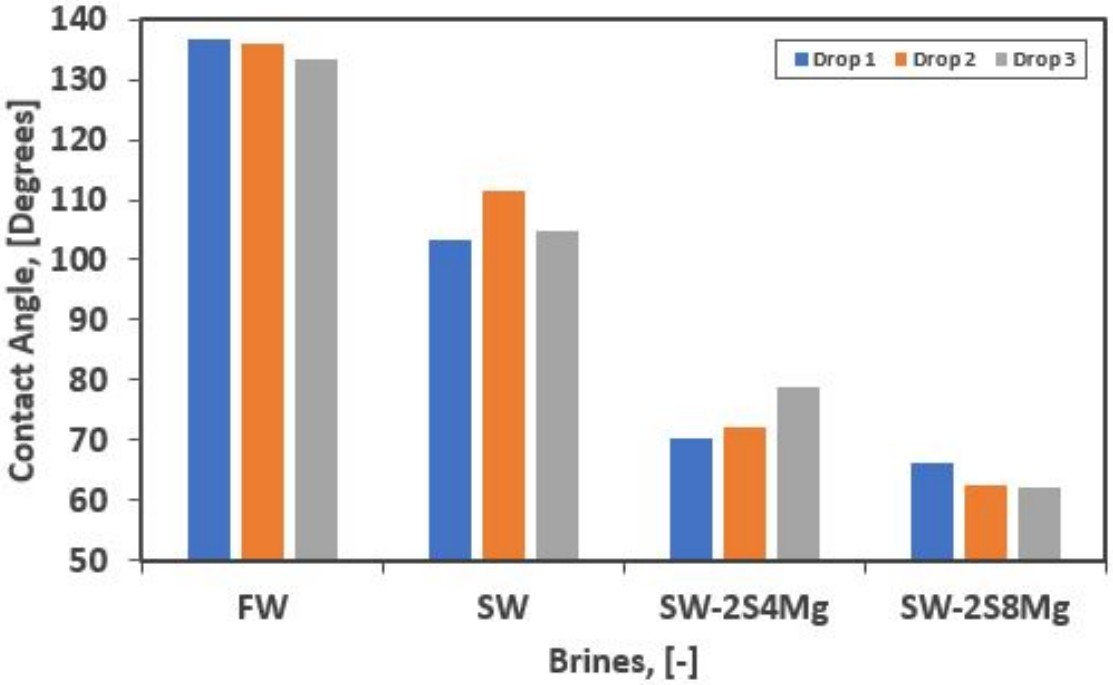

Figure 5.8: Restored chip 1 contact angles aged in different brines at 23°C

5.9 Spontaneous imbibition set up and results

This section summarises all the spontaneous imbibition experimental results on wettability alteration in limestone cores. The results are based on the newly improved experimental set up described in Section 4.2 in reference to objective 3 in Chapter 1. The new design successfully allowed for external control of the components inside the heating chamber through communication with 1.5mm diameter PTFE lines and a 3-way T-valve network. Test brines, degassed with magnetic stirrers before loading, were preheated and used in the experiment. As discussed by Tweheyo et al. (2006) and Strand et al. (2008), recoveries due to fluid expansion were minimised, and therefore all recoveries except for the first brine were due to wettability alteration. The degassing process also minimised air into the system that could have led to recovery due to gas expansion upon heating. The system degassing step described in Section 4.2.1 also helped to minimise gas effects. The Exxsol D60 used to pump fluids at the start and during change of brines was not degassed in the first experiment. A few air slugs were seen along the D-60 flow lines behind the pump. This was the main air source and was visualised by a few air bubbles in the lower neck of the Amott cells.

All brines used in the SI experiments had a substantial salinity, Table 4.2. As expected their boiling points should be below that of pure water, 100°C. At 96°C, they were all expected to boil. However, internal production in the neck of the Amott cells prevented this boiling at all time during the experiment. 15ml of test brine in the burettes also provided an extra pressure, in addition to atmospheric pressure, that prevented FW from boiling during the system initiation, degassing and temperature rise to 96°C.

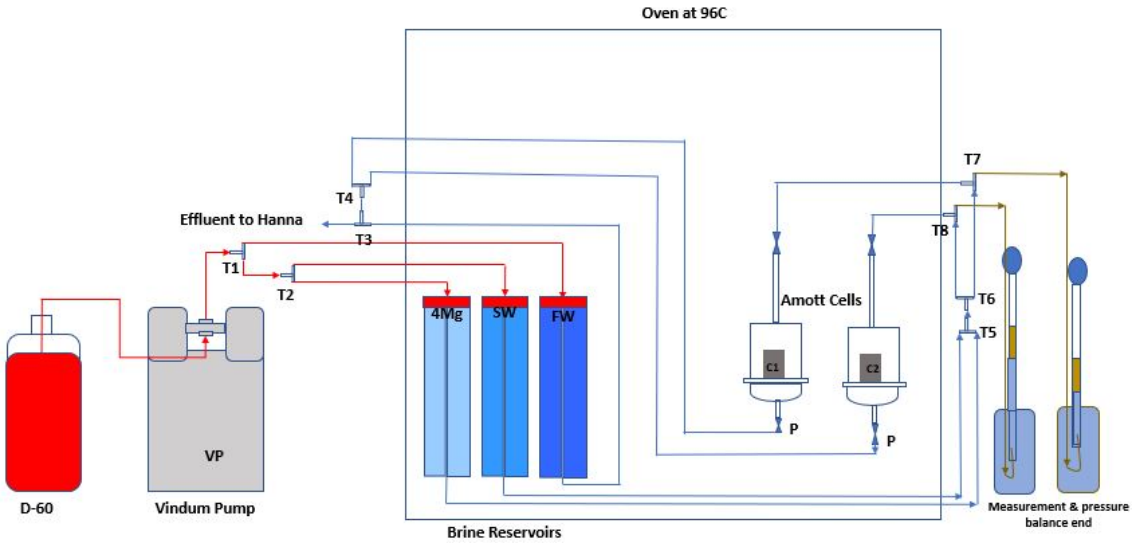

Figure 5.9: The schematic of the imbibition rig set up

5.9.1 Selective dilution of NaCl content in sea water

Ainsa core plugs B2 and B3 were used to understand the effect of selective dilution of synthetic seawater with respect to NaCl has on wettability alteration mechanisms. In line with the procedure described in Section 4.2 and Section 4.6, B2 and B3 were first imbibed with FW. With in 2 days the production from both cores had already plateaued at 16.8% and 11% for B2 nd B3 respectively. The plateau period was extended by one day and no extra production was recorded in both cores. According to Zhang et al. (2007) and Yu et al. (2008), physical properties of the core such as Swi, pore connectivity, control recovery with the first brine. Though FW is rich in Mg^{2+} and Ca^{2+} ions, these ions are not active in wettability altertaion without SO_4^{2-} in limestone core (Strand et al., 2008; Shariatpanahi et al., 2010). On the 5^{th} day, SSW was introduced. Both core responded with in a day, with B2 plateauing with an additional recovery of 6.6% . production from B3 flattened after 2 days with a total incremental recovery of 5.5% . After 3 more days, no additional production was observed. All the recoveries in this case were due to wettability alteration caused by the activity of PDIs to a limestone surface initiated by the SO_4^{2-} ions.

The cores were then exposed to 10x-NaCl-diluted synthetic seawater (0.1-NaCl-SSW). There was a delayed response to production in both cores with it being more noticeable for 2 days in B3, Figure 5.10. After the first production, a day lag to the next production was observed which points to the observation that spontaneous imbibition with 0.1-NaCl-SSW after SSW is a slow process. After more than 3 days of plateauing in both cores, total incremental recovery of 5.4% and 5.5% was recorded in both B2 and B3 respectively. The main difference between SSW and 0.1-NaCl-SSW is the NaCl which is 10 times less in 0.1-NaCl-SSW. One can therefore assert that selective dilution of SSW has a positive impact on the wettability alteration mechanisms in limestone cores. As was suggested by Yousef et al. (2012(a)), it improves the activity of PDIs at the rock-brine interface which ultimately desorb the adsorbed hydrocarbon molecules. Shariatpanahi et al. (2010) using SSW fully depleted in NaCl in the tertiary mode with SSW in the secondary mode observed no increase in recovery on limestone reservoir cores. The observation in this work contradict with what Shariatpanahi et al. (2010) made. The incremental recovery with 0.1-NaCl-SSW in this work is so substantial that they can not

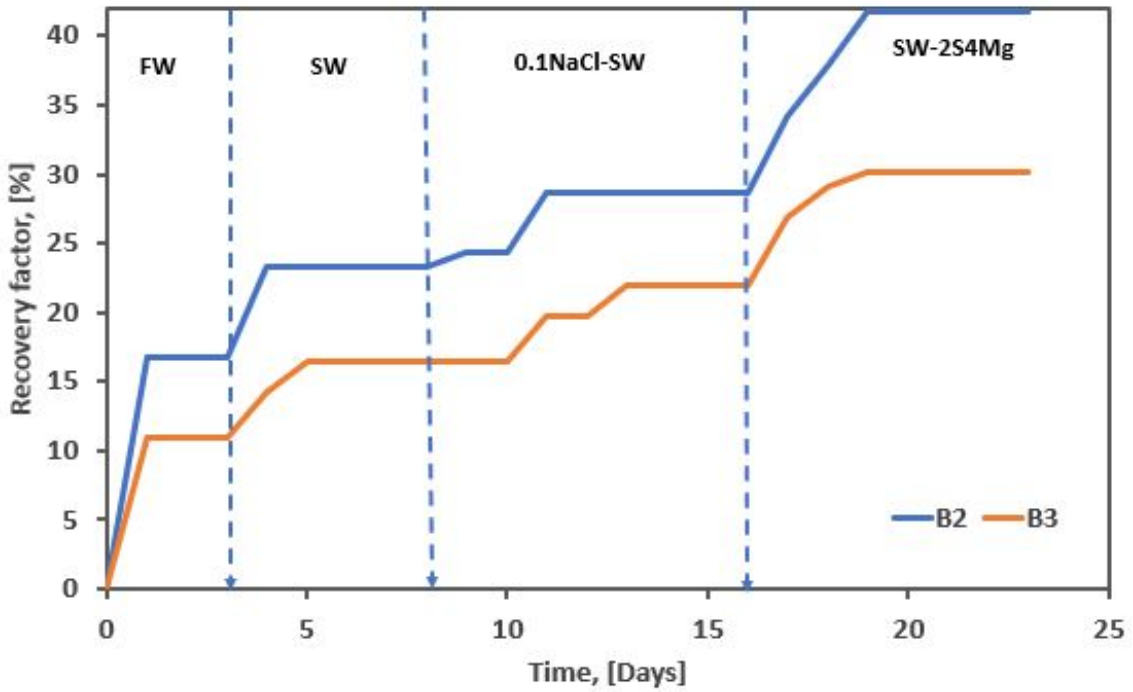

Figure 5.10: Crude oil recovery as a percentage of OIIC for Ainsa cores B2 and B3. The effect of selective dilution of NaCl in SSW on activity of PDIs at 96°C

be ignored or accrued to experimental artifacts.

After the test with 0.1-NaCl-SSW, B2 and B3 were spontaneously imbibed with 10 times NaCl-diluted SSW with $[Mg^{2+}]$ and $[SO_4^{2-}]$ respectively 4 and and 2 times above that in SSW (SSW-2S4Mg). This test was to confirm the impact of reducing the [NaCl] in SSW has on the activity of PDIs mainly the Mg^{2+} ion in SO_4^{2-}-enriched SSW. Among all tertiary modes, SSW-2S4Mg gave the largest production and most prolonged response. B2 plateaued after 8 days with an incremental recovery of 13% whereas B3 has additional recovery of 12.2% . This pointed to two observations. Selective dilution of the NaCl improves the activity of potential determining ions to a limestone surface. Also increasing the concentration of PDIs after selective dilution improves the water wetting state in previously oil wet limestone cores. The concentration effects are in line with what Strand et al. (2008) and Shariatpanahi et al. (2010) observed in limestone cores and Tweheyo et al. (2006) in chalk cores.

Selective dilution of SSW with respect to the NaCl content reduces the concentration of Na^+ and Cl^- ions. These ions are deemed none reactive to a limestone surface and do not in any way dictate the surface charge on it (Firoozabadi et al., 2015; Nazari et al., 2020). However, the two monovalent ions in the diffuse layer of the thin water film can limit access to the limestone surface for Mg^{2+}, SO_4^{2-} and Ca^{2+} ions that are important for wettability alteration. Reducing the [NaCl] creates way for the SO_4^{2-} ions to adsorb to the brine-limestone surface which ultimately cause co-adsorption of the cationic PDIs. Either cations react and form complexes with the adsorbed carboxylic groups or the Mg^{2+} substitutes for the Ca^{2+} ions to which the carboxylic groups are adsorbed. Either way the crude oil molecules get detached from the limestone surface according tho the multi-ion exchange (MIE) mechanism suggested by Zhang et al. (2005). Reducing the [NaCl] also reduces the ionic strength of SSW. This expands the debye length of the ions in the diffuse layer of the electric double layer system in the thin wa-

ter film (Hirasaki et al., 1991; Nazari et al., 2020; Firoozabadi et al., 2015; Han, 2002). The diffuse layer expands, creates strong electrostatic repulsion and more positive disjoining pressure. Ultimately stable water films are created as adsorbed oil molecules get detached from the limestone surface according to the DLE theory.

In line with the observations made concerning selective dilution of SSW as an EOR fluid, number of considerations need to made for it to be applied on a field scale pilot. A comprehensive feasibility study needs to be conducted first concerning installing and running a desalting facility that selectively removes or reduces the NaCl content in seawater. A proper salt handling or disposal program also has to be analysed comprehensively with focus on the environment. Though NaCl is deemed to be of less negative impact to the environment. However, the availability of sea water in the neighbourhood of the off-shore field under study, or in the case of the Norwegian continental Shelf fields, makes the process practically and physically implementable.

5.9.2 Brine composition: Mg^{2+} and SO_4^{2-}

Angola cores C1 and C2 were used in the study of understanding the role played by the Mg^{2+} ion in sulfate-enriched SSW varieties. Knowing that the Mg^{2+} ion is most active at high temperatures above 80°C, the experiment was conducted at 96°. At this temperature, the Mg^{2+} has preference to a limestone surface over Ca^{2+} ions. C1 and C2 were first imbibed with FW. Within 2 days production from both cores had plateaued at a recovery of 21.4% and 21.5% ,Figure 5.11. Though both cores vary significantly in physical properties, Table 5.5, their response to FW was quite a like and might be due to similar Swi values. After 5 more days of plateauing, the cores were then exposed to SSW. Again with in 2 days production from both cores had flattened with an incremental recovery of 5.5% and 10.2% and no extra recovery was made in 5 days afterwards. Recovery with SSW could be attributed to the activity of PDIs. The cores were then tested with SSW-2S4Mg. Step wise increments in recovery with both cores were observed. A similar trend that was seen in Section 5.9.1. Total additional recoveries of 4.4% and 5.7% were recorded in C1 and C2 respectively over the course of 7 days. The core were then exposed last to SSW-2S8Mg. Another delayed step wise response was observed with C2 before it plateaued with a recovery rise of 10.2% over a period of 10 days. C1 gave an additional recovery of 4.4% within the same period. 10 days were chosen so as to see whether the delayed step wise response could last longer than a week.

Before switching to the SSW-2S8Mg, the oven was cooled down to allow switch of brine as described in Section 4.2.3. When the oven was heated again to 96°C , with SSW-2S4Mg as the crossover brine, no additional production was observed over 24 hours. For a bout 10 minutes, after the temperature had risen to 96°C, brine SSW-2S4Mg was seen boiling in both Amott cell necks. The liquid levels however stayed relatively stable and brine in the lower parts also seemed calm with no observable convections. Boiling took place until when the liquid column in the external burettes balanced out the pressure deficit. Brine was then smoothly changed to SSW-2S8Mg and all production observed afterwards was accrued to it.

Incremental production with SSW-2S4Mg and even more with SSW-2S8Mg indicates that enriching SSW with Mg^{2+} ions in the presence of SO_4^{2-} ions improves the water wetting state in limestone cores. According to Strand et al. (2008) and Shariatpanahi et al. (2010), recoveries due to Mg^{2+} substitution for Ca^{2+} ions to which hydrocarbon molecules are adsorbed starts at around 80°C and increases with temperature. At the experimental temperature of 96°C and

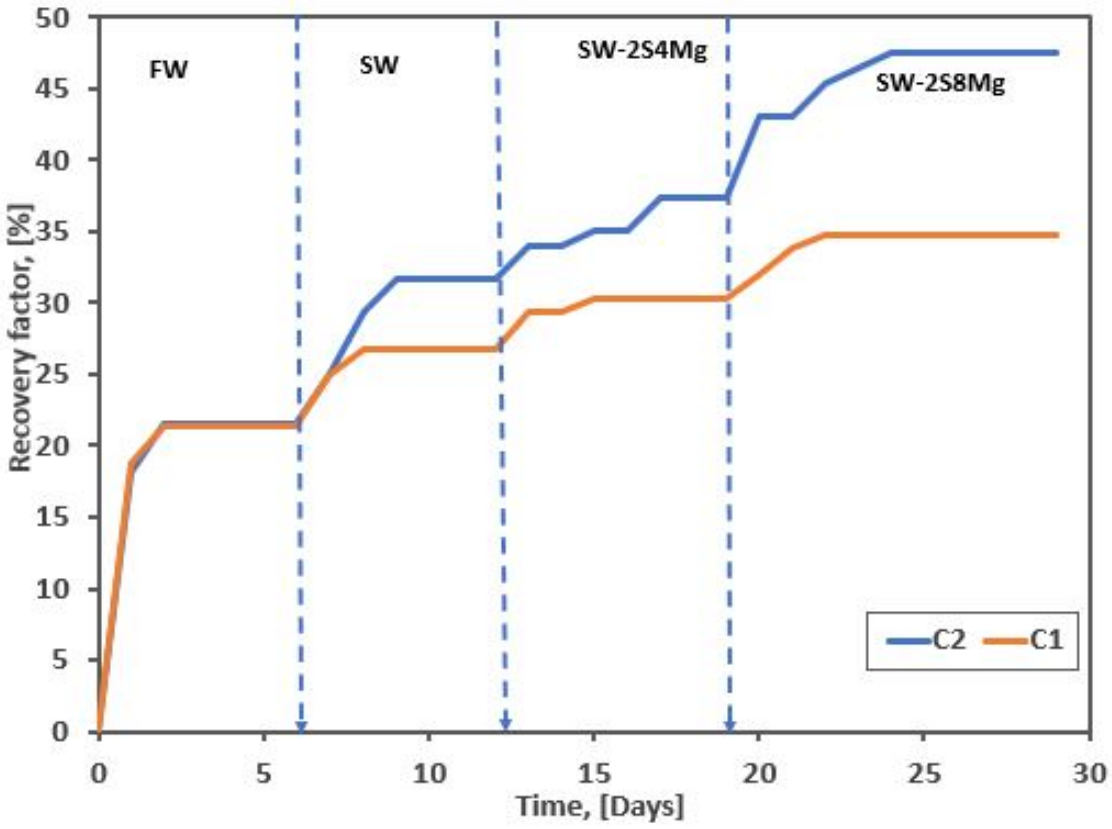

Figure 5.11: spontaneous imbibition results at 96°C. The effect of magnesium, in sulfate-enriched SSW. Oil recoveries expressed as percentage of OIIC.

with increased availability of Mg^{2+}, this substitution recovery was expected to be significant. According to the MIE mechanism, at this temperature, the Mg^{2+}..SO_4^{2-} ion pair also starts to dissociate and avail more Mg^{2+} ions that can react and form complexes with the adsorbed hydrocarbon molecules. Recovery by this process was expected to be of less occurrence since the R-COO-Ca bond is stronger and more stable than the R-COO-Mg bond. Though as was observed by Zhang et al. (2007) on a chalk surface, at 96°the Ca^{2+} is a stronger PDI to a carbonate surface with the Mg^{2+} only stabilising it in solution through ion pair formation with the SO_4^{2-} ion. Strand et al. (2008) says that in this case, in the presence of Ca^{2+} ions, wettability alteration process due the MIE mechanism is through the Ca^{2+} and SO_4^{2-} ions with marginal recovery from as a result of Mg^{2+} reactivity.

In line with the DLE mechanism, recovery by this process was not expected. With reference to Table 5.4, all brine the 4 brine used in this experiments has ion strength values above 1mol/l. With these values, the diffuse double layer collapses and recovery by this process becomes challenging to explain (Nazari et al., 2020).

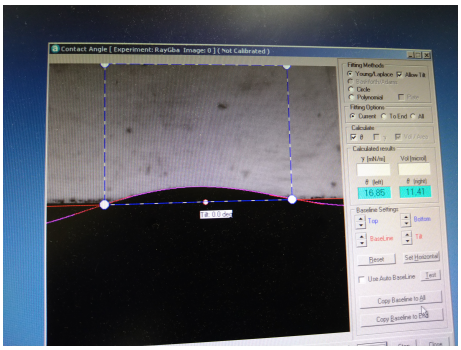

(a) Contact angle in FW after aging at 96°C. Oil droplet spreading on the surface

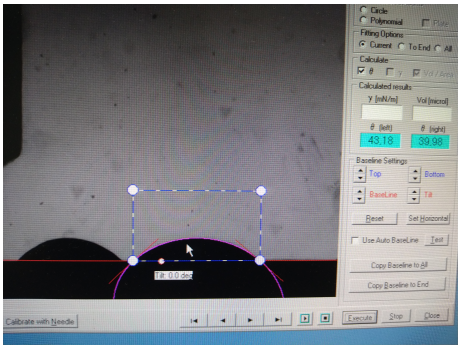

(b) Contact angle in SSW after aging at 96°C

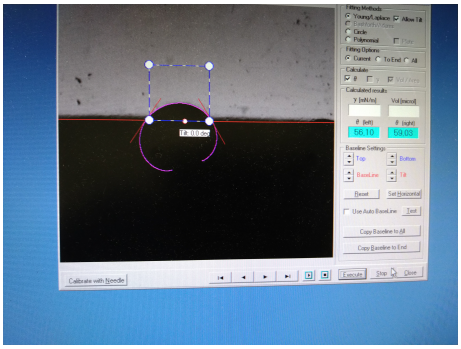

(c) Contact angles in SSW-2S4Mg after aging at 96°C

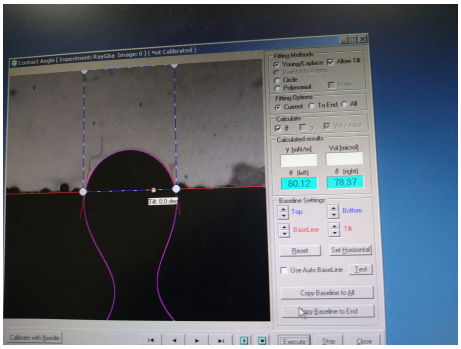

(d) Contact angles in SSW-2S8Mg after aging at 96°C

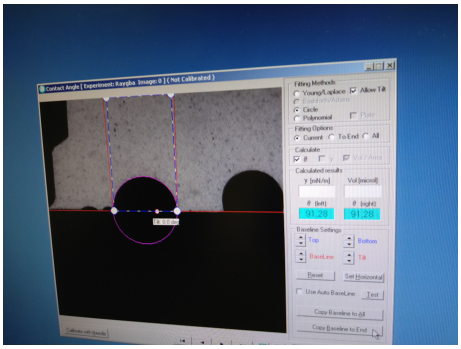

(e) Contact angle in SSW after aging for 3 days at 96°C

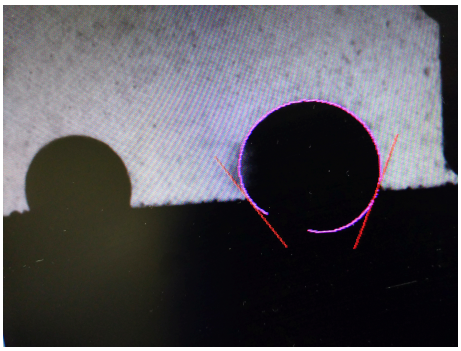

(f) Contact angles in 0.1-NaCl-SSW after aging at 96°C for 3 days. Droplet retracting from the surface

Figure 5.12: Contact angle measurement with the goniometer with either chip 1 or chip 2 aged in different brines.

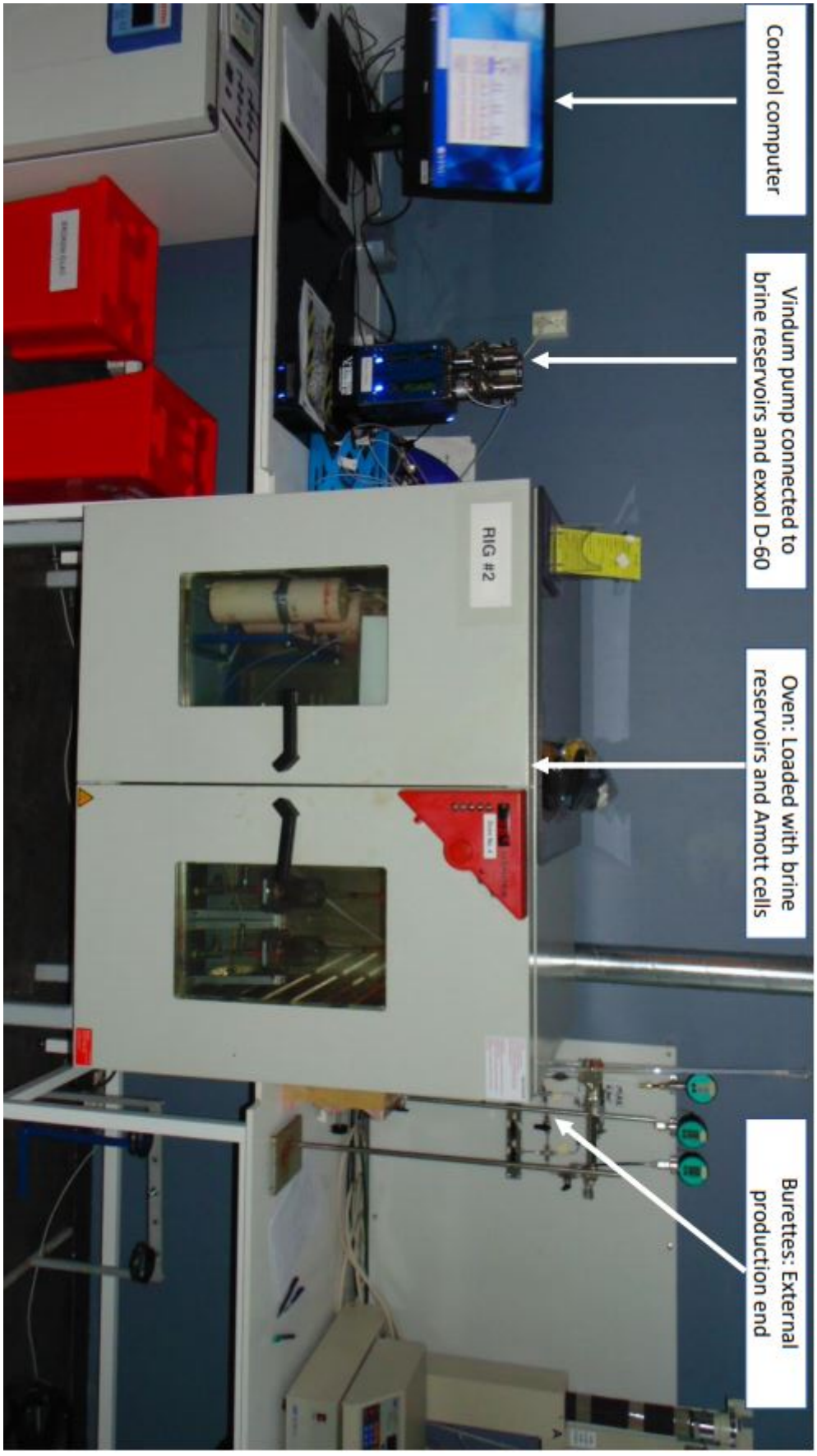

Figure 5.13: The external set up of the spontaneous imbibition rig showing the main components

Chapter 6

Conclusion

A comprehensive study on the effect of water quality in regards to spontaneous imbibition in limestone core has been successfully conducted. In reference to the main aim of the project, it has been shown that the ionic composition of brine dictates the extent of wettability changes in limestone outcrop core plugs. Altering the composition of synthetic seawater by enriching it with Mg^{2+} and SO_4^{2-} ions showed improvement in oil recoveries. Basing on the observations and result analysis, the following conclusions can be made.

- From spontaneous imbibition results, synthetic seawater imbibing in a tertiary mode after formation water is an effective wettability modifying brine in limestone core and improves oil recovery.
- Enriching synthetic seawater with SO_4^{2-} ions above the concentration in normal sea water improves the activity of potential determining ions that are responsible for wettability alteration.
- The magnesium, (Mg^{2+}) ion is an effective wettability modifier in limestone cores. Increasing its concentration in imbibing brine above that in sea water only accelerates the rate of wettability modification as has been shown with SSW-2S4Mg and SSW-2S8Mg spontaneously imbibing after SW in a serial mode.
- Enriching SW with SO_4^{2-} ions improve the activity of Mg^{2+} ions in wettability alteration process in limestone outcrop cores.
- Spontaneous imbibition results with 0.1-NaCl-SSW showed that selective dilution of sea water improves the activity of PDIsin wettability alteration.
- The use of SSW-2S4Mg after 0.1-NaCl-SSW and the high recoveries afterwards show that depleting SW in its NaCl content, and enriching it with Mg^{2+} and SO_4^{2-} improves the water wetting state that speeds up the SI process.

The following conclusions can also be made regarding contact angle measurements and zeta potential measurements

- Trough contact angle measurements, it has been shown that formation water can not improve the water wetting state of a strongly oil wet limestone core both at room temperature of 23C and at 96°C.
- Contact angle measurements have also shown that SW, SSW-2S4Mg, SSW-2S8Mg, and 0.1-NaCl-SSW are all able to improve the water wetting state on a limestone surface both at 23°C and 96°C.
- Using 0.1-NaCl-SSW has shown that selective dilution of synthetic seawater in regard to its NaCl content improves the activity of PDIs in wettability alteration.
- Reduction in contact angles with SSW-2S4Mg and SSW-2S8Mg after exposing the limestone surface to SW confirms that enriching SW with Mg^{2+} ions in presence of SO_4^{2-}

makes a limestone surface more water wet.

- Zeta potential measurements have showed that both selective dilution, (0.1-NaCl-SSW), and holistic dilution of SW, (0.1-SSW) reduce the positive charge at the limestone surface, and can therefore improve the activity of Mg^{2+}, Ca^{2+} and SO_4^{2-} ions in wettability alteration.
- In using crude oil aged powder for ZP measurements, care must be taken when using toluene in cleaning the powder not to wash away the adsorbed hydrocarbon molecules. 50% n-heptane-toluene mixture seems not be effective and may be a smaller toluene fraction could work better
- Zeta potential measurements at 25°C and 70°C showed high temperatures enhances the adsorption or activity of PDIs

The study also compared efficiencies of two aging mechanisms and the following conclusions can be made in that regard.

- A new experimental set up and procedure for dynamic aging were successfully put in place
- Basing on spontaneous imbibition results, dynamic aging is more effective in restoring a stronger initial oil wetting state in outcrop than static aging
- Even when not done under confining pressure, a continuous rate of 15ml/hour provided a good initial oil wet state
- When aging dynamically, petrophysical properties of the core material especially permeability need to be considered. In tight Angola cores C1, C2 and C3, a low rate of 1.5ml/hour was used. These cores were classified as being tight
- When aging dynamically, using a back pressure regulator to keep all light oil components in solution improves the aging efficiency

Basing on this work, all the objectives defined in Chapter 1 have been achieved. With these objectives the main goal of looking at the effect of water quality on spontaneous imbibition was achieved and tested using crude oil recoveries. Probable future work needs to look at the impact selective dilution has on the activity of Mg^{2+} ion in absence of Ca^{2+} ion on the wettability alteration process in limestone cores. More research still needs to be done to fully understand the underlying mechanism behind wettability alteration and whether the observed improved oil recoveries are due to the process itself. More research also needs to be done to understand further the efficiencies and inefficiencies of dynamic aging done under confining pressure in outcrop cores.

Bibliography

Bibliography

Anderson, William G et al. (1986). 'Wettability literature survey-part 1: rock/oil/brine interactions and the effects of core handling on wettability'. In: *Journal of petroleum technology* 38.10, pp. 1–125.

Austad et al. (2012). 'Conditions for a low-salinity enhanced oil recovery (EOR) effect in carbonate oil reservoirs'. In: *Energy & fuels* 26.1, pp. 569–575.

— (2015). 'Low salinity EOR effects in limestone reservoir cores containing anhydrite: a discussion of the chemical mechanism'. In: *Energy & Fuels* 29.11, pp. 6903–6911.

Azizov, Ilgar (2019). 'Effect of Water Quality on Wettability Alteration in Carbonates'. MA thesis. NTNU.

Butt, Hans et al. (2013). *Physics and chemistry of interfaces*. John Wiley & Sons.

Chandrasekhar, Sriram (2013). 'Wettability alteration with brine composition in high temperature carbonate reservoirs'. In:

Coulter, Beckman (2006). *Optima L series preparative ultracentrifuges instruction manual*.

Darling, Toby (2005). *Well logging and formation evaluation*. Elsevier.

Fernø, MA et al. (2010). 'Dynamic laboratory wettability alteration'. In: *Energy & Fuels* 24.7, pp. 3950–3958.

Firoozabadi, Abbas et al. (2015). 'Thin liquid films in improved oil recovery from low-salinity brine'. In: *Current Opinion in Colloid & Interface Science* 20.2, pp. 105–114.

Friedman, Gerald M (1996). 'Chalk reservoirs'. In: *Developments in Petroleum Science*. Vol. 44. Elsevier, pp. 773–795.

Graue, A et al. (1999). 'Impacts of wettability on capillary pressure and relative permeability'. In: *SCA9907, Reviewed Proc.: 1999 International Symposium of Core Analysts, Golden, Co., USA*.

Gupta, R and KK Mohanty (2011). 'Wettability alteration mechanism for oil recovery from fractured carbonate rocks'. In: *Transport in porous media* 87.2, pp. 635–652.

Han, Kenneth N (2002). *Fundamentals of aqueous metallurgy*. SME.

Hirasaki et al. (1991). 'Wettability: fundamentals and surface forces'. In: *SPE Formation Evaluation* 6.02, pp. 217–226.

— (2004). 'Surface chemistry of oil recovery from fractured, oil-wet, carbonate formations'. In: *Spe Journal* 9.02, pp. 151–162.

Hogg, RTWDW, To Wo Healy and Douglas W Fuerstenau (1966). 'Mutual coagulation of colloidal dispersions'. In: *Transactions of the Faraday Society* 62, pp. 1638–1651.

Karimi, Mahvash et al. (2016). 'Wettability alteration and oil recovery by spontaneous imbibition of low salinity brine into carbonates: Impact of Mg2+, SO42- and cationic surfactant'. In: *Journal of Petroleum Science and Engineering* 147, pp. 560–569.

Karoussi, Omid et al. (2007). 'Imbibition of sulfate and magnesium ions into carbonate rocks at elevated temperatures and their influence on wettability alteration and oil recovery'. In: *Energy & fuels* 21.4, pp. 2138–2146.

Lucia, F Jerry (2007). *Carbonate reservoir characterization: An integrated approach*. Springer Science & Business Media.

Nasralla, Ramez A et al. (2014). 'Double-layer expansion: is it a primary mechanism of improved oil recovery by low-salinity waterflooding?' In: *SPE Reservoir Evaluation & Engineering* 17.01, pp. 49–59.

Nazari, Negar et al. (2020). 'A Critical Review of the Role of Thin Liquid Films for Modified Salinity Brine Recovery Processes'. In: *Current Opinion in Colloid & Interface Science*, p. 101393.

Shariatpanahi et al. (2010). 'Evaluation of water-based enhanced oil recovery (EOR) by wettability alteration in a low-permeable fractured limestone oil reservoir'. In: *Energy & Fuels* 24.11, pp. 5997–6008.

— (2011). 'Initial wetting properties of carbonate oil reservoirs: effect of the temperature and presence of sulfate in formation water'. In: *Energy & fuels* 25.7, pp. 3021–3028.

Shariatpanahi, SF et al. (2016). 'Water based EOR by wettability alteration in dolomite'. In: *Energy & Fuels* 30.1, pp. 180–187.

Sheng, James J (2010). *Modern chemical enhanced oil recovery: theory and practice*. Gulf Professional Publishing.

Spadini, Adali et al. (2008). 'Carbonate reservoirs in Brazilian sedimentary basins'. In: *19th World Petroleum Congress*. World Petroleum Congress.

Standnes, Dag C and Tor Austad (2000). 'Wettability alteration in chalk: 1. Preparation of core material and oil properties'. In: *Journal of Petroleum Science and Engineering* 28.3, pp. 111–121.

Strand, Skule et al. (2006). 'Wettability alteration of carbonates—Effects of potential determining ions (Ca2+ and SO42-) and temperature'. In: *Colloids and Surfaces A: Physicochemical and Engineering Aspects* 275.1-3, pp. 1–10.

— (2008). '"Smart water" for oil recovery from fractured limestone: a preliminary study'. In: *Energy & fuels* 22.5, pp. 3126–3133.

Thomas, Michele Moisio et al. (1993). 'Adsorption of organic compounds on carbonate minerals: 1. Model compounds and their influence on mineral wettability'. In: *Chemical geology* 109.1-4, pp. 201–213.

Tiab, Djebbar and Erle C Donaldson (2015). *Petrophysics: theory and practice of measuring reservoir rock and fluid transport properties*. Gulf professional publishing.

Torsæter, Ole and Manoochehr Abtahi (2003). 'Experimental reservoir engineering laboratory workbook'. In: *Norwegian University of Science and Technology*.

Treiber, LE et al. (1972). 'A laboratory evaluation of the wettability of fifty oil-producing reservoirs'. In: *Society of petroleum engineers journal* 12.06, pp. 531–540.

Tweheyo, Medad Twimukye et al. (2006). 'The effects of temperature and potential determining ions present in seawater on oil recovery from fractured carbonates'. In: *SPE/DOE Symposium on Improved Oil Recovery*. Society of Petroleum Engineers.

Usui, S (1973). 'Interaction of electrical double layers at constant surface charge'. In: *Journal of Colloid and Interface Science* 44.1, pp. 107–113.

Yi et al. (2012). 'Improving waterflood recovery efficiency in carbonate reservoirs through salinity variations and ionic exchanges: A promising low-cost" Smart-Waterflood" approach'. In: *Abu Dhabi International Petroleum Conference and Exhibition*. Society of Petroleum Engineers.

Yousef, Ali A et al. (2010). 'Laboratory investigation of novel oil recovery method for carbonate reservoirs'. In: *Canadian Unconventional Resources and International Petroleum Conference*. Society of Petroleum Engineers.

— (2012(b)). 'Smart waterflooding: industry'. In: *SPE annual technical conference and exhibition*. Society of Petroleum Engineers.
— (2012(a)). 'The impact of the injection water chemistry on oil recovery from carbonate reservoirs'. In: *SPE EOR Conference at Oil and Gas West Asia*. Society of Petroleum Engineers.
Yu, Liping et al. (2008). 'Analysis of the Wettability alteration process during seawater imbibition into preferentially oil-wet chalk cores'. In: *SPE Symposium on Improved Oil Recovery*. Society of Petroleum Engineers.
Zhang et al. (2005). 'The relative effects of acid number and temperature on chalk wettability'. In: *SPE International Symposium on Oilfield Chemistry*. Society of Petroleum Engineers.
— (2006a). 'Wettability alteration and improved oil recovery in chalk: The effect of calcium in the presence of sulfate'. In: *Energy & fuels* 20.5, pp. 2056–2062.
— (2006b). 'Wettability and oil recovery from carbonates: Effects of temperature and potential determining ions'. In: *Colloids and Surfaces A: Physicochemical and Engineering Aspects* 279.1-3, pp. 179–187.
— (2007). 'Wettability alteration and improved oil recovery by spontaneous imbibition of seawater into chalk: Impact of the potential determining ions Ca2+, Mg2+, and SO42-'. In: *Colloids and Surfaces A: Physicochemical and Engineering Aspects* 301.1-3, pp. 199–208.

Appendix A

Petrophysical measurements

This appendix contains extra data on porosity and permeability measurements and any other petrophysical data about the rock material used in conducting the research.

A.1 Permeability and porosity plots

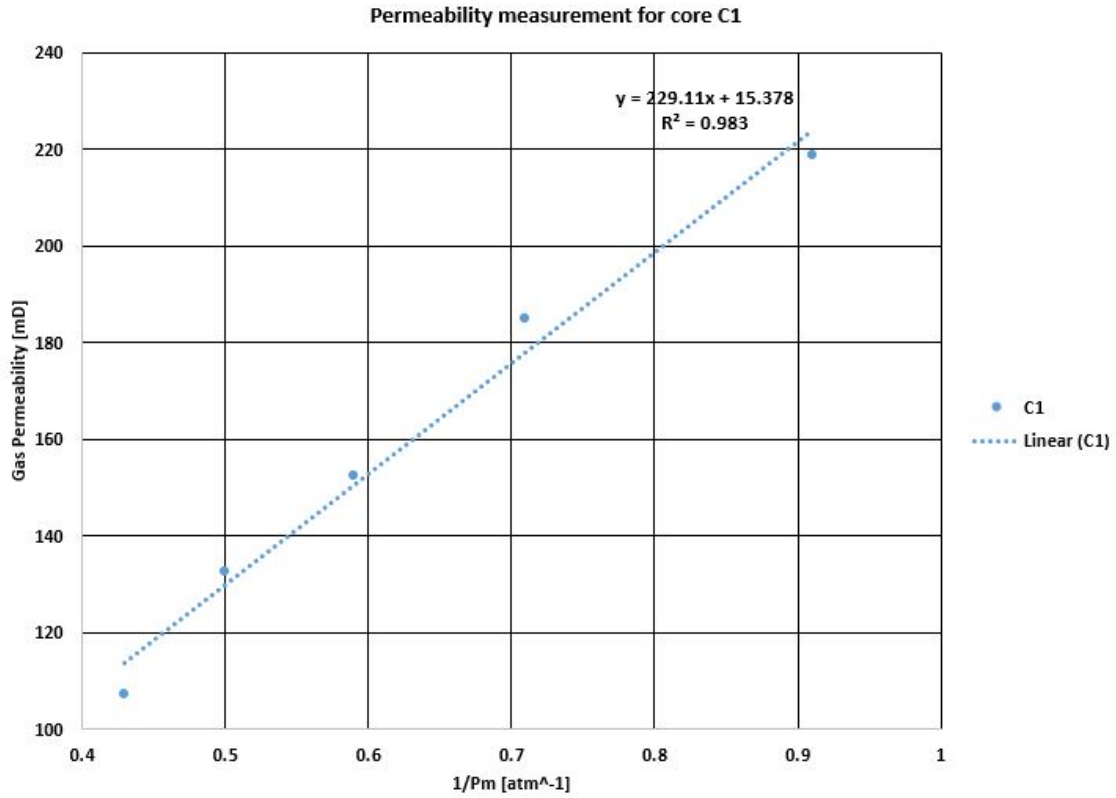

Figure A.1: Permeability plot for C1

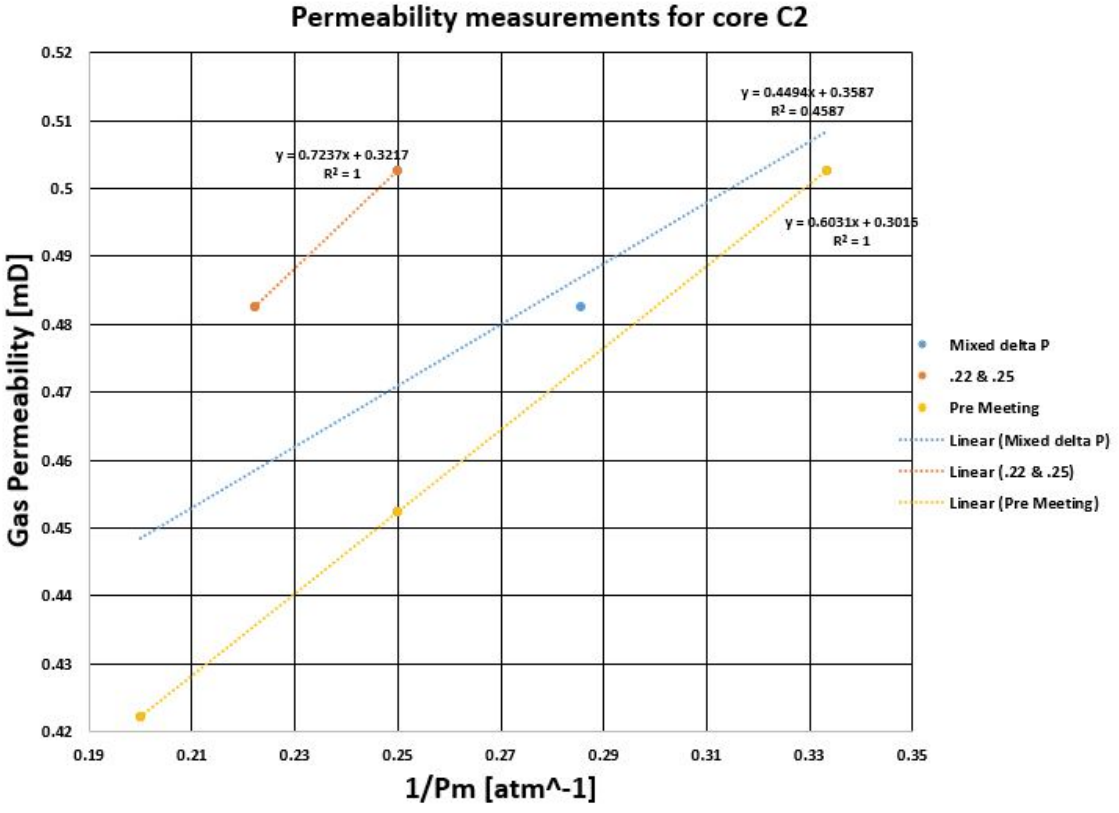

Figure A.2: Permeability plot for C2

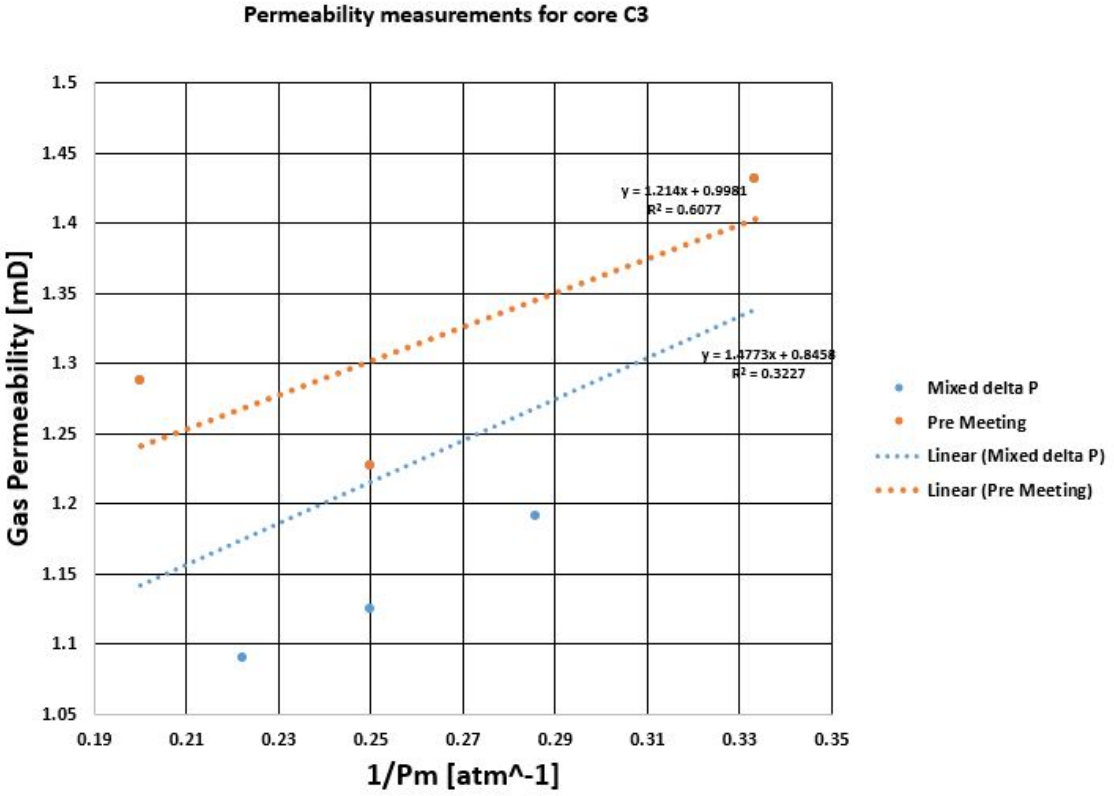

Figure A.3: Permeability plot for C3

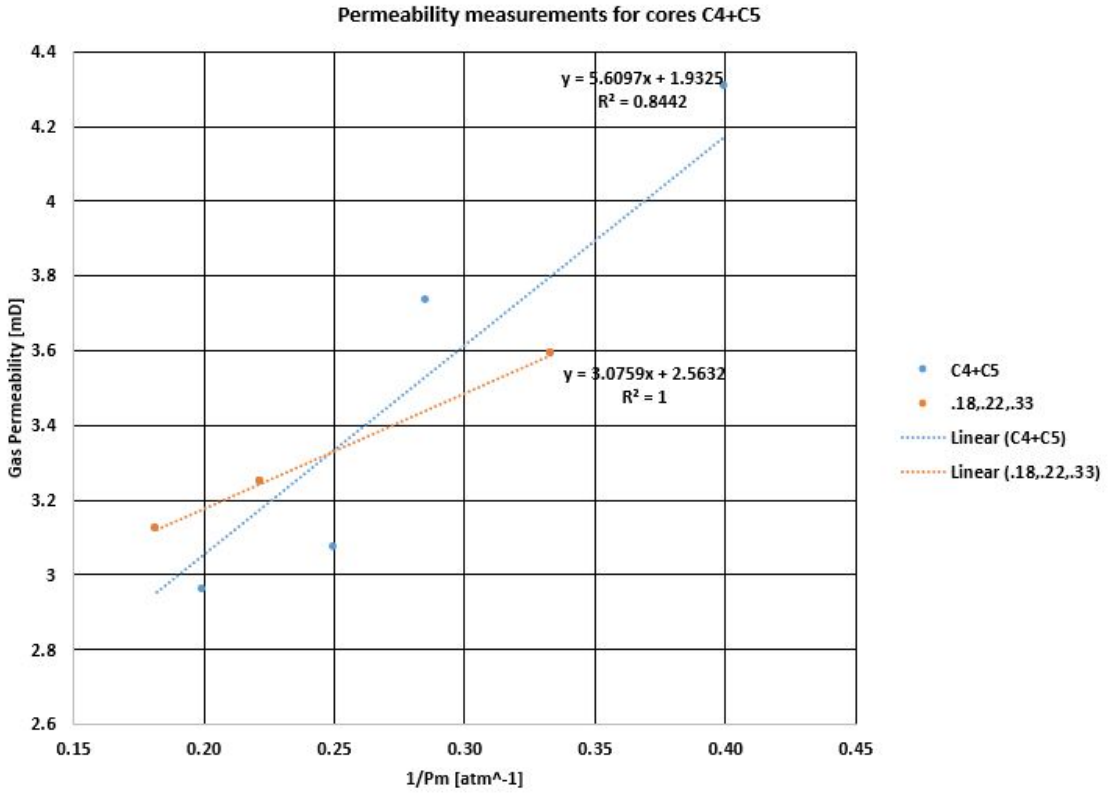

Figure A.4: Permeability plot for C4 and C5

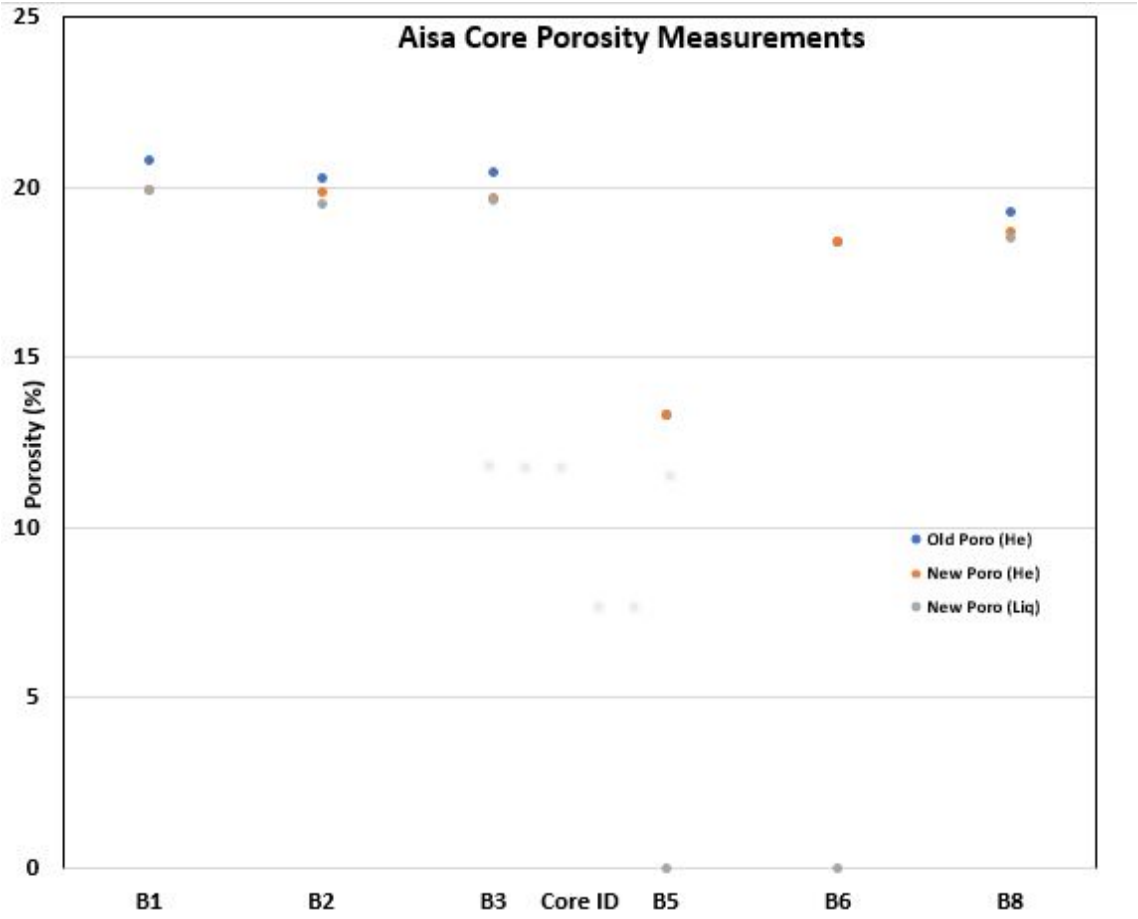

Figure A.5: Porosity cross-plot for B1, B2, B3, and B8

Appendix B

Contact angle and Zeta potential data

This Appendix contains all contact angle and zeta potential data measured in the laboratory. The experimental procedure for filtering crude oil aged rock powder for zeta potential measurements is also included.

B.1 Contact angle measurements

All measurements made on polished Angola rock material, chip 1 and 2, are provided in this section. Left and right angle are for the Young-Laplace algorithm whereas circle are for the Circle algorithm. D_i stands for the crude oil droplet site.

BRINES	FW					SSW				
DROPLETS	D1	D2	D3	D4	D5	D1	D2	D3	D4	D5
Left	168.65	169.75	168.62	166.86	169.39	168.1	168.8	167.54	165.42	167.35
Right	162.98	162.82	164.51	163.12	164.89	167.15	164.38	163.82	159.81	159.07
Circle	161.78	162.12	162.52	163.71	164.64	-	-	-	-	-

Table B.1: One crude oil droplet FW and SSW data set at 23°C

BRINES	SSW-2S4Mg					SSW-2S8Mg				
DROPLETS	D1	D2	D3	D4	D5	D1	D2	D3	D4	D5
Left	171.1	162.8	161.7	162.8	162.2	164.3	166.3	166.0	162.1	159.0
Right	159.8	155.8	153.4	154.6	153.7	158.3	158.5	165.9	159.6	158.6
Circle	-	-	-	-	-	-	-	-	-	-

Table B.2: One crude oil droplet SSW-2S4Mg and SSW-2S8Mg contact angle data set at 23°C

BRINES	FW						SSW					
DROPLETS	D1	D2	D3	D4	D5	D6	D1	D2	D3	D4	D5	D6
Left	133	137	121	130	135	-	98	111	103	123	96	104
Right	138	140	126	127	135	-	95	108	103	122	97	110
Circle	131	140	122	129	127	-	97	114	102	122	100	105

Table B.3: FW and SSW contact angle data set after 24 hours of aging at 23°C

BRINES	SSW-2S4Mg						SSW-2S8Mg					
DROPLETS	D1	D2	D3	D4	D5	D6	D1	D2	D3	D4	D5	D6
Left	70	71	78	-	-	-	62	66	59	58	60	62
Right	67	65	74	-	-	-	62	65	58	54	57	61
Circle	75	67	43	-	-	-	81	82	79	74	80	75

Table B.4: SSW-2S4Mg and SSW-2S8Mg contact angle data set after 24 hours of aging at 23°C

BRINES	FW			SSW			SSW-2S4Mg				SSW-2S8Mg			
DROPLETS	D1	D2	D3	D1	D2	D3	D1	D2	D3	D4	D1	D2	D3	D
Left	162	160	162	118	143	123	118	124	131	136	120	118	119	12
Right	169	168	168	122	141	120	117	124	147	149	120	110	118	12
Circle	162	162	162	120	139	123	121	122	133	137	125	118	118	12

Table B.5: Contact angle measurements after aging in each brine at 96°C for 24 hours

B.2 Zeta potential

[h] All zeta potential measurements are reported in Chapter 5

B.2.1 Procedure for filtration of crude oil aged rock powder

The procedure was followed to separate the crude oil-aged rock powder from crude oil. This was to enable zeta potential measurements only at the rock-brine interface and not crude oil-brine interfaces. **Procedure**

1. Prepare a 50-50% mixture of toluene and n-pentane in a 200ml beaker. This procedure needs to be done in a fume hood for both organic solvents are volatile. n-heptane dissolves light organic molecules and also reduces the dissolution strength of toluene. Toluene dissolves all organic molecules. However, organic molecules adsorbed to the rock powder should not be removed. The n-heptane fraction helps to avoid this.
2. Using a small sample of this mixture, mix it with a 20% volume of the crude oil used in aging for microscopic analysis
3. Using a pipette, place two droplets of the new mixture on a microscope glass slide
4. View the sample under a microscope for asphaltene precipitation. Asphaltene molecules would appear as flocculate particles under microscope
5. If the crude oil contains no asphaltene, mix a half of the crude oil aged sample with a 20% volume of the toluene-n-heptane mixture. Shake gently for about 20 seconds.
6. Using a 0.45vμm milipore filter paper, filter the sample-toluene-n-heptane mixture. This filter paper allows all oil molecules to go through it but not the 8μ-diameter rock powder particles.
7. When the filtration is done, carefully remove the filter paper and collect the residue (wet powder), in a glass vial
8. Place the glass vial on a heating block set at 40°C and then dry the sample with N_2 gas.
9. Whn the sample is completely dry, mix fractions of it in all test brines.
10. The brine-powder mixtures are now ready for zeta potential tests.

BRINES	Day 1			Day 3		
DROPLETS	D1	D2	D3	D1	D2	D3
Left	118	143	123	101	106	105
Right	122	141	120	106	113	114
Circle	120	139	123	105	108	114

Table B.6: Contact angle measurements in SW after aging at 96°C in 3 days

BRINES	Day 1						Day 2					
DROPLETS	D1	D2	D3	D4	D5	D6	D1	D2	D3	D4	D5	D6
Left	97	97	110	100	95	92	83	74	75	74	70	77
Right	92	85	114	104	94	106	89	76	83	74	71	72
Circle	96	97	114	105	91	93	88	68	88	71	78	79

Table B.7: Day 1 and 2 contact angles after aging in 0.1-NaCl-SSW at 96°C

BRINES	day 3					
DROPLETS	D1	D2	D3	D4	D5	D6
Left	64	71	55	53	76	75
Right	65	71	56	58	76	78
Circle	68	71	56	58	76	78

Table B.8: 3^{rd} day contact angle measurements after aging in 0.1-NaCl-SSW at 96°C

Appendix C

Experimental procedures and Risk Analysis

This appendix contains experimental procedure for the new dynamic aging and improved spontaneous imbibition set ups. It also contains risk analysis for both experiments.

C.1 Experimental procedure for dynamic aging

Mounting the core into the core holder. The procedure is in reference to the schematic shown in Figure 4.6

1. With both ends of the core holder open, connect the sleeve inlet to the vacuum source that is created by running tap water in the sink.
2. With one end of the core holder partially closed and connected to a short flow line with a T-valve to its end, gently half fill the core holder with filtered crude oil to be used in the aging process
3. With the connected T-Valve in open position, slowly let oil flow under gravity until when the first drop appears. This is to ensure that all air has been driven out of that end of the core holder. Close the T-Valve
4. With the activated vacuum, place in cores with their marked directions of flow until when the front core touches the end-piece of the core holder
5. Connect a flow line to the second end-piece of the core holder and its other end to a T-Valve. With the T-Valve open, gently hand fasten the end piece as oil flows through the connected flow line
6. Now mount the core holder on the fasting machine. With both ends of the flow lines open, fasten the end pieces as oil flows through them. All air has been driven out of the core holder system

Running the experiment

1. Activate wall pressure P1 (7 Bars) for the Isco pump.
2. Turn on all the three switches in front of the Isco Pump.
3. Define pump parameters on the pumps screen using the A, B, C, D buttons on the pump. That is the flow rate, safety pressure, style of flowing (continuous)
4. Activate sleeve pressure. All valves on the left wall to the pump should be in closed positions and T6 closed to drain. With P3 and P4 in closed positions, slowly open P3. Looking at the gauge on the gas cylinder, slowly open P4 to 35 bars. Open valves T1, T2, T3, T4 and T5 in that order

5. Start the pump using the run button. That is after clearly defining all the pump parameters
6. Activate wall pressure P2. Slowly set the back-pressure regulator to 2 bars.
7. With closed oven doors, switch on the oven and set the temperature to 96°C .
8.

Decommissioning.

1. Stop pumping by activating the stop button on the pump
2. Set the oven temperature to room temperature. Leave the set up to rest for 24 hours for it to cool from 96°C to room temp
3. Deactivate the back-pressure source by first closing P2 and leaving the regulator in closed position
4. Deactivate the sleeve pressure by first closing P3. With T6 open to drain, monitor the gauge connected to P4 until when it goes to zero. Now close P4
5. After the oven cooling, close valves, T1, T2, T3, T4, T5, and T6
6. Disconnect all flow lines and properly dispose of flow lines, crude oil, and D-60.

Changing direction of flow during aging

1. Do steps 1 to 5 under decommissioning
2. Connect the crude reservoir to the previous outlet of the core holder and connect the previous inlet to the line that goes to the back pressure regulator
3. Repeat steps 1 to 7 under Running the experiment

C.2 Experimental procedure for spontaneous imbibition experiment

After **mounting the core samples in the Amott cells** , and for Section 4.2.1

1. Filling the Amott Cells with formation water (FW)
2. Activate valve T1, to allow flow into FW.
3. Open valve T3, to allow flow into T4. Open T4 to allow flow into cell C1.
4. This way, there is a D-60 flow from the Vindum pump, that ensures a formation water flow to the C1 Amott cell
5. Switch on the desktop, to start the software which is used to control the Vindum pump
6. Set parameters such as the pump choice, flowing rate to 10ml/minute, safety pressure ($\approx$ 400 psi).
7. Start pumping via the control button on the desktop until when water flows out through T7.
8. Slowly open T4 and T3 to effluent to allow the liquid level in Amott cell on to drop to a 2ml mark in the graduated neck.
9. When cell C1 is stable, open T4 to allow flow into C2 to reach the same water level as C1 and repeat step 8. 10ml of FW is filled in each of the burettes outside for degassing and pressure balance reasons.
10. Switch on the oven power while closed, and set temperature limit to 96°C to allow the spontaneous imbibition process to commence.
11. Valves T7 and T8 should remain open to flow from the outlet of the Amott cells to the production lines during the SI process.

Changing brines: New brine, lighter than old brine

1. Open valve T1, to allow flow into T2

2. Open valve T2, to allow flow into SW.
3. Open valve T5, to allow flow from SW into T6
4. Open T6 to allow flow into T7
5. Repeat lines 5 and 7 in the degassing step , to begin pumping of D-60
6. Open T7 to allow flow into C1, and open T4 and T3 to allow effluent into hanna, (the salinity and conductivity measurement instrument) .
7. Periodic point by point salinity measurements would be made with the hanna, to establish a fully saturated setup with the new brine.
8. When the attained volume of SSW in the C1 cell (i.e when the water starts to rise into the graduated neck of the Amott cell) is reached. Open T6, to T8, to allow flow into C2, to reach the same water level as C1
9. Due to the density difference between both brines, a piston like displacement. If the salinity measurement at the effluent is same as that of SSW, then the cells are saturated with the new brine.
10. The same procedure is done when switching from SSW to SSW-2S4Mg.

Change form light brine to heavy brine, Section 4.2.3

1. In case of limited space in the oven, pump out all cumulative productions and cool down the oven to 23°C and load the new test brine reservoirs into the oven.
2. Activate valve T1, to allow flow into SSW-2S8Mg, (8Mg Reservoir).
3. Open valve T3, to allow flow into T4. Open T4 to allow flow into cell C1
4. This way, there is a D-60 flow from the Vindum pump, that ensures a SSW-2S8Mg brine to the C1 Amott cell
5. Repeat steps 5 to 7 of the degassing step.
6. With T6 open to effluent to hanna notice the salinity of the effluent brine i.e when the salinity measurement is of the new brine, which is already well known. When there is a full change of brine, open T4 to allow flow into C2 to reach the same water level as C1
7. Pumping is then stopped and oven temperature set to 96°C to allow (SI) process to continue
8. Close T6 to effluent to hanna, slowly open T3 to effluent and then open T4 to allow a back flow from C1, to allow the target level cell C1 to be attained
9. Afterwards, open T4 to C2, to allow the target volume level in the graduated neck of cell C2, to be attained
10. Valves T7 and T8 should remain open to flow from the outlet of the Amott cells to the production and 10 ml of brine put in the burettes for degassing and pressure balance reasons.

Decommissioning spontaneous imbibition set up

1. With the open production network, reduce the temperature in the oven, to room temperature
2. Ensure that all T-valves are in closed position.
3. Disconnect all flow lines

C.3 Risk Analysis

This section contains worked out risk analysis files for high temperature spontaneous imbibition (SI) and dynamic aging experiments. The risk analyses were compiled before and accordingly used in erecting rigs for both experiments. The analysis was done on excel sheets. Zoom in to clearly see the content.

RISIKOANALYSE m SPONTANEOUS IMBIBITION EXPERIMENT AT 96C # Rig #2 (Risk analysis)

Enhet/institutt:	IGP	**Dato opprettet:**	16/03/2021
Ansvarlig linjeleder (navn):		**Sist revidert:**	16/03/2021
Ansvarlig for aktiviteten som risikovurderes (navn):	Carl Fredrick Berg and Antje van der Net		
Deltakere (navn):	10003		

Beskrivelse av den aktuelle aktiviteten, området mv.:

The Spontaneous imbibition rig is used for studies of oil recovery from a core by a mechanism spontaneous imbibition of brine into an oil containg core placed inside a high temeparure-high pressure amott cells. The experiment is conducted inside the oven but also has a few external components like pumps , valves and a production system. . The conditions are 96 degree C and pressure leass than 2 bars inside the amott cell.

Activity / process	**Unwanted incident**	**Existing risk reducing measures**	**Probability (P)**	**Consequence (C)** Evaluate the				**Risk value (P x C)**	**Risk reducing measures - suggestions** Measures reducing the probability of the unwanted incident happening should be prioritized.	**Residual risk after measures being implemente**
			(1-5)	Health (1-5)						
Aktivitet/arbeidsoppgave	**Mulig uønsket hendelse**	**Eksisterende risikoreduserende tiltak**	**Vurdering av sannsynlighet (S)**	**Vurdering av konsekvens (K)** *Vurder en konsevenskategori om gangen. Menneske skal alltid vurderes.*				**Risikoverdi (S x K)**	**Forslag til forebyggende og/eller korrigendene tiltak** *Prioriter tiltak som kan forhindre at hendelsen inntreffer (sannsynlighetsreduserende tiltak) foran skjerpet beredskap (konsekvensreduserende tiltak)*	**Restrisiko etter tiltak (S x K)**
			(1-5)	Menneske (1-5)	Øk/materiell (1-5)	Ytre miljø (1-5)	Omdømme (1-5)			
Placing the core into the amott cell	Glass amott cell falling	Rat hole on the working table to support the base of the amott cell during core loading	1	1	2	0	0	3	Create a second rat hole on the table for to support the second amott cell yet to be loaded. Use platic gloves with good grip on the amott cells	1
Placing the core into the amott cell	accidentally squezzing your fingers against the amott cell	Plastic rubber floves with a rough texture	1	2	0	0	0	2	2.Dosconnect the sleeve source if connected.	3 (5 = 1)
Placing the core into the amott cell	Amott glass cracking due to over pressure caused by the fastening clamp	Adjustable screw on the nut	1	2	2	0		4	Do not force the clamp to close when its not possible. Visit the operating manual for the amott cell	1
Placing amott cell I the oven	Amott cell Falling from a supportine clamo	Weight on the clamo base	1	0	1	0	1	2		
Placing amott cells in the oven	Cracking or breaking the graduated neck of the amott cell	A red plactic nut the connects glass amott cell to metallic components above the graduated neck	3	0	3	0	0	9	Using finger like clamps to support mojority of the weights of the components above the amott graduated neck.	2
Connecting amott cell system to t	Cracking or breaking the graduated neck of the amott cell	A red plactic nut the connects glass amott cell to metallic and other components above the graduated neck	3	0	3	0	0	9	Consider making majority of the connections between components before making the last connection between them and the graduated neck of the amott cell	1
During spontaneous imbibition	Amott cell bsurtsing/cracking due to pressure build up in the system	A 2 bar pressure relief valve connected directly to the amott cell. The amott cell glass material and shape can withstand pressure up to 10 bars	1	0	3	0	0	3	Leave the production system open to atmospheric pressure	0
Pumping of Exxsol D-60	Spillage of Exxsol D-60 from its reservoir due to tripping	Placing the d Exxsol D-60 reservoir in the fume hood and and on a flat surface	1	0	0	1	0	1	Fasten and place two small holes, for flow line and pressure balance, in the lid of the Exxsol D-60 reservoir.	0
Pumping of Exxsol D-60	Bursting the 1.5mm diameter PTFE flow lines due to over pressure. They can withstand pressure up to 35 bars	A safety pressure of 27 bars (400psi) has been set with the pump to automatically stop pumping when pressure anes beyond 27 bars	1	1	1	0	0	2	Keep monitoring the vindum pump for pressure build up	1
Pumping of Exxsol D-60	Exxsol D-60 reservoir empty	Reservoirs larger than 1 litre avialble	1	0	3	0	2	5	Keep monitoring the Exxsol D-60 reservoir especially duing pumping sessions	
Brine reservoirs	Falls during clamping and spontaneous imbibtion at 96C	Reservoirs stands and adjustable clamps	2	2	0	0	0	4	Use short reservoir stands for minimise fall effects	1
Brine reservoirs	Leakage during spontaneous imbibtion at 96C	Hot surface gloves available	3	5	0	0	0	15	Keep atleast 30cm from the oven. Do a leakage test before rising the oven temeperature above room temperature	1
Pumping during spontaneous imbibtion at 96C	Exxsol D-60 pumped into the amott cell	Brine reservoir volume gretaer than the amott cell and flow line svolume combined.	3	0	3	0	2	15	Keep monitoring flow lines during pumping sessions. Install a piston in brine reservoirs	3
Oven opening at 96C	Contacting hot surfaces and inhaling hot gas	Hot surface gloves available and gas masks	3	1	0	0	0	3	Cool down the oven to room temeparure before opening it otherwise wear a full ppe for high temperaure high pressure conditions.	1
Pumping for prduction	Flooding bureates and spilling produced oil	Production only in the graduated neck of the amott cell. Oil spill can not exceed 10 ml (Pore volume limited)	1	0	1	3	0	4	Consider limiting production only in the graduated neck of the amott cell	1
Switching between brines	Pumping Exxsol D-60 into a wrong reservoir and so pressure build up due to no flow	Marked valves and flow lines among reservoirs	2	0	1	0	1	4	Update the experimental procedure to properly incorporate switch between lines and valves	1
Production systems	Bureate falling	Clamps to support the bureate	1	1	1	1	0	3		
Switching between brines	Back flow due to pressure imbalance in the system and hydrostatic heads	Production system connected to atmospheric pressure for pressure balance	2	0	1	1	0	4	Putt amott cells and brine reservoirs athe same elevation. Also elevations of pumping and production systems need to be considered to minimise hysdrostatic heads.	1

RISIKOANALYSE m Dynamic aging under sleeve pressure of 20 bars # Rig #1 (Risk analysis)

Enhet/institutt:	IGP	**Dato opprettet:**	18/02/2021
Ansvarlig linjeleder (navn):		**Sist revidert:**	18/03/2021
Ansvarlig for aktiviteten som risikovurderes (navn):	Carl Fredrick Berg and Antje van der Net		
Deltakere (navn):	10003		

Beskrivelse av den aktuelle aktiviteten, området mv.:

The flooding rig is used to perform dynamic aging in carbonare core samples at elevated temperatures. Flow rates of about 2ml/hr is set using in the ISCO pump. The pressure difference across the core is monitored over time through the pressure gauges connected at the inlet and outlet of the core holder. To avoid liquid bypassing the core, a sleeve is set aroung 19-20 bar that presses around the core by use of nitrogen supply from a gas bottle. The sleeve is a closed system. When conducting the experiments at high temperature (96°C), a back pressure regulator is used and set to 2 bar. ISCO pump is used to drive the fluids into the cylinders. The driving fluid is EXXSOL D-60 that pushes the cylinder piston in motion to direct the Heidrun oil into the core. The effluent production (oil) is collected in the oven in a graduated container.

Activity / process	**Unwanted incident**	**Existing risk reducing measures**	**Probability (P)**	**Consequence (C)** Evaluate the Health (1-5)				**Risk value (P x C)**	**Risk reducing measures - suggestions** Measures reducing the probability of the unwanted incident happening should be prioritized.	**Residual risk after measures being implemented (S x K)**
Aktivitet/arbeidsoppgave	**Mulig uønsket hendelse**	**Eksisterende risikoreduserende tiltak**	**Vurdering av sannsynlighet (S)**	**Vurdering av konsekvens (K)** *Vurder en konsevenskategori om gangen. Menneske skal alltid vurderes.*				**Risikoverdi i (S x K)**	**Forslag til forebyggende og/eller korrigerende tiltak** *Prioriter tiltak som kan forhindre at hendelsen inntreffer (sannsynlighetsreduserende tiltak) foran skjerpet beredskap (konsekvensreduserende tiltak)*	**Restrisiko etter tiltak (S x K)**
			(1-5)	Menneske (1-5)	Øk/materiell (1-5)	Ytre miljø (1-5)	Omdømme (1-5)			
mounting the core in the core holder with vacuum from flowing water	wrong mounting of the core: cell leakage, maximum volume gas release; unlimited air from 7bar flow line. Accidendtal connection to the sleeve source	1.Pressure test/leakage test implemented in procedure.	1	2	1	0	0	3	2.Dosconnect the sleeve source if connected.	3 (5 + 1)
	Core holder Falling during core mounting	Flat working space	1	3	1	0		4	Protective wear, shoes, lab jacket, glasses	4
								0		
Back pressure supply	Breakage of PTFE lines. They are certified to withstand 35 bar of pressure (507 psi).	Supply of pressurized air is only less than 3 bar. Set BP = 2bar.	1	1	1	1	0	3		
Setting the sleeve pressure	damaged sleeve or wrong mounting: over pressurizing the system by supply of the gas bottle	Choke on gas bottle allows maximum 60 bar pressure. Valve mounted between regulator And sleeve. Allows for slow pressurization and leak testing.	1	2	3	1	1	7	Recommend changing the choke to 25-30 bar; but currently not available in required range. Wear PPE	5
Filling the inlet and outlet tubings connected directly to the coreholder	Spillage of crude oil	Working in the fume hood is not possible. Wear protective gears including proper mouth mask and turn on the ventilation of the oven, without temperature. Low flow rates and temperature	3	0	1	0	0	3	Update protocol. Work on flat surface. Low flowrates.	4
Setting flow rate and injection pressure using injection pump (ISCO pump)	Rise in pressure during the injection and breaking the lines (Max. 35 bar). Spill of fluids	A safety pressure has been set to 450 psi (31 bar). The pump warns when 30bars are reached	2	1	1	0	0	4	Keep monitoring the set up for pressure build up	4
Flow lines	Bursting due to pressure rise caused by clogging	Isco Pump warning when pressure exceeds 30 bars. Oil is filtered at room temperature, wax particles can be filtered out, which reduced the risk of plugging.	2	1	2	0	0	6	Keep monitoring the set up for pressure build up	3
Core holder stands	Tripping/ fall over	Flat working space and core holders	2	2	2	2	0	12	Use PPE and keep using flat working space	3
Location of bottle with pumping fluid for iscopump	Reservoir tips/breaks resulting in spill of <1 L Exxsol-D60 .	Reservoir is placed in fume hood. Modified bottle cap avoids quick release of fluid.	2	1	0	0	0	2		
Aging at 96 degrees	Burns due to hot oven	Hot surface gloves available, protocol such that oven is not to be opened during aging.	1	5	0	0	0	5	Update protokol. Keep atleast 30cm from the oven	1
Operating the flood rig at elevated temperature:	human expoure to heat: inhalation of released gasses, heat, skin contact.	Procedure; No activities in the oven at high tempertures. Possible risk of leakage detected during high T; procedure is to turn off the oven. But in the event of opening, also ensure PPE is used	2	1	0	0	1	4	Update procedure	
volume of reservoir is used up: Oil	Oil; Pump oil displaces piston which presses the oil in the system. If piston is lowered till the bottom the pump builds up pressure in the system.	The maximum pump pressure is set in the pump. Max pump pressure= 700bar. Limit is set to 450 psi (31 bar), which is lower than max line pressure of 35 bar.	2	1	2	0	0	6	Consider leaving a volume of 50ml in the crude reservoir to avoid the piston reaching all the way to the bottom of the reservoir. Update protocol; check status fluid levels	0
Pumping at 96C	Valves leak due to high temperature expansion and pressure from pumping	Low flow rates and leakage test at low temperature. Visualization of leakage on blue paper. Expected leakage small. Can be accepted. If not acceptable; procedure, reduce temperature to RT before repairment of leakage	3	0	1	1	0	6	Wrap a small foil of Teflon around the male end of valves. Slowsly increase the temperature in the oven from room to 96C	
Elevated temperature, up to 96° C.	Ignition of flammable liquids. Exxsol D60 is combustible, with flash pont=62° C. Crude oil is highly flammable.	Closed flow line system. Rig is inside Binder oven. No ignition sources are present. Cap on bottle with the production fluid (small hole to avoid pressurizing)	1	2	2	0	1	5		
Overnight flooding	Experiment failure / equipment failure during night: Sleeve breakage, line breakage, power failure, loss of pressurized air.	Low flowrates minimize fluid spill. Binder cabinet shields most components against harm to rest of lab. Campus security checks labs outside working hours.	2	0	2	0	0	4	Keep monitoring the set up before leaving it overnight	0
Core dismounting: sleeve pressurized	Sudden gas pressure release. Will core shoot out? / gas accumulation at inlet?	Volume= max 100cm3; 20 bar= 2 liter. Pressure release is mounted. Gas is nitrogen. Suffocation danger is limited if gas flow line from gas bottle is closed.	1	2	1	0	1	4	Use manometer to check pressure is released. Update procedure	0
Decommisioning	Oil leakage during decommisioning	Installed valve behind and ahead of the core holder ; further dismounting in the fume hood.	2	1	0	2	0	6	Cover table surfaces with table paper to avoid tripping due to oil smoothing??	2
Core dismounting: spill	Spill of crude oil and D-60	Only small amounts (<5ml) of crude oil should be left in core holder/core Use of end caps to avoid spill out of flow lines and valves befre transport to the fumehood. Use of protective gear incl mask; use of oven ventilation.	2	1	0	0	0	2	Update Procedure; Work on falt surfaces and use PPE and turn on the ventilation of the oven. Condiser using valves or flow-killing plugs	0
Core dismounting: hot fluid / vapor	Ignition of flammable liquids. Skin burns.	Core should never be dismounted while at high temperatures (>50 degC). There are no ignition sources involved.	1	2	1	1	1	5	Store combustible fluids far away from the oven	1
Use of 3 way valves, core outlet	valve turned the wrong way: core outlet, flow in bypass / blocking outlet	Set a safety pressure to 450 psi.	2	1	2	0	0	6	update procedure, instruct on use of 3-way valve	2
Continuous collection of core flood effluent	Container full (not large enough to collect all fluids).	adapt size to maxium amount of effluent produced.	2	1	1	0	0	4		
	Decommisioning- Burns due to hot surfaces in the oven	Switch off the oven and leave it overnight to cool before opening it	3	3	0	0		9		
	Decommisioning- Oil spills	Valves behind and ahead of ghe core holder	3	1	0	0	0	3	Update the decommisoning proceedure	0
	Decommision- Sleeve pressure release	Proper operation of chokes on the gas cylinder and the sleeve drain	2	1	0	0	0	2	Update the decommisoning proceedure	0